EFFECTS OF TRANSIENT LONG WAVES ON NONLINEAR PROCESSES IN RANDOM WAVES

A Thesis

by

XIN YANG

Submitted to the Office of Graduate and Professional Studies of
Texas A&M University
in partial fulfillment of the requirements for the degree of

MASTER OF SCIENCE

Chair of Committee,	James M. Kaihatu
Committee Members,	Achim Stössel
	Jens Figlus
Head of Department,	Sharath Girimaji

August 2019

Major Subject: Ocean Engineering

ABSTRACT

Much effort has been devoted to the numerical modeling of nonlinear wave propagation in shallow water during the last several years. Boussinesq equations are important because they balance the effect of nonlinear terms and dispersion relation and make it possible to find solutions including waves of permanent form. However, Boussinesq equations are not valid in intermediate and deep water depth. There are generally two methods to extend the limitation. One approach is to extend the Boussinesq equation by improving the linear properties. The other one is the nonlinear mild-slope equation, which has the fully dispersion relation and shoaling property.

Kaihatu and Kirby's mild-slope nonlinear wave transformation model is a parabolic model in frequency domain. The time series measurement should be treated with Fast Fourier Transformation before simulation. The model is built for random wave fields. In Kaihatu and Kirby (1995), the model has been proved good simulation performance on the basis of the data of random wave field from Mase and Kirby (1992) experiments. However, if the model is applied in field work, it can be an interesting question whether the transient long wave will affect the model simulation.

The NEES Tsunami and Swell experiments conducted at Oregon State University produced solitary waves in random wave fields and recorded the wave heights at different gauges. Hence, this thesis makes use of Kaihatu and Kirby (1995) model to simulate this soliton plus random waves data to investigate the effect of transient long waves on the simulation of random waves. The performance of the model will be evaluated when handling the soliton plus random wave field. A MATLAB code of the model is built in reference to the original code in Fortran fixed format.

The spectra of the data and model results are compared to evaluate the performance of model qualitatively. The frequency scale is divided into three areas, infragravity area ($0 \leq f \leq \frac{f_{peak}}{2}$), swell area ($\frac{f_{peak}}{2} \leq f \leq \frac{3f_{peak}}{2}$) and sea area ($\frac{3f_{peak}}{2} \leq f$), and the energy in each area is calculated on the basis of both experiment data and model results for comparison. The root-mean-square of the wave height is calculated to evaluate the energy prediction of the model. The skewness and the

asymmetry are calculated to evaluate the performance of the model in prediction of the wave shape change during the propagation. Generally, the addition of the soliton has a significant influence on the wave field and the performance of the model. The larger the amplitude of the soliton, the larger the effect of the soliton on the nonlinear processes in random waves, and with that the poorer the performance of the model in prediction of spectra.

DEDICATION

To my father, Junlin Yang, my mother, Pin Chen, and my girlfriend, Lu Dong.

ACKNOWLEDGMENTS

At the end of the 2014, when the ship industry and ocean engineering shrank to an unacceptable level because of the low price of petroleum, I decided to apply for a master of science degree in America. Partially because I couldn't be recommended as graduate student without examination, I wanted to find another possibility for my career. I still remembered the day when I received the admission from Texas A&M University. It was at the mid of May and I had already accept the reality that I was rejected by Texas A&M University. I was hanging out with my girlfriend but not in a mood totally. The new email from Ocean Engineering Department at Texas A&M University informed me that I was admitted. It lit me. I knew that a new challenge but also an opportunity came to me. I was excited. I successfully threw myself out of the comfort zone.

I was still unsure about what topic I was interested in for research at the end of the first year at Texas A&M University. I can get A through learning, asking , memorizing and thinking but it was a hard choice for me since I hadn't taken part in a research ever. At that time, I was taking the *Turbulence Process* from Dr. Girimaji. I was impressed by numerical modeling of nonlinear process. I wanted to try numerical modeling. I just felt it was cool to use formula and codes to predict the physic phenomena. It was useful, meaningful and even elegant to me. Some senior recommended me to have a look Dr. Kaihatu's personal website. I read all the contents on his website. I even printed one of his publication, *Parameterization of maximum significant wave heights in coastal regions due to hurricanes*, and read it even though I couldn't understand it at all. But I thought it was so cool that I wanted to learn more about. I feel shamed that I was so rude that I just came in Dr. Kaihatu's office without appointment. But I also feel lucky that Dr. Kaihatu accepted me anyway.

It was hard but also interesting at the beginning. I started to learn about the knowledge of nonlinear wave mechanics and Fortran. I love to derive formulae, which may be unconsciously influenced by my father, a mathematics professor. However, I was unable to connect the formulae to the physic meaning. I was also a rookie in coding. Hence, in the every week meeting, I had

tons of questions about derivation, meaning of terms and stupid bugs in codes to ask Dr. Kaihatu. Sometimes, I think I understand the point, but I then find I totally misunderstood it or forgot something really simple. It is a spiral stairs for me to make progress and study something. This research experience teaches me a lot, the most important thing is that research is something I want for my career. I just don't want to stop when I just scratch the surface. My curiosity makes me to continue for a more complete cognitive world.

I need to say thank you to my advisor, Dr. James M. Kaihatu. He has aided me tremendously with his advice, his patience and his help. Every time he told me that his time was limit and our meeting should be short, but it turned out another hour was spent on my questions. Sometimes, it is hard for me to express my grateful because of the language, but this experience is one of the most important things for my career life. My committee, consisting of Dr. Achim Stössel and Dr. Jens Figlus, deserve my thanks for agreeing to serve.

I also want to say thank you to my classmates, Xu Chang, Yu Wang, Alexander Freddo and Mourya Penugonda. They gave me a lot of advice about research. Every time I have some crazy idea or questions, they were willing to have a discussion with me.

Finally, I need to thank my parents. They finance my master of science program and it is not easy for a common family in China. They are open-mind and give their son to make decisions for his life freely. I hope I made you all proud. I also need to say thanks to my girlfriend for her company and patience. It is really hard to have a long-distance relationship. I hope everything goes well in the future.

CONTRIBUTORS AND FUNDING SOURCES

Contributors

This work was supported by a thesis committee consisting of Dr. James M. Kaihatu of the Department of Civil Engineering and and Dr. Achim Stössel of the Department of Oceanography and Dr. Jens Figlus of the Department of Ocean Engineering.

The data used in this thesis is provided by Dr. James M. Kaihatu.

All other work conducted for the thesis was completed by the student independently.

Funding Sources

There is no outside funding contributions to acknowledge related to this research.

TABLE OF CONTENTS

Page

LIST OF FIGURES

FIGURE Page

LIST OF TABLES

TABLE Page

1. INTRODUCTION AND LITERATURE REVIEW

1.1 Introduction

In 2004 India Tsunami, it was observed that the solitary wave created by earthquake traveled a long distance to the shoreline. It is an interesting and meaningful question that what effect the solitary wave has on the random wave processes in shoaling and breaking.

The nonlinear process in wave propagation affects wave shapes. The wave shapes have a significant effect on the sediment transport. Hence, the research on water wave propagation is meaningful to coastal engineering, offshore engineering and understanding of sediment transport. The linear theory is valid in most cases for investigating wave energy flux and wave-structure interaction problems. However, in order to learn about the shape change during wave propagation, the sediment transport and some other physic phenomena, it is necessary to extend wave theory to nonlinear wave theory. Many numerical models have been built based on the nonlinear wave theory to investigate the wave propagation at the coastal.

Kaihatu and Kirby (1995) built a mild-slope model for nonlinear wave transformation. This model has the same dispersion relation and shoaling properties as linear theory and the same order of accuracy in nonlinearity with weakly nonlinear extended Boussinesq equation model. This thesis uses the model of Kaihatu and Kirby (1995) to investigate the interaction between soliton and random wave field.

In the derivation of Kaihatu and Kirby's (1995) model, the quadratic nonlinear terms are treated by wave triad resonant interactions. This actually implicates that the signal input should be periodic. Discrete Fourier transformation used in derivation of model also actually stands on the premise that the signal is periodic. Additionally, the dissipation mechanism used in the model is from Thornton and Guza (1983), which is for random wave shoaling. Hence, it is reasonable to say that the model is built for random waves.

In Kaihatu and Kirby (1995), the model has been proved good simulation performance on the

basis of the data from Mase and Kirby experiments. Kaihatu and Kirby's mild-slope nonlinear wave transformation model is a parabolic model in frequency domain. The time series measurement should be treated with Fast Fourier Transformation before simulation. Theoretically, every function can be treated with Fourier Transformation. Hence, a signal of random wave field mingled with transient long waves can also be transformed by Fourier transformation and taken as input data. It is worth investigation whether the transient long wave like soliton will affect the performance of the model.

The NEES Tsunami and Swell experiment conducted at Oregon State University produced solitary waves in random wave fields. This thesis makes use of the model of Kaihatu and Kirby (1995) to simulate this soliton plus random waves data to investigate the effect of transient long waves on the simulation of random waves. A MATLAB code of the model is built in reference to the original code in Fortran fixed format. Chapter 2 of the thesis derives the one-dimensional mild slope model for nonlinear wave propagation and treats the data from Mase and Kirby (1992) experiment to verify the validity of MATLAB version code. In Chapter 3, for comparison, the simulation results of purely random wave fields are given firstly. Then, the spectra of data and modeling results for soliton plus random waves are compared. The effect of transient long waves on nonlinear process in random waves can be shown intuitively through the comparison between purely random wave and soliton plus random wave. To quantify the effect of transient long wave, H_{rms} (root mean square of wave height), skewness and asymmetry of experimental data and model results are calculated and compared. The energy of infragravity scale, swell scale and sea scale have been calculated and compared with the experimental data to show the performance of the model in prediction of the energy distribution in the frequency domain.

1.2 Literature Review

Under the influence from air pressure, free water surface has a tendency to deform. The gravity and surface tension apply on the water body at the same time. Water wave is a manifestation of the balance of the forces mentioned above, which maintain the smooth and continuous water surface. The nature of wave is propagation of energy. Under the external influence, potential energy is

transformed into kinetic energy of water particles, the wave is formed. Wave number, wave height and wave frequency decide the features of the wave. The energy is transported in certain direction, certain range and at certain frequency.

As the wave propagates toward the shoreline, the water depth decreases, the amplitudes of the waves increase due to the conservation of the energy flux at the same time, which is called shoaling. However, these are linear wave problems. The nonlinear behavior inherent in ocean waves becomes more evident in shallow water. The shapes of wave become more asymmetric and change to ones with sharp crests and flat troughs in shallow water. The wave will break at one point, where the wave amplitude cannot increase any more and the wave form is crushed. Wave breaking causes the dissipation of the wave field. Many of these nonlinear wave behavior are describable using wave-wave energy exchange between frequencies (Freilich & Guza, 1984[1]). Moored structures can resonate with the long waves. Wave breaking, long shore currents and sediment transport are all related to the shapes of the shoaling waves. The analytical solution to the propagation of nonlinear waves and wave breaking is impossible with the present mathematics tools. Hence, it is necessary to develop numerical model to simulate the wave propagation.

The linear theory is applicable when the water waves have small amplitudes. Under this assumption, the free surface boundary conditions can be expanded by Taylor expansion at the mean water level. The wave elevation is assumed to be infinitesimal and the nonlinear terms in the boundary conditions are neglected. However, in the shallow water wave, the application of linear theory can be stringent. The linearized shallow-water approximation can be useful only if the following conditions are satisfied:[2]

$$\mu \equiv kh \ll 1 \qquad and \qquad \delta \equiv \frac{A}{h} \ll 1 \tag{1.1}$$

where k is wave number, h is water depth, A is wave amplitude.

The second condition is difficult to meet for shallow water waves. The increase of the amplitude during shoaling can be derived from linearized equations of motion. There are also some empirical equations used to anticipate the amplitude. However, the spectral evolution, nonlinear energy

exchange, prediction of the shape of waves and other effects are beyond linear theory. Therefore, nonlinearity needs to be considered.

The Airy theory was developed under the assumption that the pressure at one point in the fluid was equal to the hydrostatic pressure of the fluid volume above that point.[3] Boussinesq (1871) derived a set of equations which are expanded to the second order of small quantities. Many methods have been developed to derive these two theories. The formalism of Benny (1966) and Peregrine (1967) are utilized and referred widely in the later literature. The difference between Airy and Boussinesq equations is that Boussinesq equations kept the terms proportional to μ^2 but Airy theory omitted these terms.

Airy's theory for long waves results in the following equations:[2]

$$\eta_t + \bigtriangledown_h \cdot [(\delta\eta + 1)\bar{\mathbf{u}}] = 0, \tag{1.2}$$

$$\bar{\mathbf{u}}_t + \delta\bar{\mathbf{u}} \cdot \bigtriangledown_h \bar{\mathbf{u}} + \bigtriangledown_h \eta = 0, \tag{1.3}$$

$$P = \delta\eta - z. \tag{1.4}$$

In contrast, Boussinesq Theory results in these equations:

$$\eta_t + \bigtriangledown_h \cdot [(\delta\eta + 1)\bar{\mathbf{u}}] = 0, \tag{1.5}$$

$$\bar{\mathbf{u}}_t + \delta\bar{\mathbf{u}} \cdot \bigtriangledown_h \bar{\mathbf{u}} + \bigtriangledown_h \eta - \frac{\mu^2}{3} \bigtriangledown_h^2 \cdot \bar{\mathbf{u}}_t = 0, \tag{1.6}$$

$$P = \delta\eta - z + \frac{\delta\mu^2}{2}(z^2 + 2z) \bigtriangledown_h \cdot \bar{\mathbf{u}}_t. \tag{1.7}$$

The η is wave elevation. The $\bigtriangledown_h$ denotes the horizontal gradient. The h denotes the water depth. The $\bar{\mathbf{u}}$ is the depth-averaged horizontal velocity, which is defined by $\bar{\mathbf{u}} = \frac{1}{H}\int_{-1}^{\delta\eta} dz \bigtriangledown_h \phi$, where ϕ is defined as potential function.

The parameter δ actually quantify the effect of nonlinearity and μ accounts for the effect of dispersion. For Airy theory, the $O(\mu^2)$ terms are dismissed, which means non-dispersive. For Boussinesq equation, the effect of nonlinearity and dispersion are retained to $O(\delta)$ and $O(\mu^2)$

respectively. When δ and μ are both infinitesimal, the equations from linear theory are obtained.

In the Airy theory, the wave cannot propagate in permanent form. However, it is contradicted by the existence of solitary wave, which is transient long wave of small amplitude and propagates without change of shape. The Boussinesq equations have the solitary wave as one of their solutions This paradox in long wave was not resolved until a paper by Ursell (1953). Ursell found a parameter, $\eta_0\lambda^2/h^3$, played a fundamental role in solving the long wave paradox. This parameter is named Ursell number, which also can be written as:

$$U_r = \frac{\delta}{\mu^2} \tag{1.8}$$

where δ is the nonlinearity parameter:

$$\delta = \frac{a_0}{h_0} \tag{1.9}$$

and μ is the dispersion parameter:

$$\mu = k_0 h_0 \tag{1.10}$$

where h_0 is a characteristic water depth, k_0 is a characteristic wave number, a_0 is a characteristic wave amplitude.

Ursell (1953)[3] suggested that linear wave theory is applicable when $U_r \ll 1$; Boussinesq equation work when U_r has a finite value ($U_r = 1$); and Airy theory (nonlinear long wave) is applicable when U_r is large ($U_r \gg 1$).

Korteweg & de Vries (1895) derived a single equation, KdV equation, which is actually the one-dimensional version of the Boussinesq equations. These two sets of equations can be solved to describe the propagation of the wave in permanent form in constant depth. Different kinds of models have been developed based on these two sets of equations. Peregrine (1967)[4] derived the Boussinesq equations from the Euler equation for waves on a beach of mild uniform slope. Mei (1983) re-derived the Boussinesq equations from the boundary value problem and assumed that the vertical velocities in the water column are much smaller than horizontal velocities. Hence, he expanded the potential function as a power series in the vertical coordinate and used the scaling

method to retain the terms to $O(\delta)$ and $O(\mu^2)$ to achieve the Boussinesq equations. Freilich and Guza (1984) derived frequency-domain models from the one-dimensional equations of Peregrine (1967) and performed the comparison with the field data.

Extended Boussinesq's Equations

One fundamental problem of the models based on Boussinesq equations is that they are only valid in shallow water depth (small μ^2, where $\mu = kh$).[5] Starting from Witting (1984), efforts have been devoted to extending the application of the Boussinesq equations by changing the dispersive characteristics of the Boussinesq equations to apply to deeper depth. Witting (1984) started from the integral form of governing equations and then used the Taylor expansion to find the relation between vertically averaged horizontal velocity and surface velocity. He used the fluid velocity at the bottom to create the representation for irrotational two-dimensional waves, resulting in numerical model which incorporated both long wave theory and Boussinesq theory and used a tridiagonal matrix solve to perform the simulation. However, his method is applicable only in one-dimension.

Madsen et al. (1991)[6] developed an improved Boussinesq model by deriving an improved dispersion relation and then determining the terms in the Boussinesq equations which would have had to lead to these terms. They started with the summary of different types of Boussinesq equations and introduced a free parameter B in the phase celerity and group velocity. They made an approximation of the dispersion term in the Boussinesq equation which was decided by the free parameter B. Then they tuned the parameter B to achieve the smallest percentage error.

In his method, the dispersion property is also improved, but at the same time, the introduction of the fifth order derivative increases the complexity of the numerical solution. This fifth order derivative was an effect of the improved dispersion relation.

Madsen and Sørensen (1992) extended the model of Madsen et al. (1991) to a slowly varying bathymetry from deep to shallow water. Madsen and Sørensen (1993) investigated frequency domain formulations of the model of Madsen et al. (1991) for wave evolution over a flat bottom. The equations of Madsen et al. (1991) had been further investigated by Schäffer and Madsen (1995)[7],

Madsen and Schäffer (1998)[8] and Madsen and Schäffer (1998)[8].

Nwogu (1993)[9] used the velocity at an arbitrary elevation to derive a new set of Boussinesq equations from Euler equations rather than the bottom velocity or vertically averaged velocity. The new set of Boussinesq equations contains an additional frequency dispersion term in the continuity equation. The arbitrary depth z_α can be chosen to obtain the best fit between the linear dispersion relation of the model and the exact dispersion relation for a wider range of water depths. This method introduced the free parameter α naturally from the representation of continuity and momentum equations via the velocity at an arbitrary depth. Hence, from intermediate depth to deep water, the linear dispersion property can be decided by the choice of the velocity variable. The linear dispersion property becomes very similar to those of the first-order Stokes waves if the velocity chosen is closed to that at the mid-depth. However, his method has the similar drawback to Madsen et al. (1991). The highest order of the spatial derivatives in Nwogu's equation is one order higher than that in the common Boussinesq's equation, which brings up more difficulty to achieve numerical solution.

Chen and Liu (1995)[10] rederived the modified Boussinesq equation given by Nwogu (1993) in terms of a velocity potential on an arbitrary elevation and the free surface displacement. They started from the boundary value problem and used the velocity potential at an arbitrary depth to express the velocity potential function. They derived the linear properties of their potential version of Boussinesq's equation given by Nwogu (1993). They determined the free parameter $\alpha = -0.3855$ by minimizing the sum of relative errors of the phase and group velocities over the range $0 \leq h/\lambda_0 \leq 0.5$. Then they substituted finite Fourier series of potential into Boussinesq's equation and combined equations into one equation in terms of velocity potential only. They remarked that it should be taken attention whether the combination of two equations would harm the dispersion property during the substitution and successive approximation. In their small-angle parabolic model, they assumed that the variation of the wave field in the y-direction is small and then they moved the terms containing y-derivatives to the right-hand side to take the equation as a fourth-order ordinary differential equation about x. In their angular-spectrum parabolic model,

they first decomposed the wave field with trigonometric polynomials into a series of wave modes. Then they impose another assumption that $(h - D) \sim O(\epsilon)$, where D donates reference depth, the deviation of the actual depth from the reference depth is of the same order of magnitude as the typical wave amplitude. Therefore, they can apply the same method used in small angle parabolic model to obtain a parabolic approximation. The accuracy of their model depends on the difference between the wavenumber of the forcing term and their characteristic wavenumber of the equation. However, their model is not applicable for a broad-banded spectrum. The parabolic approximation of the angular-spectrum model is restricted to the assumption about depth so that the model is not applicable for relatively deep water.

Mild-Slope Equation

An alternative approach involves the use of the mild-slope equation formalism. Mild-slope theory is developed to simulate the wave refraction, diffraction and shoaling. It is initially a linear model from the approximation of linear shallow-water theory, in which the vertical structure of the waves is ignored, and the slope of the seabed is extremely small.

The mild-slope equation (2.11) is firstly derived by Berkhoff (1972), which is widely used in the later literature. He started from boundary value problem with mild slope and made the assumption to expend the potential function into a power series. Then he took the integral of the governing equation and made simplification under different case of the relation between μ (μ=kh) and ν ($\nu = \mu\epsilon^{\frac{1}{2}} = h/\sqrt{\lambda L}$, λ is the wave length and L is the length scale of bathymetric features).

$$\bigtriangledown \cdot (cc_g \bigtriangledown \Phi) + \omega^2 \Phi c_g / c = 0[11] \tag{1.11}$$

where c is wave celerity, c_g is group velocity, Φ is the potential function. Smith and Sprinks (1975) developed a model based on mild-slope equation for refraction and scattering. They derived the mild-slope equation with Green's identity, which is a more direct method and is applied in Kaihatu and Kirby (1995). In the model of Smith and Sprinks (1975)[12], they tried to simulate the group and phase velocity to extend the linear shallow-water theory for mild slope.

Radder (1979)[13] derived the parabolic approximation based on the mild-slope equation. He started from Helmholtz equation, which is reduced from (2.11), without loss of generality. Then he assumed that the wave propagated mainly in the x direction and split the equation into a transmitted field and a reflected field. He achieved the parabolic approximation of the transmitted field by omitting the reflected field term in the equation of transmitted field. Lozano and Liu (1980)[14] derived a parabolic approximation to the linearized water wave theory in mild slope bathymetry via an asymptotic method. The introduction of parabolic approximation has greatly increased the efficiency of numerical calculation of mild-slope equations.

Bryant (1973)[15] investigated the efficacy of developing fully-dispersive models with non-linearity. His research was made into the evolution, from a sinusoidal initial wave train, of long periodic waves with small but finite amplitude propagating in one direction over water in a uniform channel. His model is different, which is built to be periodic in space and evolving in time. Furthermore, Bryant (1974)[16] showed that the phase velocity and harmonic amplitudes of his spatially periodic solution matched those of the cnoidal waves of Korteweg & de Vries (KdV) equation.

Keller (1988)[17] derived coupled nonlinear equations for the amplitudes of two small-amplitude resonantly interacting gravity waves from the exact Euler equations, form the nonlinear shallow water theory , and from the Boussinesq equations. He showed that, in the shallow water limit, the equations reduced to identical forms.

Agnon et al. (1993)[18] derived a fully-dispersive nonlinear evolution equation for shoaling gravity waves, describing the process all the way from deep to shallow water. Agnon et al. (1993) started from the boundary value problem in mild-slope water depth. They used Taylor expansion about the mean water level on the free surface boundary condition and substituted the Fourier transform of potential function describing the evolution of the frequency spectrum Φ. In order to obtain a single evolution equation, Agnon et al. (1993) found a solution written as a superposition of a term representing the free waves and the other associated with locked waves to the Laplace equation with the bottom boundary problem. Hence, they achieved the evolution equation by substituting the solution into the combined free surface boundary condition where the

surface displacement has been eliminated. The model of Agnon et al. (1993) incorporated the fully dispersion relation and nonlinear evolution. Kaihatu and Kirby (1995) extended this model into two-dimensional propagation and applied parabolic approximation to make it more practical. Kaihatu and Kirby (1995) also included the dissipation mechanism in the surf zone. Tang and Ouelette (1997)[19] extended the model of Kaihatu and Kirby by including diffraction and bottom slope effects in the nonlinear terms of their model.

The model of Kaihatu and Kirby (1995) is applicable for periodic wave field because periodicity in time is assumed during the derivation of the model. When the Fourier series is substituted into the time dependent mild slope equation, the inherent assumption of a time-periodic signal is established. Hence, when we use the model of Kaihatu and Kirby (1995), the data should be transformed into frequency domain by Fast Fourier Transformation firstly. Fast Fourier Transformation is actually an optimized algorithm of discrete Fourier transformation. It is able to transform any time dependent signal into signal in frequency domain. It arouses the question that how the model performs if the signal of random wave interacting with transient long wave is input.

This thesis makes use of the model Kaihatu and Kirby (1995) to treat amplitude signals of soliton plus random wave. The performance of the model will evaluated in the comparison of spectra, root-mean-square of wave height, energy of waves in different scales of frequency, the skewness and the asymmetry. Both the energy and wave shape prediction will be included in the evaluation. Additionally, it can be investigated whether the nonlinear processes of random waves described in the physic model will be affected by transient long waves.

2. KAIHATU AND KIRBY (1995) NUMERICAL MODELING OF LONG WAVES

2.1 Introduction of Model

In this section, the numerical model used in this paper to describe the propagation of wave from deep to shallow water will be derived. The mild-slope equation is developed in the approach of Smith and Sprinks (1975). However, the equation is not readily applicable for an open coastal area because the equation is elliptic and the entire boundary conditions are required to do the numerical calculation. To make the parabolic approximation of the mild-slope equation, Kaihatu & Kirby (1995) made the assumption that the wave propagates primarily in the x-direction, so that wave-related variations can be considered as slow in the y-direction. The derivatives of amplitudes can be scaled to drop high-order terms in the equation. Additionally, in order to factor out any y-dependence from the phase function, the method of Lozano and Liu (1980) is used, where the wave-number function is defined as y-averaged reference phase function.

2.2 The Boundary Value Problem

We begin from the water wave boundary value problem for the velocity potential ϕ:

$$\bigtriangledown^2\phi = \bigtriangledown_h^2\phi + \phi_{zz} = 0; \qquad -h \le z \le \eta \tag{2.1}$$

$$\phi_z = -\bigtriangledown_h h \cdot \bigtriangledown_h\phi; \qquad z = -h \tag{2.2}$$

$$gz + \phi_t + \frac{1}{2}(\bigtriangledown_h\phi)^2 + \frac{1}{2}(\phi_z)^2 = 0; \qquad z = \eta \tag{2.3}$$

$$\eta_t - \phi_z + \bigtriangledown_h\eta \cdot \bigtriangledown_h\phi = 0; \qquad z = \eta \tag{2.4}$$

It is reasonable to assume that the depth varies slowly to such a degree that the local values of wave-related parameters can be used.

We want to achieve the solvable nonlinear boundary value problem, using ϵ as the nonlinearity parameter (where $\epsilon = ka$, where k is wave number and a is wave amplitude). Taylor series are used to expand the free surface boundary conditions about $z = 0$ and retain terms to $O(\epsilon^2)$:

$$\nabla_h^2\phi + \phi_{zz} = 0; \qquad -h \le z \le 0 \tag{2.5}$$

$$\phi_z = -\nabla_h h \cdot \nabla_h\phi; \qquad z = -h \tag{2.6}$$

$$g\eta + \phi_t + \frac{1}{2}(\nabla_h\phi)^2 + \frac{1}{2}(\phi_z)^2 + \eta\phi_{zt} = O(\epsilon^3); \qquad z = 0 \tag{2.7}$$

$$\eta_t - \phi_z + \nabla_h\eta \cdot \nabla_h\phi - \eta\phi_{zz} = O(\epsilon^3); \qquad z = 0 \tag{2.8}$$

Many methods have been developed to solve and simplify the boundary value problem. Separation of variables have been used in many methods. Bryant (1972) expanded the surface displacement $\eta(x,t)$ in the Fourier series and created the compatible Fourier series expansion of $\phi(x,y,t)$, which satisfied the governing equation and bottom boundary equation resulting in formulas for the Fourier amplitudes. Smith and Sprinks (1975)[12] used the Green's second Identity to derive the mild-slope equation. Their methods are different, but they both used the solutions from the linear theory achieved by separation of variables.

First, we assume a superposition of solutions:

$$\phi(x,y,z,t) = \sum_{n=1}^{N} f_n(k_n,h,z)\tilde{\phi}_n(k_n,\omega_n,x,y,t) \tag{2.9}$$

where ω_n is the angular frequency and k_n is the wave number of the n^{th} frequency component, and:

$$f_n = \frac{coshk_n(h+z)}{coshk_nh} \tag{2.10}$$

The frequency ω_n and the wave number k_n are related by the linear dispersion relation:

$$\omega_n^2 = gk_ntanhk_nh \tag{2.11}$$

Then we need to combine the dynamic free surface condition and kinematic free surface condition to eliminate the η. It is straightforward that we need to take derivative of (2.7) respect to t and take

horizontal divergence of (2.7), which results in:

$$\eta_t(g+\phi_{zt})+\eta\phi_{ztt}+(\phi_{tt}+\frac{1}{2}(\bigtriangledown_h\phi)_t^2+\frac{1}{2}(\phi_z)_t^2)=0 \tag{2.12}$$

$$\bigtriangledown_h\eta(g+\phi_{zt})+\eta\bigtriangledown_h\phi_{zt}+\bigtriangledown_h\phi_t=0 \tag{2.13}$$

Substituting (2.7), (2.12) and (2.13) into (2.8), we can get:

$$\phi_z=-\frac{1}{g}[\phi_{tt}+\frac{1}{2}(\bigtriangledown_h\phi)_t^2+\frac{1}{2}(\phi_z)_t^2-\frac{1}{2g}(\phi_t)_{zt}^2+\bigtriangledown_h\cdot(\phi_t\bigtriangledown_h\phi)]; \qquad z=0 \tag{2.14}$$

We use Green's second identity on the variables f_n and $\tilde{\phi}_n$ (Smith and Sprinks, 1975[12]):

$$\bigtriangledown_h\cdot\left(\int_{-h}^{0}f_n^2dz\bigtriangledown_h\tilde{\phi}_n\right)-\int_{-h}^{0}f_{nz}^2dz\tilde{\phi}_n=-f_n\tilde{\phi}_{nz}|_{z=0}+O(\epsilon,\alpha^2) \tag{2.15}$$

where α is a parameter characterizing the bottom slope. For our purpose it is assumed that

$$\alpha\leq O(\epsilon) \tag{2.16}$$

According to (2.10), we can also get that:

$$f_n(0)=1 \tag{2.17}$$

$$f_{nz}(0)=\frac{\omega_n^2}{g} \tag{2.18}$$

$$\int_{-h}^{0}f_n^2dz=\frac{(CC_g)_n}{g} \tag{2.19}$$

$$\int_{-h}^{0}(f_{nz})^2dz=\frac{\omega_n^2}{g}(1-\frac{C_{gn}}{C_n}) \tag{2.20}$$

where C_n is the wave celerity and C_{gn} is the group velocity of the n^{th} component. Substituting (2.9), (2.14), (2.17), (2.18), (2.19), (2.20) into (2.15), we can get a time-dependent mild-slope

equation with nonlinear coupling between modes:

$$\begin{aligned}
&\tilde{\phi}_{tt} - \bigtriangledown_h \cdot [(CC_g)_n \bigtriangledown_h \tilde{\phi}_n] + \omega_n^2(1 - \frac{C_{gn}}{C_n})\tilde{\phi}_n \\
=&\frac{1}{2}\left\{\sum_l \sum_m \left[\frac{\omega_l^2 + \omega_m^2}{g^2}(\tilde{\phi}_{l_t}\tilde{\phi}_{m_t})_t - \frac{\omega_l^2\omega_m^2}{g^2}(\tilde{\phi}_l\tilde{\phi}_m)_t\right]\right. \\
&\left. - \sum_l \sum_m \left[(\bigtriangledown_h\tilde{\phi}_l \cdot \bigtriangledown_h\tilde{\phi}_m)_t + \bigtriangledown_h \cdot (\tilde{\phi}_{l_t} \bigtriangledown_h \tilde{\phi}_m) + \bigtriangledown_h \cdot (\tilde{\phi}_{m_t} \bigtriangledown_h \tilde{\phi}_l)\right]\right\}
\end{aligned} \tag{2.21}$$

2.3 Wave Interaction and Resonance

In order to achieve the equations in frequency domain, it is convenient to make use of Fourier transformation to factoring out the time dependence. According to (2.21), there are nonlinear summations on the right side of the equation. It is obvious that wave interactions happen among different modes since some quadratic terms are introduced. Thus, it is necessary to have a discussion about the wave interaction and triad resonance in the nonlinear wave domain question.

The free surface boundary condition is expanded to $O(\epsilon^2)$. The combined boundary condition thus retains the terms of $O(\epsilon^2)$. Referring to Benney (1962), four wave interactions need to be considered if we retain the nonlinearity to $O(\epsilon^3)$.

The combined boundary equation reducing to the second order is:

$$\frac{\partial^2\phi}{\partial t^2} + g\frac{\partial\phi}{\partial z} = -\frac{1}{2}(\bigtriangledown_h\phi)_t^2 - \frac{1}{2}(\phi_z)_t^2 + \frac{1}{2g}(\phi_t)_{zt}^2 - \bigtriangledown_h \cdot (\phi_t \bigtriangledown_h \phi) \tag{2.22}$$

We will assume that the total solution to (2.22) is combined with linear part and nonlinear part. According to the linear theory, the linear part of a spatially and temporarily periodic solution is:

$$\phi_0 = \sum_n (a_n(\epsilon t)e^{i\psi_n} + a_n(\epsilon t)^\star e^{-i\psi_n}) \tag{2.23}$$

where the asterisk denotes the complex conjugate amplitude.The phase function ψ is:

$$\psi = (\vec{k} \cdot \vec{x} - \omega t) \tag{2.24}$$

where $\vec{k}$ is the wave number vector. We assume that ω and $\vec{k}$ satisfy the linear dispersion relation and amplitude a and $a^\star$ are slow variants in time. It is reasonable to assume that the total solution is:

$$\phi = \phi_0 + \phi_1 = \sum_n (a_n(\epsilon t)e^{i\psi_n} + a_n^\star(\epsilon t)e^{-i\psi_n}) + \epsilon\phi_1 \tag{2.25}$$

Substituting (2.25) into (2.22), it is obvious that on the left-hand side we have:

$$\frac{\partial^2\phi_0}{\partial t^2} + g\frac{\partial\phi_0}{\partial z} = 0 \tag{2.26}$$

So we can get:

$$\begin{aligned} &\frac{\partial^2\phi_1}{\partial t^2} + g\frac{\partial\phi_1}{\partial z} = \\ &A(\omega,\vec{k})\sum_m\sum_l (a_m(\epsilon t)e^{i\psi_m} + a_m(\epsilon t)^\star e^{-i\psi_m})\cdot(a_l(\epsilon t)e^{i\psi_l} + a_l(\epsilon t)^\star e^{-i\psi_l}) \end{aligned} \tag{2.27}$$

which is truncated to $O(\epsilon^2)$. $A(\omega,\vec{k})$ is an amplitude function which consists of the coefficients generated by the derivatives.

From (2.27), we can see that the quadratic terms in the combined boundary condition give rise to the products of exponential functions:

$$e^{i(\psi_l+\psi_m)} \tag{2.28}$$

$$e^{i(\psi_l-\psi_m)} \tag{2.29}$$

$$e^{i(-\psi_l+\psi_m)} \tag{2.30}$$

$$e^{i(-\psi_l-\psi_m)} \tag{2.31}$$

The homogeneous solution to (2.27) is:

$$\phi_1 \sim e^{i\psi_n} + c.c. \tag{2.32}$$

So the product terms will oscillate at ψ_n if any of the following conditions are satisfied:

$$\psi_n = \psi_m + \psi_l \tag{2.33}$$

$$\psi_n = \psi_m - \psi_l \tag{2.34}$$

$$\psi_n = -\psi_m + \psi_l \tag{2.35}$$

$$\psi_n = -\psi_m - \psi_l \tag{2.36}$$

implying:

$$\vec{k}_n = \vec{k}_m + \vec{k}_l \tag{2.37}$$

$$\vec{k}_n = \vec{k}_m - \vec{k}_l \tag{2.38}$$

$$\vec{k}_n = -\vec{k}_m + \vec{k}_l \tag{2.39}$$

$$\vec{k}_n = -\vec{k}_m - \vec{k}_l \tag{2.40}$$

and

$$\omega_n = \omega_m + \omega_l \tag{2.41}$$

$$\omega_n = \omega_m - \omega_l \tag{2.42}$$

$$\omega_n = -\omega_m + \omega_l \tag{2.43}$$

$$\omega_n = -\omega_m - \omega_l \tag{2.44}$$

The interaction includes resonance and bounding wave. According to the definition, the bounding waves are primary harmonics and higher harmonics that never increase energy and stay small. They violate the slowly varying assumption as well. The resonance is dominant mechanism for energy exchange among the wave components resonant. Therefore, the other terms are omitted except the triad resonant terms. The time dependence can be completely factored out when (2.41), (2.42), (2.43) and (2.44) are satisfied , and only resonant interactions are retained. In this way, the

time dependence is factored out and the model is transferred into frequency domain.

2.4 Time-Harmonic Wave Propagation in Two Dimensions & Parabolic Approximation

We intend to achieve the time-harmonic wave propagation model in two dimension from (2.21). Hence, we can factor out the time dependence by using Fourier transformation. We can assume that:

$$\tilde{\phi}_n(x,y,t) = \frac{\hat{\phi}_n}{2} e^{-i\omega_n t} + \frac{\hat{\phi}_n^\star}{2} e^{i\omega_n t} \tag{2.45}$$

Substituting (2.45) into (2.21) and making use of the resonance condition discussed in the previous section, we can get a time-harmonic wave equation:

$$\begin{aligned}
&\bigtriangledown_h \cdot [(CC_g)_n \bigtriangledown_h \hat{\phi}_n] + k_n^2 (CC_g)_n \hat{\phi}_n = -\frac{i}{4}\left[\sum_{l=1}^{n-1} 2\omega_n \bigtriangledown_h \hat{\phi}_l \cdot \bigtriangledown_h \hat{\phi}_{n-l}\right. \\
&\left. + \omega_l \hat{\phi}_l \bigtriangledown_h^2 \hat{\phi}_{n-l} + \omega_{n-l} \hat{\phi}_{n-l} \bigtriangledown_h^2 \hat{\phi}_l + \frac{\omega_l \omega_{n-l} \omega_n}{g^2} (\omega_l^2 + \omega_l \omega_{n-l} + \omega_{n-l}^2) \hat{\phi}_l \hat{\phi}_{n-l}\right] \\
&-\frac{i}{2}\left[\sum_{l=1}^{N-n} 2\omega_n \bigtriangledown_h \hat{\phi}_l^\star \cdot \bigtriangledown_h \hat{\phi}_{n+l} + \omega_{n+l} \hat{\phi}_{n+l} \bigtriangledown_h^2 \hat{\phi}_l^\star - \omega_l \hat{\phi}_l^\star \bigtriangledown_h^2 \hat{\phi}_{n+l}\right. \\
&\left. - \frac{\omega_l \omega_{n+l} \omega_n}{g^2} (\omega_l^2 - \omega_l \omega_{n+l} + \omega_{n+l}^2) \hat{\phi}_l^\star \hat{\phi}_{n+l}\right]
\end{aligned} \tag{2.46}$$

We take one of the nonlinear terms as the example of the derivation. In (2.21), we have a nonlinear term:

$$-\frac{1}{2} \sum_l \sum_m \frac{\omega_l^2 \omega_m^2}{g^2} (\tilde{\phi}_l \tilde{\phi}_m)_t \tag{2.47}$$

Applying the wave resonant interaction condition, it is reasonable to assume a basic frequency and wave number that satisfy the following relation:

$$\omega_n = n \cdot \omega \tag{2.48}$$

$$k_n = n \cdot k \tag{2.49}$$

Substituting (2.45) into (2.47), we can get:

$$
\begin{aligned}
-\frac{i\omega}{2}\sum_{l}\sum_{m}\frac{\omega_l^2\omega_m^2}{g^2}\Bigg[&\frac{\hat{\phi}_l\hat{\phi}_m}{4}(-l-m)e^{-i\omega(l+m)t}\\
&+\frac{\hat{\phi}_l^\star\hat{\phi}_m}{4}(l-m)e^{-i\omega(m-l)t}\\
&+\frac{\hat{\phi}_l\hat{\phi}_m^\star}{4}(m-l)e^{-i\omega(l-m)t}\\
&+\frac{\hat{\phi}_l^\star\hat{\phi}_m^\star}{4}(m+l)e^{i\omega(m+l)t}\Bigg]
\end{aligned}
\tag{2.50}
$$

We retain the terms oscillating at $e^{in\omega t}$, so we can apply the resonance conditions:

$$n-l-m=0 \qquad m=n-l \tag{2.51}$$

$$n-m+l=0 \qquad m=n+l \tag{2.52}$$

$$n-l+m=0 \qquad m=l-n \tag{2.53}$$

$$n+m+l=0 \qquad m=-n-l \tag{2.54}$$

Then we can get:

$$-\frac{i}{2}\sum_{l}\left[\frac{\omega_l^2\omega_{n-l}^2\omega_n}{g^2}\frac{\hat{\phi}_l\hat{\phi}_{n-l}}{4}+\frac{\omega_l^2\omega_{n+l}^2\omega_n}{g^2}\frac{\hat{\phi}_l^\star\hat{\phi}_{n+l}}{4}+\frac{\omega_l^2\omega_{l-n}^2\omega_n}{g^2}\frac{\hat{\phi}_l\hat{\phi}_{l-n}^\star}{4}\right] \tag{2.55}$$

The conjugate term can be omitted as it does not contribute. Then we fix the limits of the summation operator.

First term: $n-l\geq 1$ or $l\leq n-1$

Second term: $n+l\geq 1$ or $l\geq 1-n$

Third term: $1\leq l-n\leq N$ or $1\leq l\leq N-n$

Therefore, we can get:

$$-\frac{i}{2}\left[\sum_{l=1}^{n-1}\frac{\omega_l^2\omega_{n-l}^2\omega_n}{g^2}\cdot\frac{\hat{\phi}_l\hat{\phi}_{n-l}}{4}+\sum_{l=1}^{N-n}\frac{\omega_l^2\omega_{n+l}^2\omega_n}{g^2}\frac{\hat{\phi}_l^\star\hat{\phi}_{n+l}}{4}+\sum_{l=n+1}^{N}\frac{\omega_l^2\omega_{l-n}^2\omega_n}{g^2}\frac{\hat{\phi}_l\hat{\phi}_{l-n}^\star}{4}\right] \tag{2.56}$$

The equation (2.46) is an elliptic equation. It is not practical to do numerical calculation based on elliptic equation as all of the boundary conditions are required, since $\hat{\phi}_n$ is a function of x and y, some spatial assumptions are needed to do further simplification of the equation. We assume that:

$$\begin{aligned}\hat{\phi}_n(x,y) &= -\frac{ig}{\omega_n}A_n(x,y)e^{i\int k_n(x,y)dx} \\ \hat{\phi}_n^{\star}(x,y) &= -\frac{ig}{\omega_n}A_n^{\star}(x,y)e^{-i\int k_n(x,y)dx}\end{aligned} \tag{2.57}$$

where the complex amplitude A_n is assumed to vary slowly in the spatial coordinates. The wave is assumed to propagated primarily in the x-direction, so we only include integral of the wave number with respect to x in the complex exponential function. Substituting (2.57) into (2.46) gives:

$$\begin{aligned}&[(CC_g)_n A_{nx}]_x + 2i(kCC_g)_n A_{nx} + i(kCC_g)_{nx}A_n \\ &+ \left[(CC_g)_n (A_n e^{i\int k_n(x,y)dx})_y\right]_y e^{-i\int k_n(x,y)dx} \\ =&\frac{1}{4}\sum_{l=1}^{n-1} RA_l A_{n-l}e^{i\int(k_l+k_{n-l}-k_n)dx} + \frac{1}{2}\sum_{l-1}^{N-n} SA_l^{\star}A_{n+l}e^{i\int(k_{n+l}-k_l-k_n)dx}\end{aligned} \tag{2.58}$$

where

$$R = \frac{g}{\omega_l\omega_{n-l}}[\omega_n^2 k_l k_{n-l} + (k_l + k_{n-l})(\omega_{n-l}k_l + \omega_l k_{n-l})\omega_n] - \frac{\omega_n^2}{g}(\omega_l^2 + \omega_l\omega_{n-l} + \omega_{n-l}^2) \tag{2.59}$$

$$S = \frac{g}{\omega_l\omega_{n+l}}[\omega_n^2 k_l k_{n+l} + (k_{n+l} - k_l)(\omega_{n+l}k_l + \omega_l k_{n+l})\omega_n] - \frac{\omega_n^2}{g}(\omega_l^2 - \omega_l\omega_{n+l} + \omega_{n+l}^2) \tag{2.60}$$

In order to make parabolic approximation of (2.58), we need to get rid of the second-order derivative term with respect to x or y. Yue and Mei (1980) introduced the parabolic approximation by assuming the wave propagating in the x direction and making use of the Laplace equation to scaling the derivatives of amplitude function with respect to x and y. Here, we use the scaling approach

of Yue and Mei (1980)[20] to order the derivatives of A_n:

$$\frac{\partial A_n}{\partial x} = O(\epsilon^2) \tag{2.61}$$

$$\frac{\partial A_n}{\partial y} = O(\epsilon) \tag{2.62}$$

Hence, the first term in (2.58) can be dropped. Since we only retained integral of the wave number with respect to x in the exponential function, the derivative of A_n about x is assumed to be smaller than that about y for balance. Then we need to factor out the dependence of y from the phase function, since the integral is only taken in the x direction. We make use of the method of Lozano and Liu (1980)[14], where they define a y-averaged wave number $\bar{k}_{n0}(x)$ as a reference phase function. Thus, we rewrite (2.57) as:

$$\begin{aligned} \hat{\phi}_n(x,y) &= -\frac{ig}{\omega_n} a_n(x,y) e^{i\int \bar{k}_{n0}(x)dx} \\ \hat{\phi}^\star_n(x,y) &= -\frac{ig}{\omega_n} a^\star_n(x,y) e^{-i\int \bar{k}_{n0}(x)dx} \end{aligned} \tag{2.63}$$

which gives:

$$\begin{aligned} A_n(x,y) &= a_n(x,y) e^{i(\int \bar{k}(x)_{n0}dx - \int k_n(x,y)dx)} \\ A^\star_n(x,y) &= a^\star_n(x,y) e^{-i(\int \bar{k}(x)_{n0}dx - \int k_n(x,y)dx)} \end{aligned} \tag{2.64}$$

Substituting this into (2.58), we can get:

$$\begin{aligned} &2i(kCC_g)_n a_{nx} - 2(kCC_g)_n(\bar{k}_{n0} - k_n)a_n + i(kCC_g)_{nx} a_n + [(CC_g)_n (a_n)_y]_y \\ =&\frac{1}{4}\left(\sum_{l=1}^{n-1} R a_l a_{n-l} e^{i\int (k_{l0} + k_{(n-l)0} - k_{n0})dx} + 2\sum_{l-1}^{N-n} S a^\star_l a_{n+l} e^{i\int (k_{(n+l)0} - k_{l0} - k_{n0})dx} \right) \end{aligned} \tag{2.65}$$

This is the parabolic model of the nonlinear mild-slope equation in Kaihatu (1995). The one-

dimensional version is:

$$A_{nx} + \frac{(kCC_g)_{nx}}{2(kCC_g)_n} A_n = \\ -\frac{i}{8(kCC_g)_n} \left(\sum_{l=1}^{n-1} RA_l A_{n-l} e^{\int (k_l + k_{n-l} - k_n) dx} + 2 \sum_{l=1}^{N-n} SA_l^{\star} A_{n+l} e^{i \int (k_{n+l} - k_l - k_n) dx} \right) \tag{2.66}$$

which is used in my applications.

One drawback of this model is that it can be only applied for small angles of incidence. Kaihatu (2001)[21] added a second-order correction to a free-surface boundary condition used to derive the model formula. Wide-angle propagation terms are also included in the model. It will not be discussed in detail in this thesis , since it focuses on the effects of the transient wave on the wave simulation and the waves in the experiment propagate in one direction.

2.5 Dissipation Mechanism

When waves approach the shoreline, the amplitudes of the waves continue to increase along with the decrease of the water depth. In contrast to a monochromatic wave, the random waves do not have a specific breakpoint. Once the waves start to break, the turbulence dissipation is the dominant dissipation mechanism. There are two dissipation models commonly used for random waves, Battjes and Janssen (1978) and Thornton and Guza (1983). [5]

Battjes and Janssen (1978)[22] started from the wave energy balance:

$$\frac{\partial P_x}{\partial x} + D = 0 \tag{2.67}$$

in which P_x is the x-component of the time-mean energy flux per unit length, x is the horizontal direction normal to the shoreline. D is the time mean dissipation per unit area. Then they assumed self-similarity in the surf zone, such that:

$$H(x) = \gamma h(x) \tag{2.68}$$

where $H(x)$ is the wave amplitude varying in x direction and $h(x)$ is the water depth function about x. γ is a coefficient of $O(1)$. Then they wrote the assumption stated above in terms of the probability distribution of the wave heights, which is assumed to be of the Rayleigh-type. The probability that at a given point a height is associated with a breaking wave, Q_b, is expressed with H_{rms} and H_m:

$$\frac{1-Q_b}{lnQ_b} = -\left(\frac{H_{rms}}{H_m}\right)^2 \tag{2.69}$$

where H_{rms} is the root mean square of the wave field and H_m is a maximum possible wave height for each depth h.

In order to specify the quantitative estimation of H_m, Battjes and Janssen (1978) chose Miche's criterionfor the maximum height of periodic waves of constant form and modified it for some freedom of adjustment:

$$H_m = 0.88k^{-1}tanh(\gamma kh/0.88) \tag{2.70}$$

Battjes and Janssen (1978) estimated the energy dissipation rate in a broken wave from that in a bore of corresponding height. They use order-of-magnitude estimates according to Lamb (1932) to achieve the expression for energy dissipation:

$$D = \frac{\alpha}{4}Q_b\bar{f}\rho g H_m^2 \tag{2.71}$$

where $\bar{f}$ is the mean frequency of the wave field.

The energy flux P was estimated by linear approximation:

$$P_x = Ec_g \tag{2.72}$$

$$E = \frac{1}{8}\rho g H_{rms}^2 \tag{2.73}$$

$$c_g = \left[\frac{2\pi f}{k}\left(\frac{1}{2} + \frac{kh}{sinh2kh}\right)\right]_{f=\bar{f}} \tag{2.74}$$

Hence, H_{rms} can be solved by this closed system.

The drawback of the Battjes and Janssen model is that the probability that a wave amplitude is associated with a breaking wave at a given point is estimated by a wave height distribution with a sharp cut-off. The prediction of the model about H_{rms} agrees with the observation generally. However, there is considerable inflexibility with such a sharp cut-off.

Thornton and Guza (1983)[23] extended the model of Battjes and Janssen (1978) by accounting for the transformation of the wave height probability distribution through the surf zone. They did some comparison between Rayleigh distribution and field data of wave height to show that wave height distribution can be described well by Rayleigh distribution even in the surf zone. They used a weighted Rayleigh distribution to include the transformation of the wave height distribution during the surfing zone, which enable some of the waves to break later after they pass the criteria for wave breaking. The big difference between Battjes and Janssen (1978) and Thornton and Guza (1983) is that the former used a sharp cut-off of the Rayleigh distribution to model the wave breaking but Thornton and Guza (1983) did not. Mase and Kirby (1992) included the dissipation mechanism in their shoaling model and made the comparison with a laboratory experiment. We also take the formulas developed in Mase and Kirby (1992).

$$\begin{aligned} &A_{nx} + \frac{(kCC_g)_{nx}}{2(kCC_g)_n} A_n + \alpha_n A_n = \\ &-\frac{i}{8(kCC_g)_n} \left(\sum_{l=1}^{n-1} R A_l A_{n-l} e^{\int (k_l + k_{n-l} - k_n) dx} \right. \\ &\left. +2 \sum_{l=1}^{N-n} S A_l^{\star} A_{n+l} e^{i \int (k_{n+l} - k_l - k_n) dx} \right) \end{aligned} \tag{2.75}$$

where:

$$\alpha_n = \alpha_{n0} + \left(\frac{f_n}{f_{peak}}\right)^2 \alpha_{n1} \tag{2.76}$$

$$\alpha_{n0} = F\beta(x) \tag{2.77}$$

$$\alpha_{n1} = (\beta(x) - \alpha_{n0}) \frac{f_{peak}^2 \sum_{n=1}^{N} |A_n|^2}{\sum_{n=1}^{N} f_n^2 |A_n|^2} \tag{2.78}$$

$$\beta(x) = \frac{3\sqrt{\pi}}{4\sqrt{gh}} \frac{B^3 f_{peak} H_{rms}^5}{\gamma^4 h^5} \tag{2.79}$$

$$H_{rms} = 2\sqrt{\sum_{n=1}^{N} |A_n|^2} \tag{2.80}$$

and where f_{peak} is the peak frequency of the spectrum. The free parameters B, F and γ should be tuned to achieve the best simulation. For the data of the experiment of Mase and Kirby (1992), their values are 1.0, 0.5 and 0.6 respectively.

2.6 Numerical Method

In this section, we discuss the numerical method used to solve (2.66), the Runge-Kutta method. The Runge-Kutta method achieves the accuracy of a Taylor series approach without requiring the calculation of higher derivatives. The equation (2.66) can be written in the following form:[24]

$$\frac{dy}{dx} = f(x, y) \tag{2.81}$$

Transforming (2.81) into numerical form, we can get:

$$y_{i+1} = y_i + \phi h \tag{2.82}$$

where the slope ϕ is called an increment function, which can be treated as the slope over the interval of function y. The increment function can be written in general form as

$$\phi = a_1 k_1 + a_2 k_2 \cdots + a_n k_n \tag{2.83}$$

where the a_n are constants and k_n are:

$$k_1 = f(x_i, y_i) \tag{2.84}$$

$$k_2 = f(x_i + p_1 h, y_i + q_{11} k_1 h) \tag{2.85}$$

$$k_3 = f(x_i + p_2 h, y_i + q_{21} k_1 h + q_{22} k_2 h) \tag{2.86}$$

$\vdots$

$$k_n = f(x_i + p_{n-1} h, y_i + q_{n-1,1} k_1 h + q_{n-1,2} k_2 h + \cdots + q_{n-1,n-1} k_{n-1} h) \tag{2.87}$$

where p and q are constants. The most popular Runge-Kutta method is classical fourth-order Runge-Kutta method:

$$y_{i+1} = y_i + \frac{1}{6}(k_1 + 2k_2 + 2k_3 + k_4)h \tag{2.88}$$

where

$$k_1 = f(x_i, y_i) \tag{2.89}$$

$$k_2 = f\left(x_i + \frac{1}{2}h, y_i + \frac{1}{2}k_1 h\right) \tag{2.90}$$

$$k_3 = f\left(x_i + \frac{1}{2}h, y_i + \frac{1}{2}k_2 h\right) \tag{2.91}$$

$$k_4 = f(x_i + h, y_i + k_3 h) \tag{2.92}$$

According to the above discussion, the equation (2.66) can be written in the form of (2.81)

$$\begin{aligned} A_{nx} &= -\frac{(kCC_g)_{nx}}{2(kCC_g)_n} A_n \\ &- \frac{i}{8(kCC_g)_n} \left(\sum_{l=1}^{n-1} R A_l A_{n-l} e^{\int (k_l + k_{n-l} - k_n) dx} + 2 \sum_{l=1}^{N-n} S A_l^{\star} A_{n+l} e^{i \int (k_{n+l} - k_l - k_n) dx} \right) \end{aligned} \tag{2.93}$$

The process of application of Runge-Kutta method is showed below:

$$k_1 = A_{nx,i} \tag{2.94}$$

$$A^{\star} = A_{n,i} + \frac{1}{2}k_1 dx \tag{2.95}$$

$$k_2 = f(x + \frac{1}{2}dx, A^{\star}) \tag{2.96}$$

$$A^{\star\star} = A_{n,i} + \frac{1}{2}k_2 dx \tag{2.97}$$

$$k_3 = f(x + \frac{1}{2}dx, A^{\star\star}) \tag{2.98}$$

$$A^{\star\star\star} = A_{n,i} + k_3 dx \tag{2.99}$$

$$k_4 = f(x + dx, A^{\star\star\star}) \tag{2.100}$$

$$A_{i+1} = A_i + \frac{1}{6}(k_1 + 2k_2 + 2k_3 + k_4)dx \tag{2.101}$$

where $A^{\star}$, $A^{\star\star}$ and $A^{\star\star\star}$ denote the middle term during calculation and f denotes the numerical calculation of derivative of A about x.

2.7 Application in Mase and Kirby (1992)

As mentioned before, this thesis makes use of the nonlinear mild-slope parabolic model of Kaihatu & Kirby (1992). The model was originally coded in Fortran fixed format. This thesis transfers the model into MATLAB version. In order to verify the applicability and validity of the MATLAB version, the Case 2 data of Mase and Kirby (1992)[25] is utilized.

Mase and Kirby Case 2 made use of the Pierson-Moskowitz spectrum with $f_p = 1.0Hz$ (f_p is the peak frequency) to simulate random waves. Figure 2.1 shows a sketch of the experimental setup. Water surface elevations were measured by wave gauges at water depths of 47 cm, 35 cm, 30 cm, 25 cm, 20 cm, 17.5 cm, 15 cm, 12.5 cm, 10 cm, 7.5 cm, 5.0 cm, and 2.5 cm over a $\frac{1}{20}$ plan beach. The sampling rate is $\triangle t = 0.05sec$, recording a total of 15000 points. In order to compare with the result of Kaihatu (1994)[26], the same data processing method is applied. The Case 2 data is divided into 7 realizations of 2048 points each. First, a Fast Fourier Transformation (FFT) is applied to each realization. The reason to choose 2048 (2^{11}) is to satisfy the requirement of FFT.

Hence, the spectrum for each realization is obtained. The very high frequencies are not covered by nonlinear triad interactions, so only the lower 256 frequency components would be modeled, yielding a frequency range from $0.0098Hz \leq f \leq 2.5088Hz$.

The comparisons are shown in Figures 2.2 through 2.7. The model performs well generally and reflects that shown in Kaihatu (1994) and Kaihatu and Kirby (1995). In the range from the half of the peak frequency to the peak frequency, the model simulates the wave field accurately. Though the trends are predicted well, at frequencies higher than peak frequency, the model over-predicts the energy of this part. The deviation from the data could be caused by the under-prediction of the dissipation with the dissipation mechanism of Thornton and Guza (1983). The breaking model of Thornton and Guza (1983) simulates the root mean square of the wave height after wave breaking and does not investigate the wave breaking process in the time domain or in the frequency domain. Kaihatu and Kirby (1995) and Kaihatu (2001) took the dissipation terms in Thornton and Guza (1983) and weighted the terms to f^2. The results give an accurate reproduction of third-moment wave shape statistics taken from data.

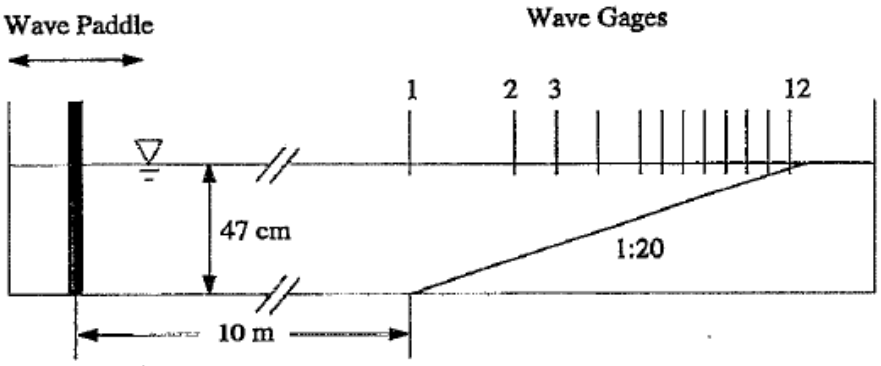

Figure 2.1: Experimental setup of Mase and Kirby (Taken from Kaihatu and Kirby, 1995)[25]

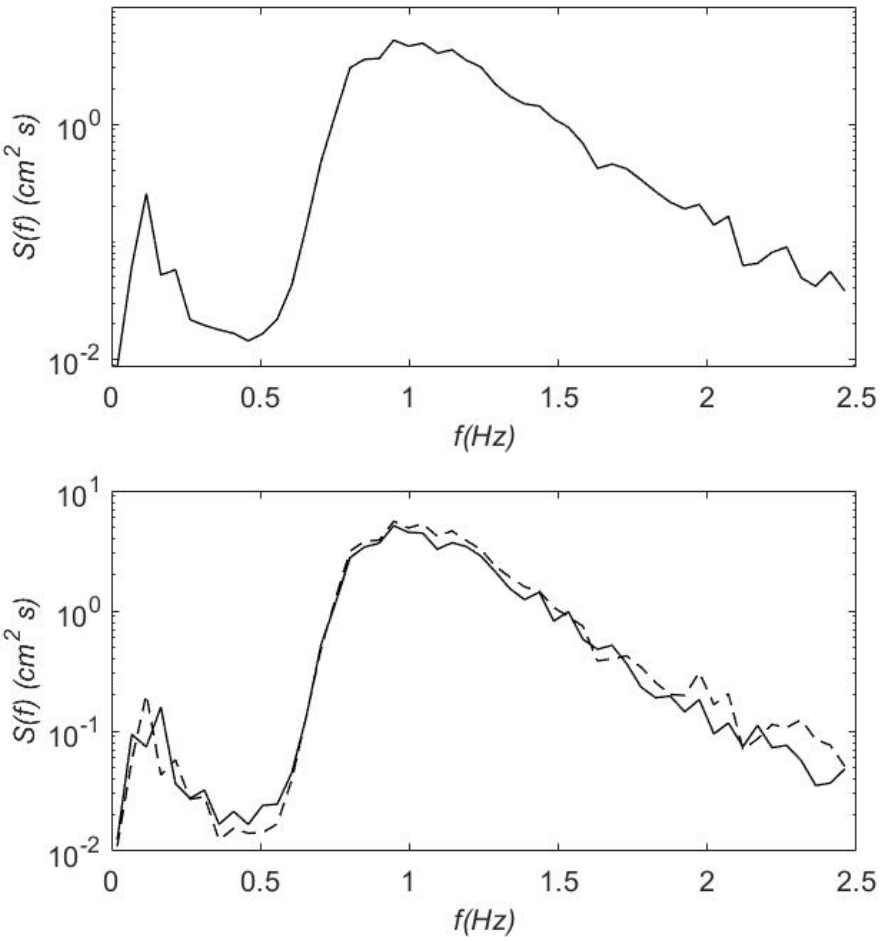

Figure 2.2: Comparison of Model Results and Experiment Data Based on Case 2 of Mase and Kirby (1992). Experiment Data (-), Model of Kaihatu & Kirby (- -). (Top) Input Spectra at d=47 cm; (Bottom) d=35 cm.

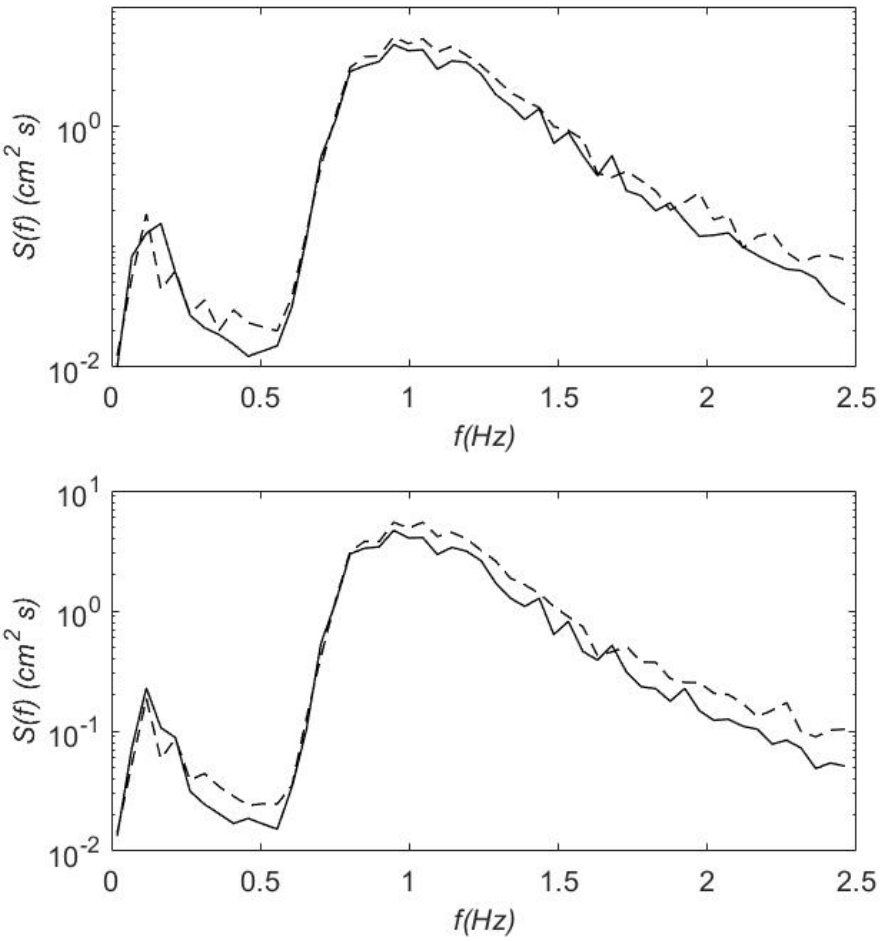

Figure 2.3: Comparison of Model Results and Experiment Data Based on Case 2 of Mase and Kirby (1992). Experiment Data (-), Model of Kaihatu & Kirby (- -). (Top) Spectra at d=30 cm; (Bottom) d=25 cm.

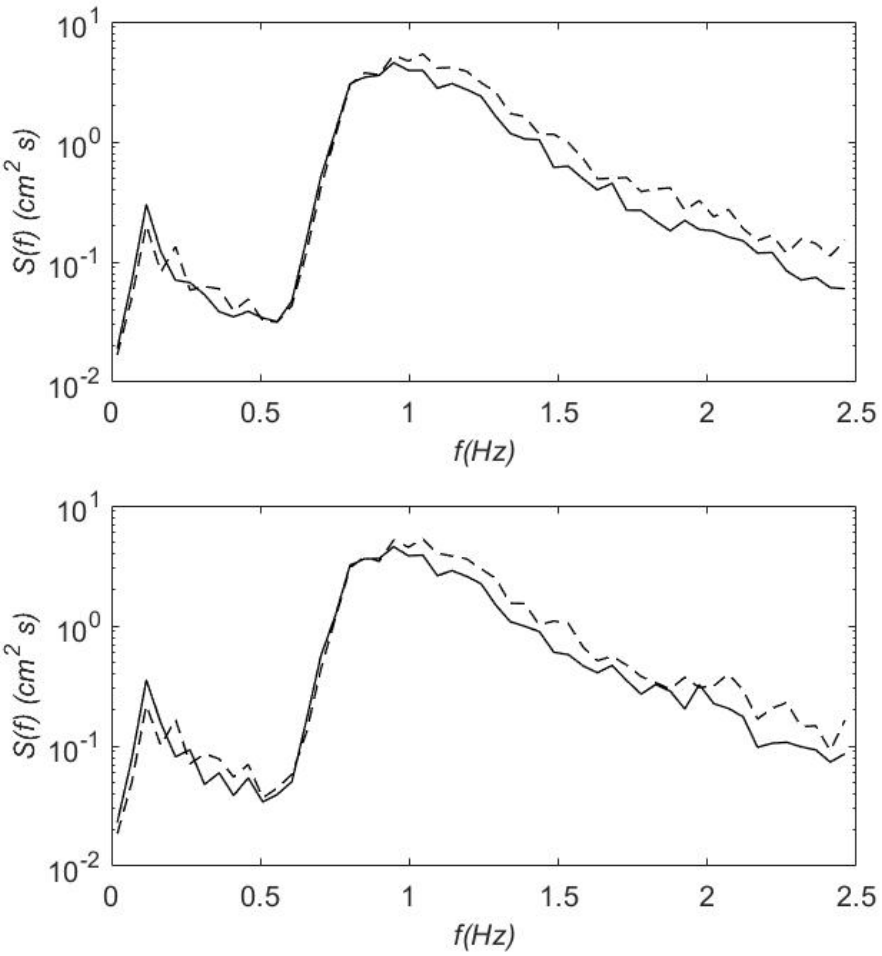

Figure 2.4: Comparison of Model Results and Experiment Data Based on Case 2 of Mase and Kirby (1992). Experiment Data (-), Model of Kaihatu & Kirby (- -). (Top) Spectra at d=20 cm; (Bottom) d=17.5 cm.

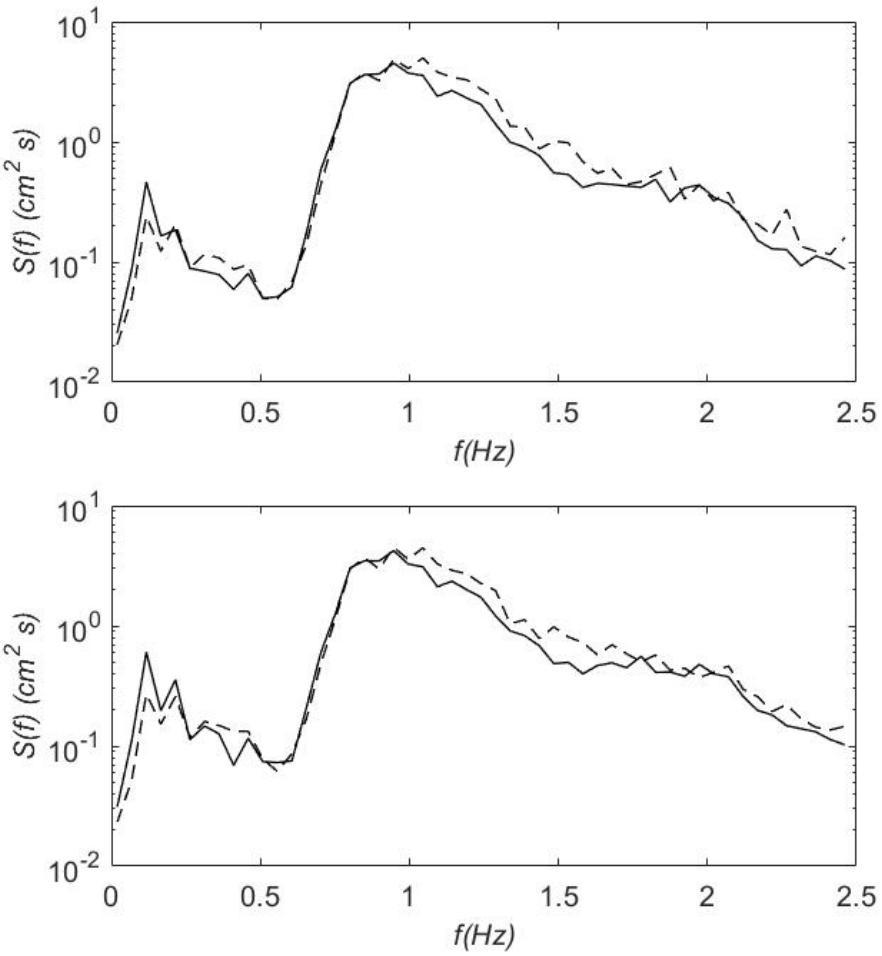

Figure 2.5: Comparison of Model Results and Experiment Data Based on Case 2 of Mase and Kirby (1992). Experiment Data (-), Model of Kaihatu & Kirby (- -). (Top) Spectra at d=15 cm; (Bottom) d=12.5 cm.

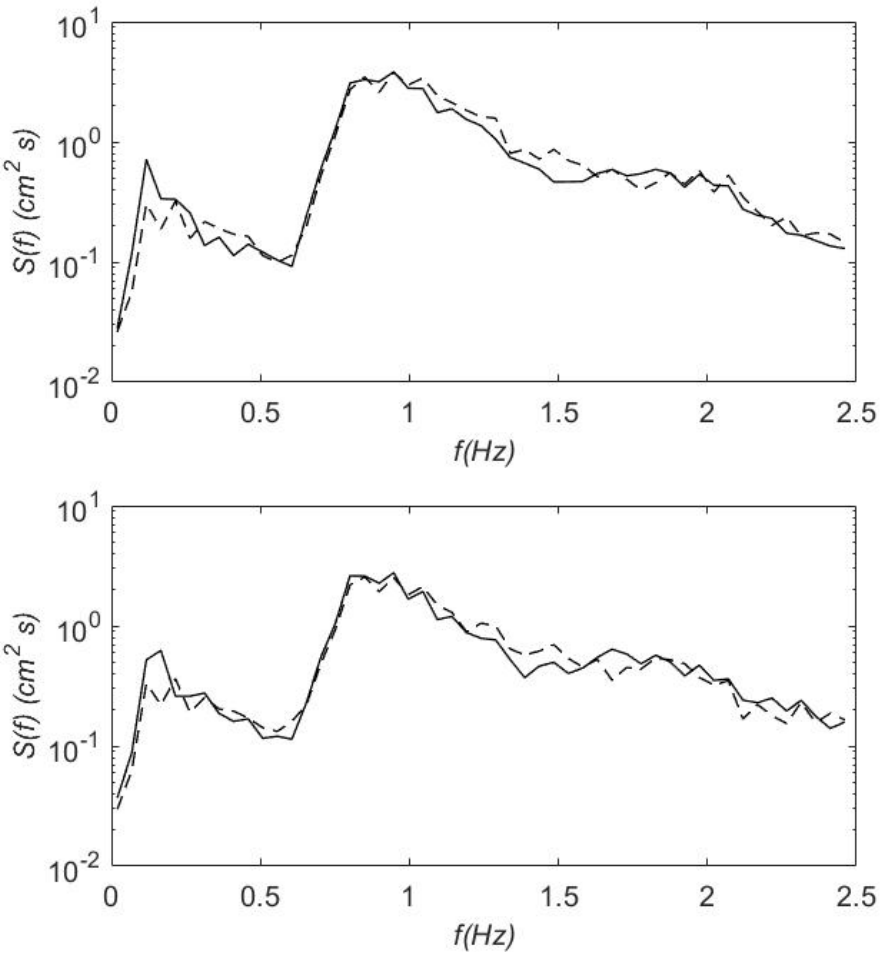

Figure 2.6: Comparison of Model Results and Experiment Data Based on Case 2 of Mase and Kirby (1992). Experiment Data (-), Model of Kaihatu & Kirby (- -). (Top) Spectra at d=10 cm; (Bottom) d=7.5 cm.

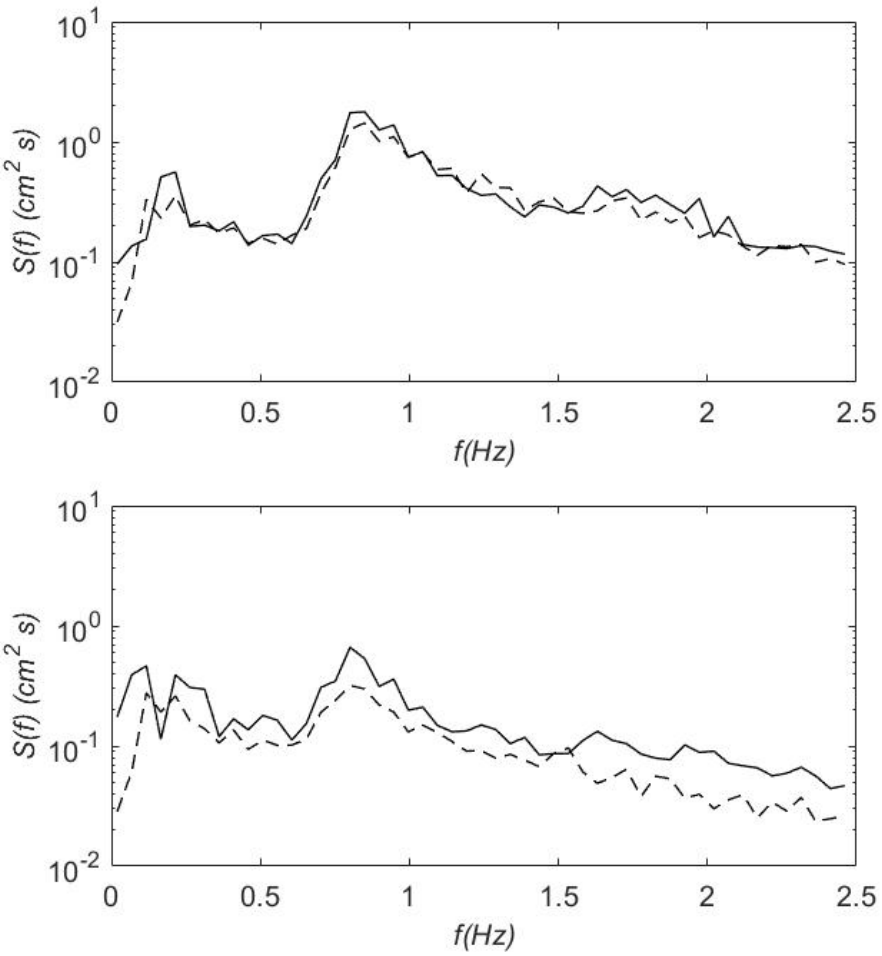

Figure 2.7: Comparison of Model Results and Experiment Data Based on Case 2 of Mase and Kirby (1992). Experiment Data (-), Model of Kaihatu & Kirby (- -). (Top) Spectra at d=5 cm; (Bottom) d=2.5 cm.

3. APPLICATION FOR DATA FROM NEES TSUNAMI AND SWELL EXPERIMENT AT OREGON STATE UNIVERSITY

3.1 Introduction of Experiment

Experiments on combining Tsunami and swell were conducted at Oregon State University. The data from three of these experiments will be used to evaluate the performance of model and investigate the effect of soliton. In the experiments, the wave heights were measured and recorded at the sampling interval of 0.02 s by instruments at 18 gauge points, which were set at different water depths.

In the first experiment, three cases of measurement of the wave heights, purely random wave field, purely soliton and solitary wave plus random waves (Case 1, Case 2 and Case 3), will be treated by the model of Kaihatu and Kirby (1995) respectively. In the case for purely random wave (Case 1), the peak frequency is 0.125 Hz and the wave height of random wave is 1 m. In the case for purely soliton (Case 2), the wave height is 0.85 m. In the case for soliton plus random wave (Case 2), the peak frequency (f_p) is 0.125 Hz, the wave height of the random wave is 1 m and the wave height of the soliton is 0.85 m. For the purely random wave, one trial was taken and lasted 21 minutes. For the soliton, one trial was taken and took 39 seconds. For the soliton plus random wave case, seven trials were taken and each one lasted 5 minutes.

In the second and third experiment, the laboratory setup is the same as the previous experiment except that the wave height of the soliton is 0.5m and 0.7 m respectively. Figure (3.1) shows a sketch of the experiment bathymetry. Water surface elevation is measured at different water depths. The depth profile and gauge locations are given by the tables:

Gauge Point Location					
Gauge 1	0 m	Gauge 7	21.94 m	Gauge 13	34.76 m
Gauge 2	3.65 m	Gauge 8	25.70 m	Gauge 14	36.57 m
Gauge 3	7.32 m	Gauge 9	27.41 m	Gauge 15	38.40 m
Gauge 4	10.96 m	Gauge 10	29.34 m	Gauge 16	40.35 m
Gauge 5	14.62 m	Gauge 11	31.08 m	Gauge 17	41.98 m
Gauge 6	18.28 m	Gauge 12	33.00 m	Gauge 18	43.99 m

Table 3.1: The Gauge Points' Location In the Experiment

Water Depth Profile		
Distance From x=0	Depth (from-to)	Slope
0 to 10.97 m	2 m	0
10.97 to 14.62 m	2 to 1.69 m	1:12
14.62 to 43.99 m	1.69 to 0.001 m	1:24

Table 3.2: The Water Depth Profile In the Experiment

For purely random wave case, the data of wave amplitude at each wave gauge will be split into 15 realizations of 4096 points . First, they will be treated by Fast Fourier transformation. For each trial of soliton plus random wave field, the data of wave height at each gauge point will be split into 4 realization of 4096 points. They will be also transformed into amplitudes in frequency domain. The average of realizations is achieved to stabilize the spectrum estimation. Additionally, the band average is used to smooth the plots. Three neighbor points are averaged to represent the center of this scale.

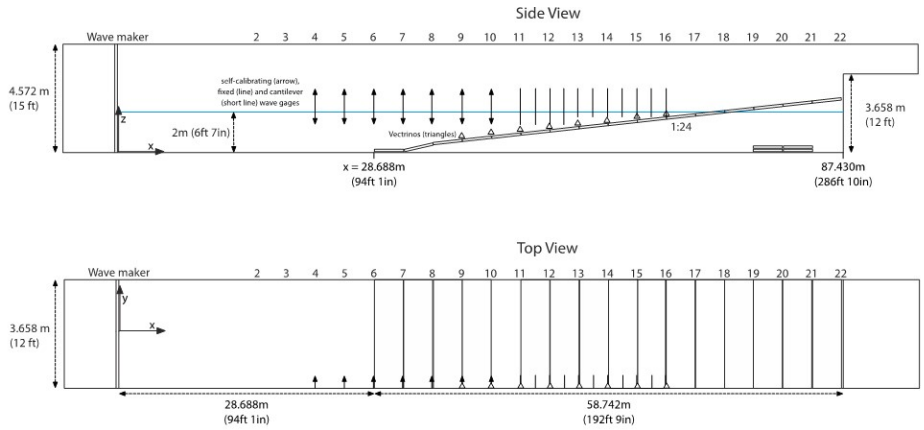

Figure 3.1: The Experiment Bathymetry and Gauge Points' setup for NEES Tsunami and Swell Experiment at Oregon State University[27]

The data is treated in the same method which is used for Mase and Kirby (1992) experiment. Fast Fourier Transformation is applied to each realization. The lower 128 frequency components are modeled, yielding a frequency range from $0.0122Hz \leq f \leq 1.5503Hz$, which contains about 80% of the wave energy. It is reasonable to truncate the spectrum for the lower 128 frequency components since the peak frequency is 0.125 Hz and the energy at the higher frequency is small. In addition, the wavemaker is not designed to generate waves with a frequency higher than $1Hz$. The spectra have been treated with band average, where band width is three, to smooth the plots.

3.2 Experiment 1: Set The Wave Height of Soliton 0.85 m

In this section, the comparisons between spectra for data obtained in the Experiment 1 and the prediction of fully-dispersive nonlinear mild-slope model are shown. There are a total of nine trials in Experiment 1. Trial 1 is the measurement of pure random wave. Trial 2 is the measurement of pure soliton. The rest of the trials are the measurement of soliton plus random wave.

The experiment keeps the position of the soliton in the random wave train unchanged. Hence, the experiment is an ergodic process. The statistic properties of the seven trials of soliton plus random wave should be similar. For this reason, the data and model results of Trial 6 are chose as a representation for ensemble in this section without loss of generality. Experiment 2 and Experiment

3 are treated in similar way.

The comparisons between model results and data of Trial 1 are shown from Figure 3.2 to Figure 3.10. The model results show good consistency with the data, especially in the infragravity wave and swell wave area. The model predicts the peak frequency energy well and the error ratio is not larger than 5% until the wave approach the No.11 gauge point($d = 1.01m$). The deviation at the peak frequency does not grow until $d = 1.01\ m$. The frequency scale is divided into three areas, infragravity area ($0 \leq f \leq \frac{f_{peak}}{2}$), swell area ($\frac{f_{peak}}{2} \leq f \leq \frac{3f_{peak}}{2}$) and sea area ($\frac{3f_{peak}}{2} \leq f$). In the infragravity and swell area, the model performs well at most gauges. Notably, the deviation of energy density in the sea area is relatively large from $x = 10.96\ m$ and $d = 2\ m$. This deviation increases until $x = 18.28\ m$ and $d = 1.54\ m$. However, from $x = 25.70\ m$ and $d = 1.23\ m$, the model results show good prediction in the sea area. The reason for the over-prediction is unclear. But it should be noted that the deviation has not kept growing along the wave propagation. It means that the error has not been amplified along with the iteration. The deviation in the sea area might result from errors in the dissipation mechanism and the truncation of the data.

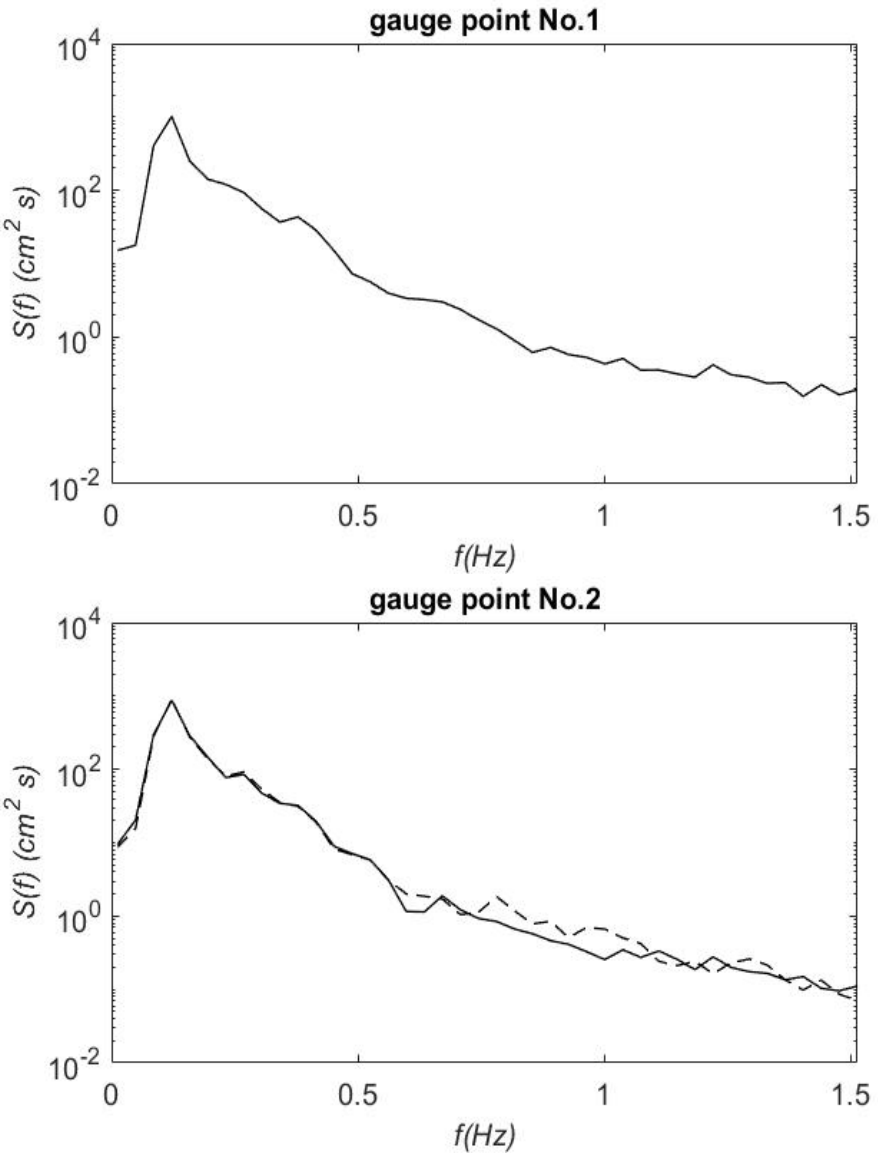

Figure 3.2: Comparison of Model Results and Experiment Data From NEES Tsunami and Swell Experiment(Purely random). Experiment Data (-), Model of Kaihatu & Kirby (- -). (Top) Input Spectra at x=0 cm (d=2 m); (Bottom) x=365 cm (d=2 m).

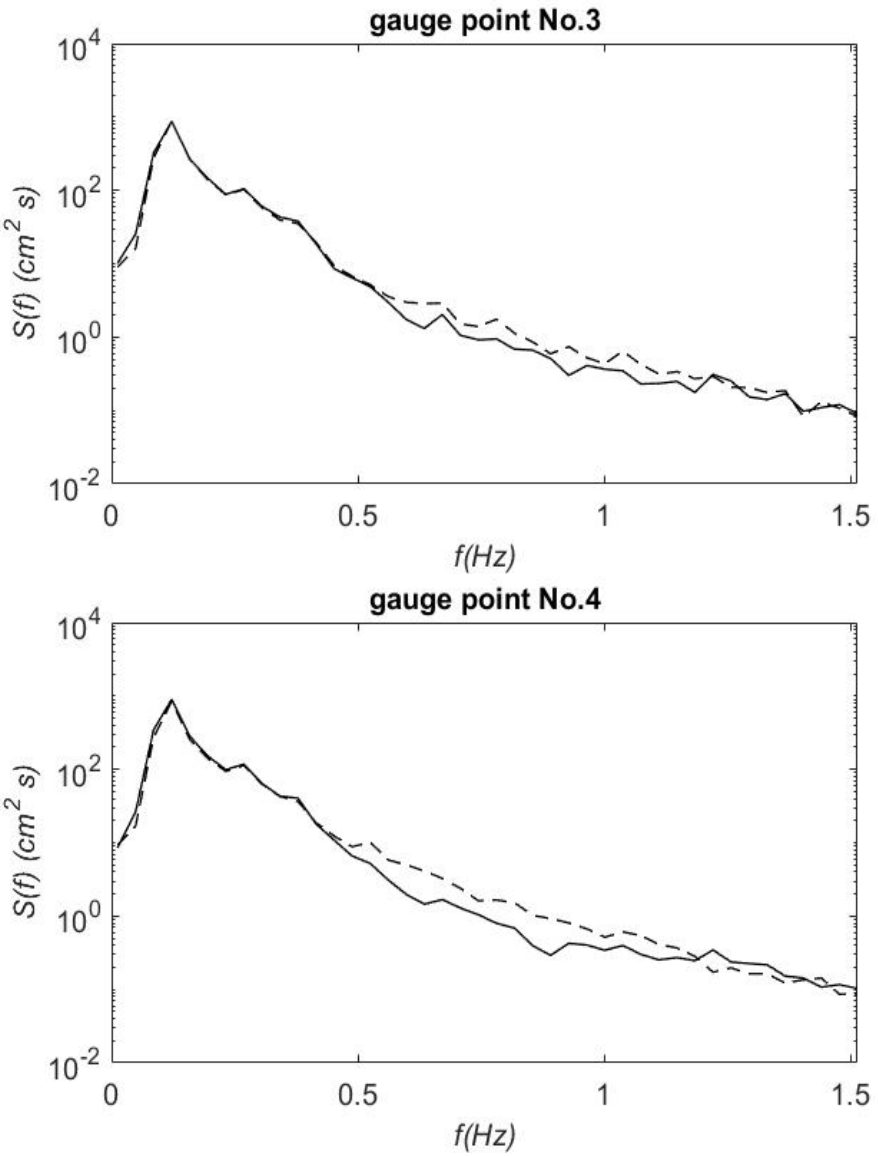

Figure 3.3: Comparison of Model Results and Experiment Data From NEES Tsunami and Swell Experiment(Purely random). Experiment Data (-), Model of Kaihatu & Kirby (- -). (Top) Spectra at x=732 cm (d=2 m); (Bottom) x=1096 cm (d=2 m).

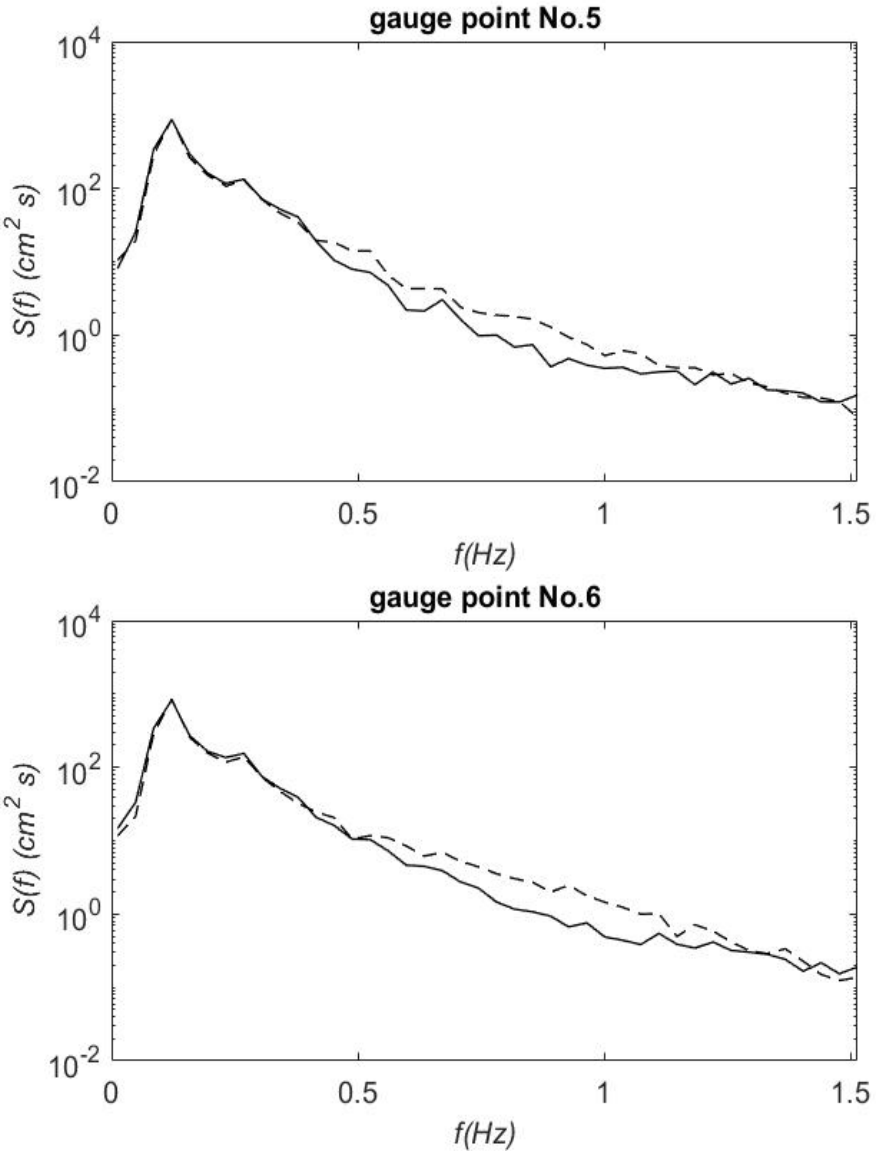

Figure 3.4: Comparison of Model Results and Experiment Data From NEES Tsunami and Swell Experiment(Purely random). Experiment Data (-), Model of Kaihatu & Kirby (- -). (Top) Spectra at x=1462 cm (d=1.69 m); (Bottom) x=1828 cm (d=1.54 m).

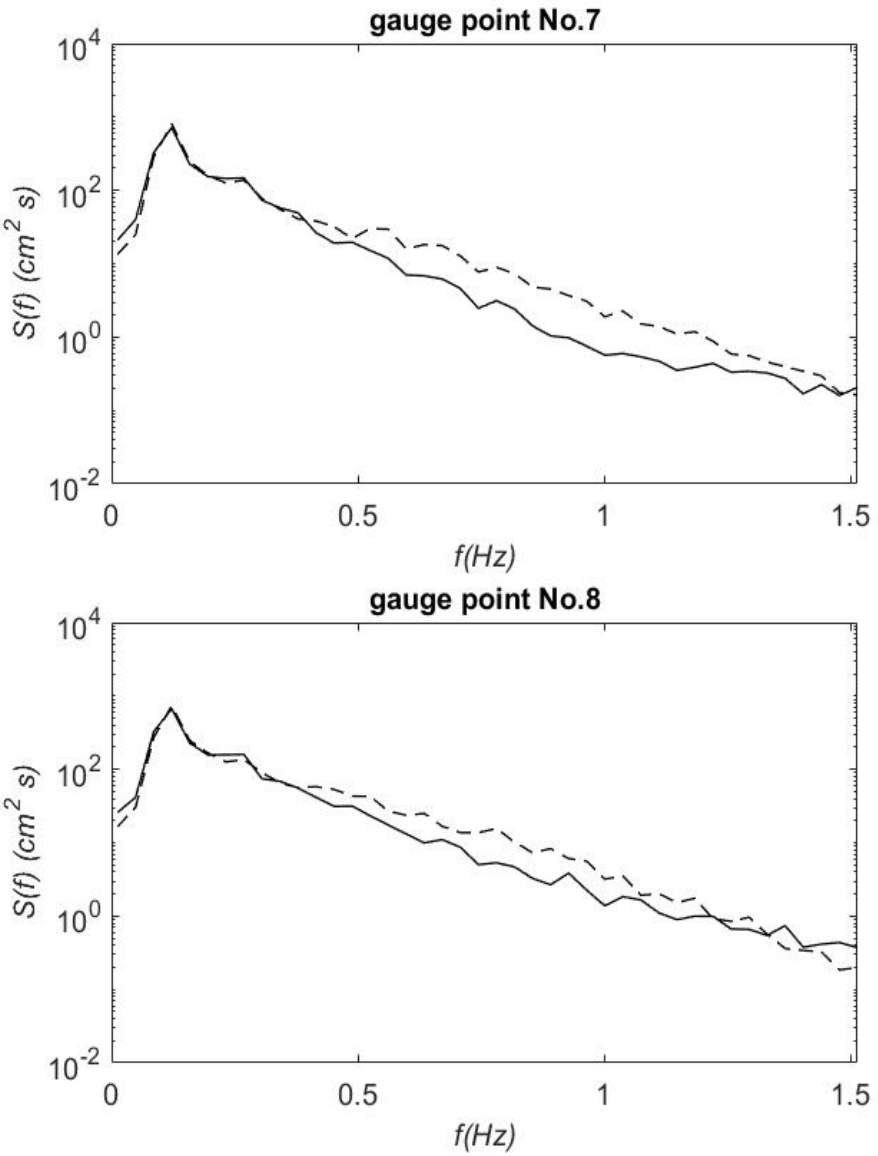

Figure 3.5: Comparison of Model Results and Experiment Data From NEES Tsunami and Swell Experiment(Purely random). Experiment Data (-), Model of Kaihatu & Kirby (- -). (Top) Spectra at x=2194 cm (d=1.39 m); (Bottom) x=2570 cm (d=1.23 m).

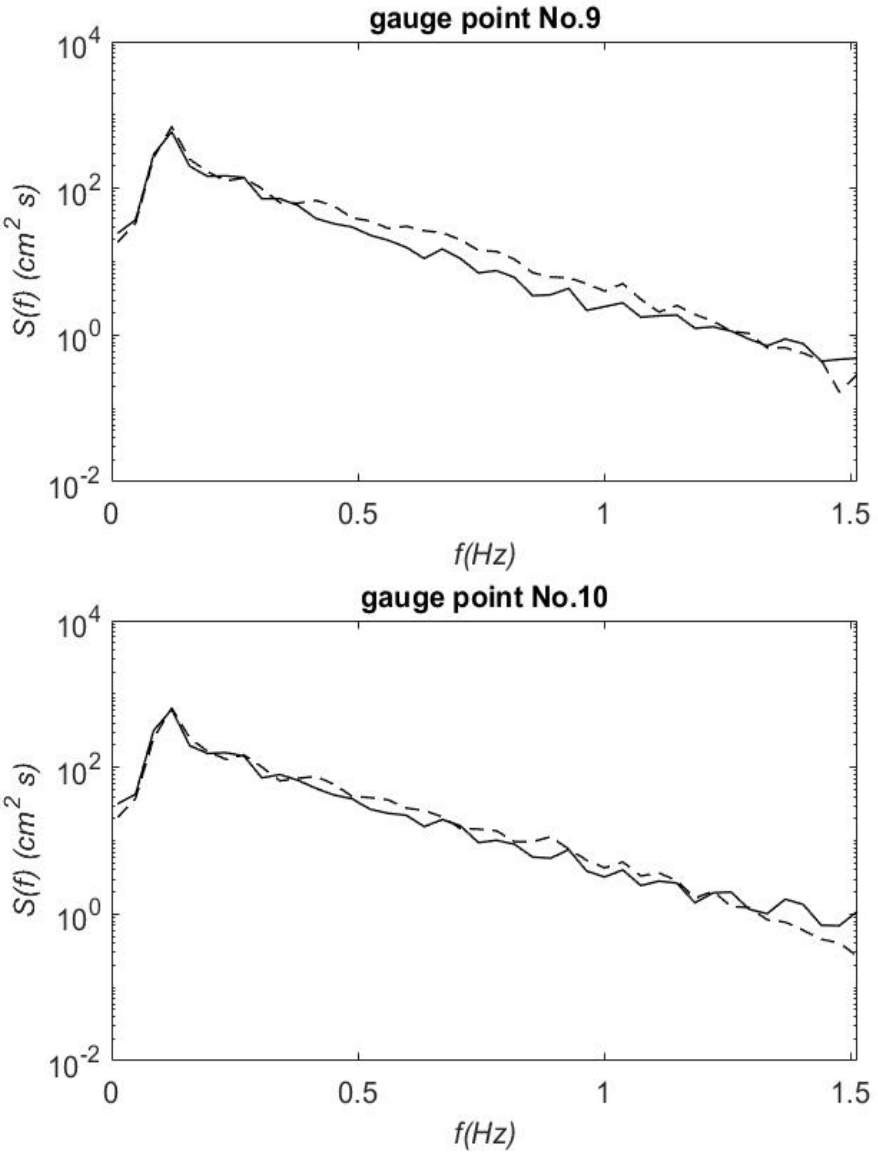

Figure 3.6: Comparison of Model Results and Experiment Data From NEES Tsunami and Swell Experiment(Purely random). Experiment Data (-), Model of Kaihatu & Kirby (- -). (Top) Spectra at x=2741 cm (d=1.16 m); (Bottom) x=2934 cm (d=1.08 m).

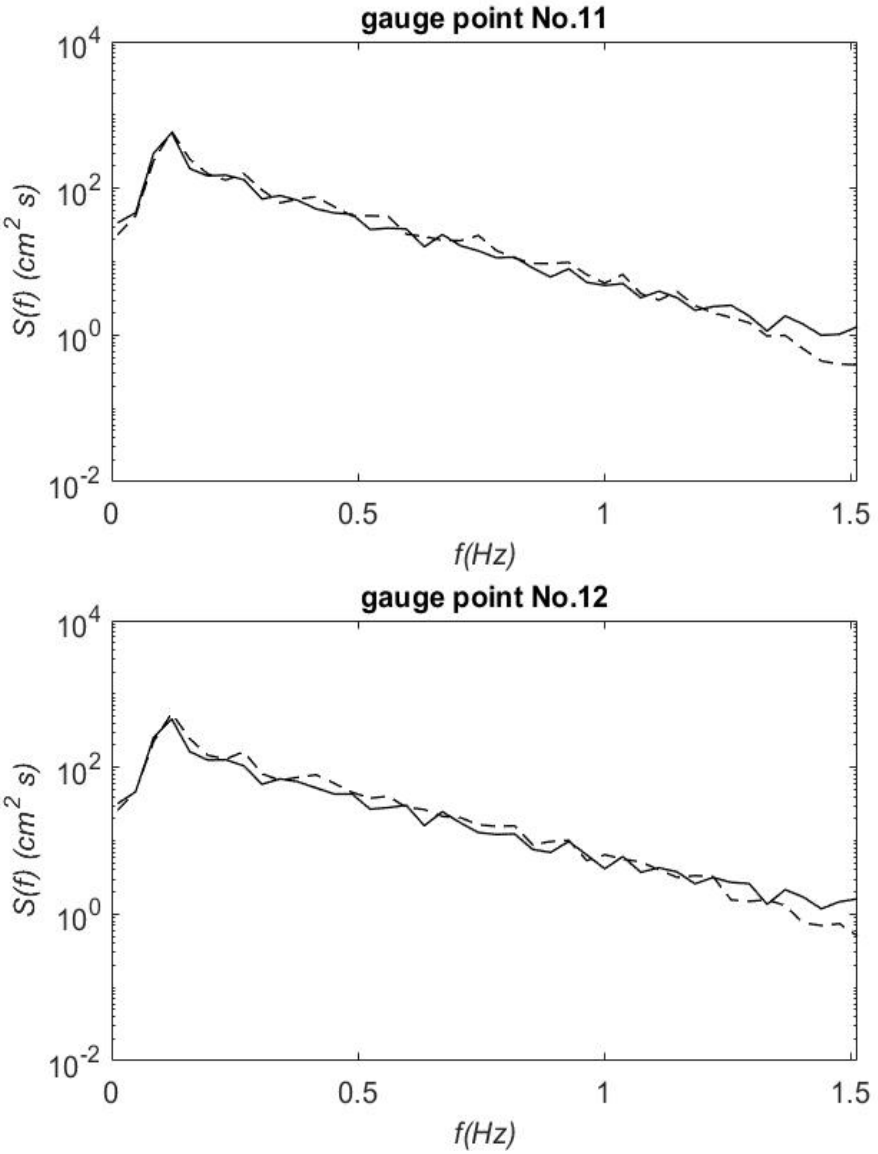

Figure 3.7: Comparison of Model Results and Experiment Data From NEES Tsunami and Swell Experiment(Purely random). Experiment Data (-), Model of Kaihatu & Kirby (- -). (Top) Spectra at x=3108 cm (d=1.01 m); (Bottom) x=3300 cm (d=0.93 m).

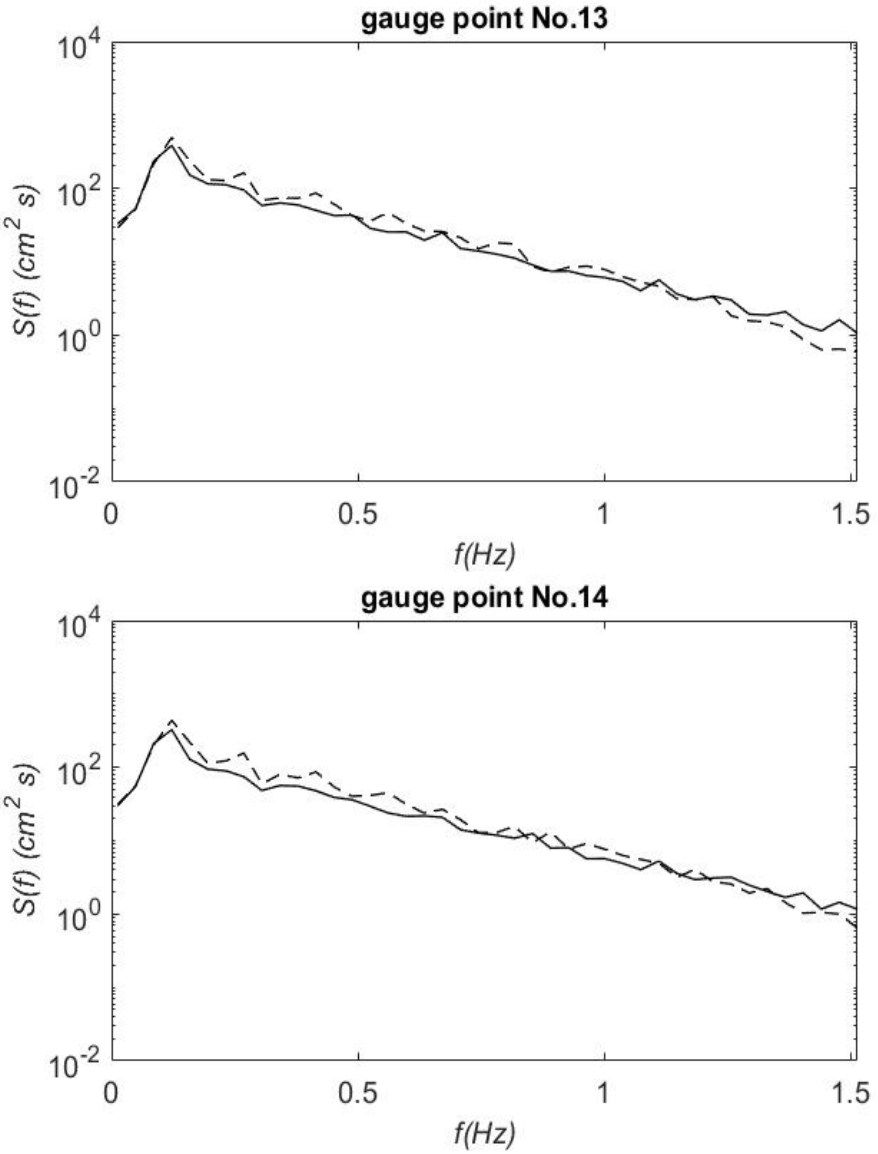

Figure 3.8: Comparison of Model Results and Experiment Data From NEES Tsunami and Swell Experiment(Purely random). Experiment Data (-), Model of Kaihatu & Kirby (- -). (Top) Spectra at x=3476 cm (d=0.85 m); (Bottom) x=3657 cm (d=0.78 m).

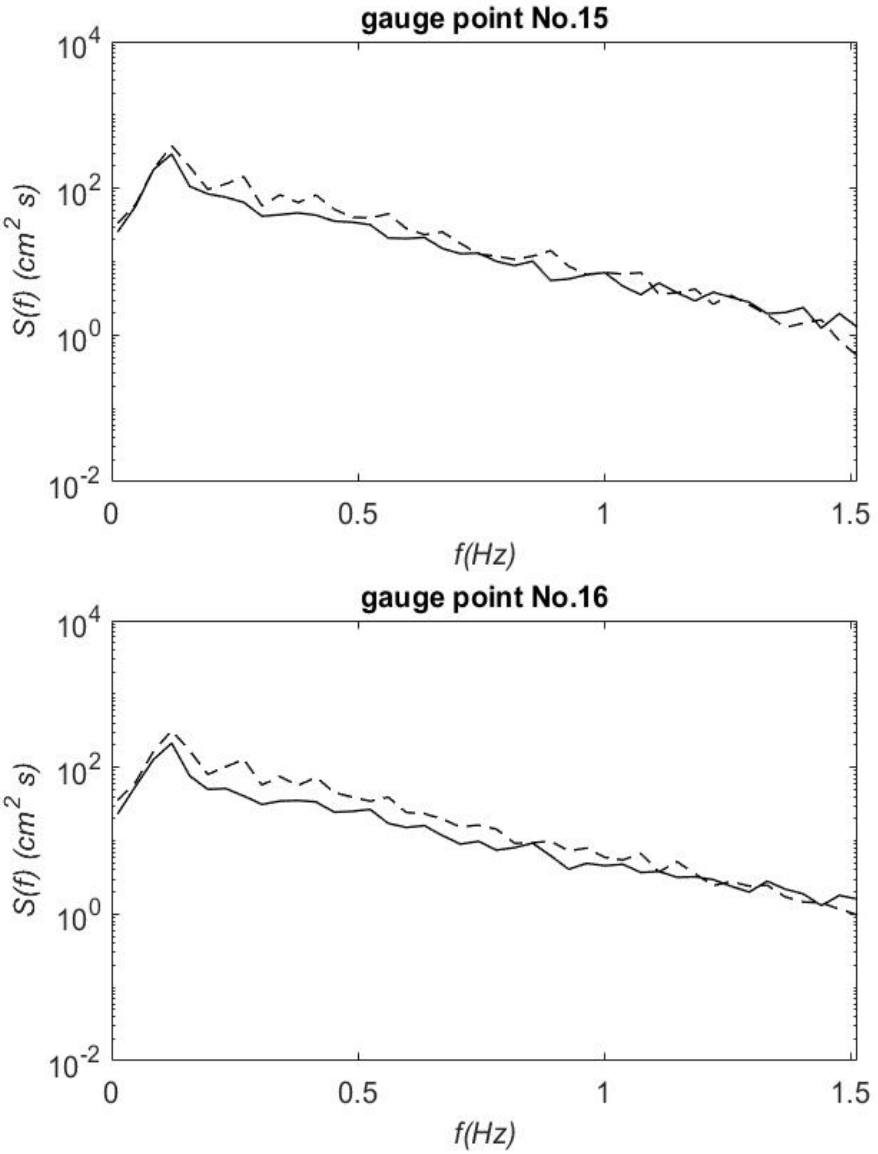

Figure 3.9: Comparison of Model Results and Experiment Data From NEES Tsunami and Swell Experiment(Purely random). Experiment Data (-), Model of Kaihatu & Kirby (- -). (Top) Spectra at x=3840 cm (d=0.70 m); (Bottom) x=4035 cm (d=0.62 m).

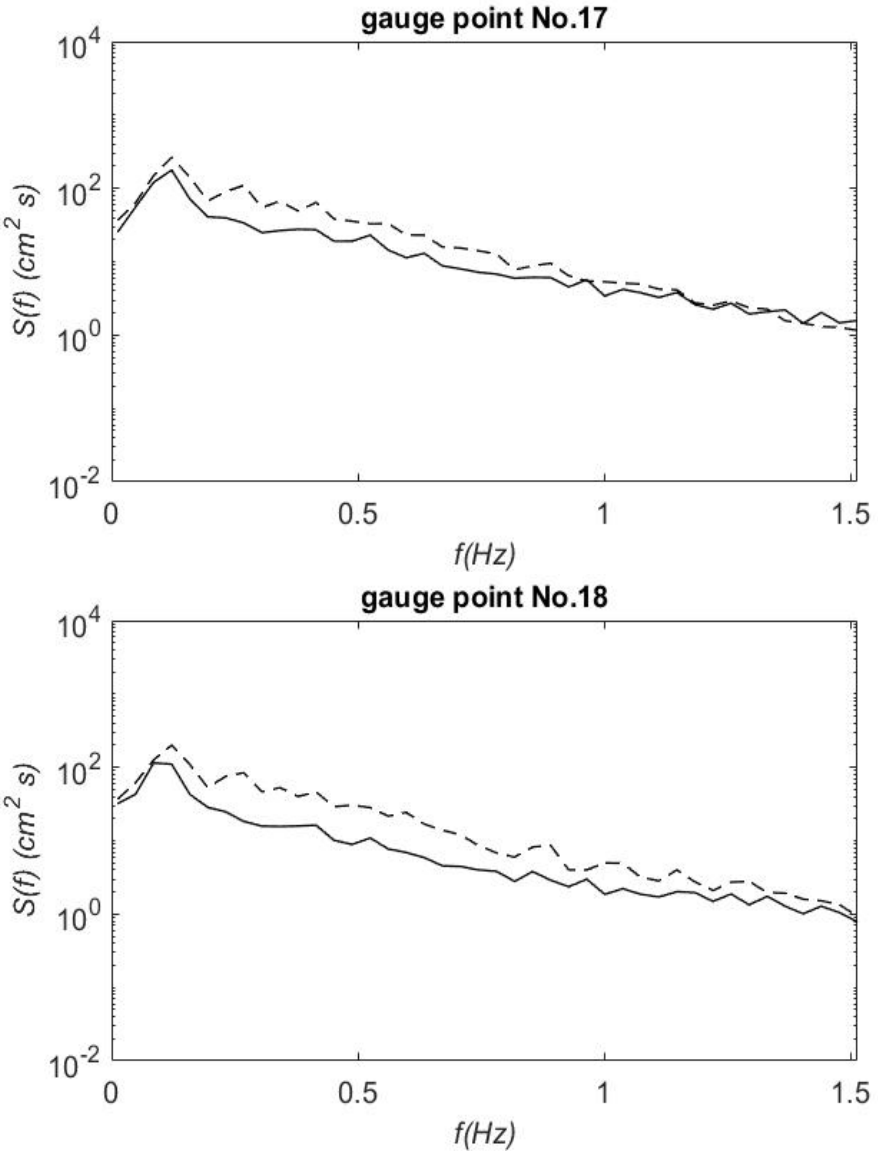

Figure 3.10: Comparison of Model Results and Experiment Data From NEES Tsunami and Swell Experiment(Purely random). Experiment Data (-), Model of Kaihatu & Kirby (- -). (Top) Spectra at x=4198 cm (d=0.55 m); (Bottom) x=4399 cm (d=0.47 m).

The fully dispersive mild slope model is built based on the assumption that the wave field is periodic since the discrete Fourier series is used in derivation. However, the solitary wave is a transient wave. The soliton is a permanent form wave, which can be described in the form of an aperiodic analytic function. The Fourier transformation can transfer any time dependent function or signal into a spectrum, no matter whether it is periodic. An analytic soliton can be transformed

into frequency domain by continuous Fourier transformation.

However, Fast Fourier Transformations used in the model inherently describe functions in terms of discrete frequencies. Hence, the usage of discrete Fourier transformation can have an effect on model simulation of the data related to soliton. However, It is still meaningful to make comparisons between spectra for data and model results of soliton plus random wave to evaluate the performance of the model.

The model results of soliton plus random wave in Trial 6 are shown from Figure 3.11 to Figure 3.19 and the spectra for measurement at corresponding gauge points is plotted for comparison. The spectra for measurement of soliton plus random wave are more fluctuating than those for purely random wave. It may be caused by the addition of soliton energy and the discrete Fourier transformation. The plot shape at the peak frequency is flat rather than peaky. The soliton interaction, which adds energy, is a likely reason. However, the model still shows a good prediction of the energy density at the peak frequency. The deviation of the model results and data does not increase until $d = 0.93$. In the infragravity area, the model under-predicts the energy density almost at the beginning of the propagation. Therefore, it can inferred that the effect of soliton is evident in the low frequency area of the spectra. The accuracy of the model simulation at higher frequency is also much lower than that of the simulation of purely random wave. The performance of the model will be further evaluated based on higher-order statistical properties in section 3.5.

In Experiment 1, the wave height of the random wave is 1 m and that of the soliton is 0.85 m. The model predicts the evolution of spectra well generally. However, the model under-predicts the energy in the infragravity area almost at the beginning. Additionally, the model over-predicts the energy density at the higher frequency remarkably. As has been mentioned before, the energy density in the infragravity area and swell area has been increased under the effect of soliton. Though the energy density at the peak frequency has not undergone substantial increase, the spectrum here is flat rather than peaked. The nonlinear process transfers the energy at lower frequency to higher frequency. At the same time, the dissipation mechanism from Thornton and Guza (1983) may not work for soliton. Therefore, the energy at the higher frequency has not been dissipated as much

as it ought to be. These changes of the spectra brought by soliton can be the main reason for the larger deviation of the prediction.

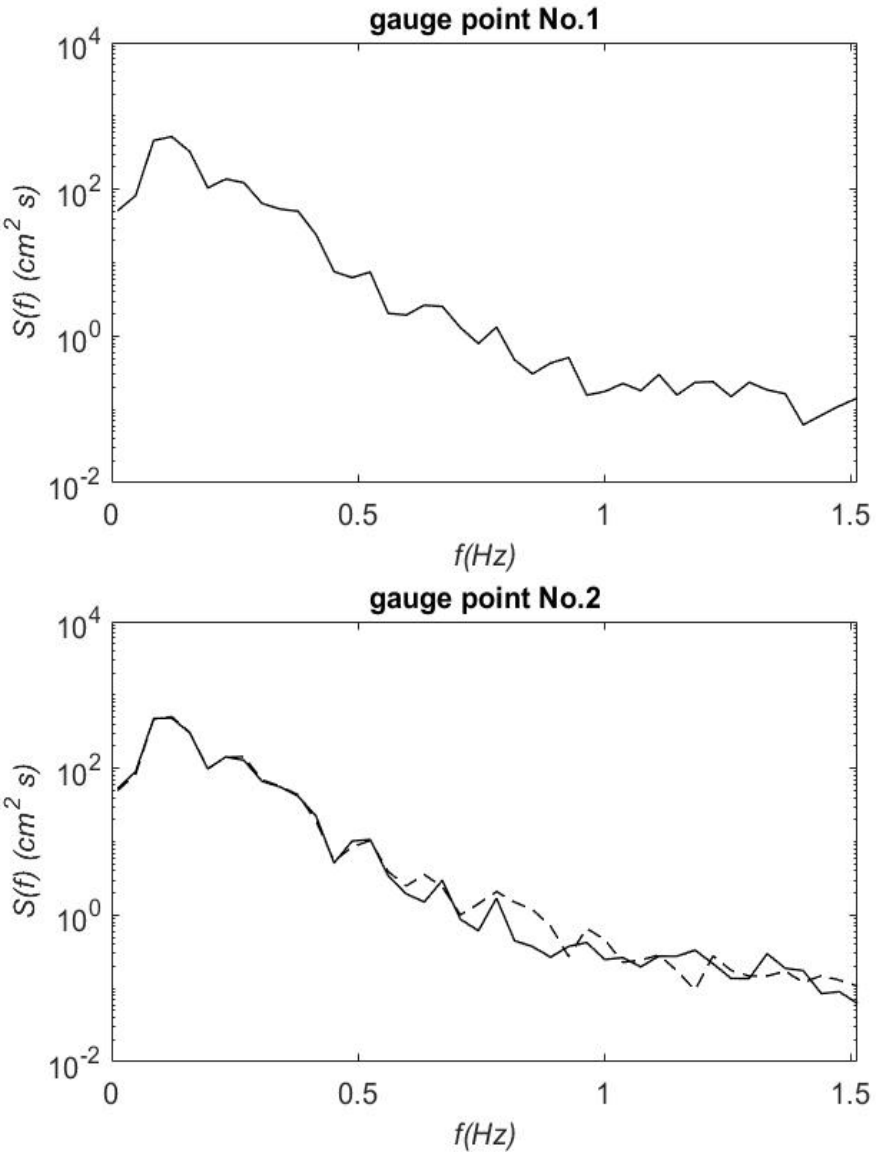

Figure 3.11: Comparison of Model Results and Experiment Data From NEES Tsunami and Swell Experiment(Soliton plus random). Experiment Data (-), Model of Kaihatu & Kirby (- -). (Top) Input Spectra at x=0 cm (d=2 m); (Bottom) x=365 cm (d=2 m).

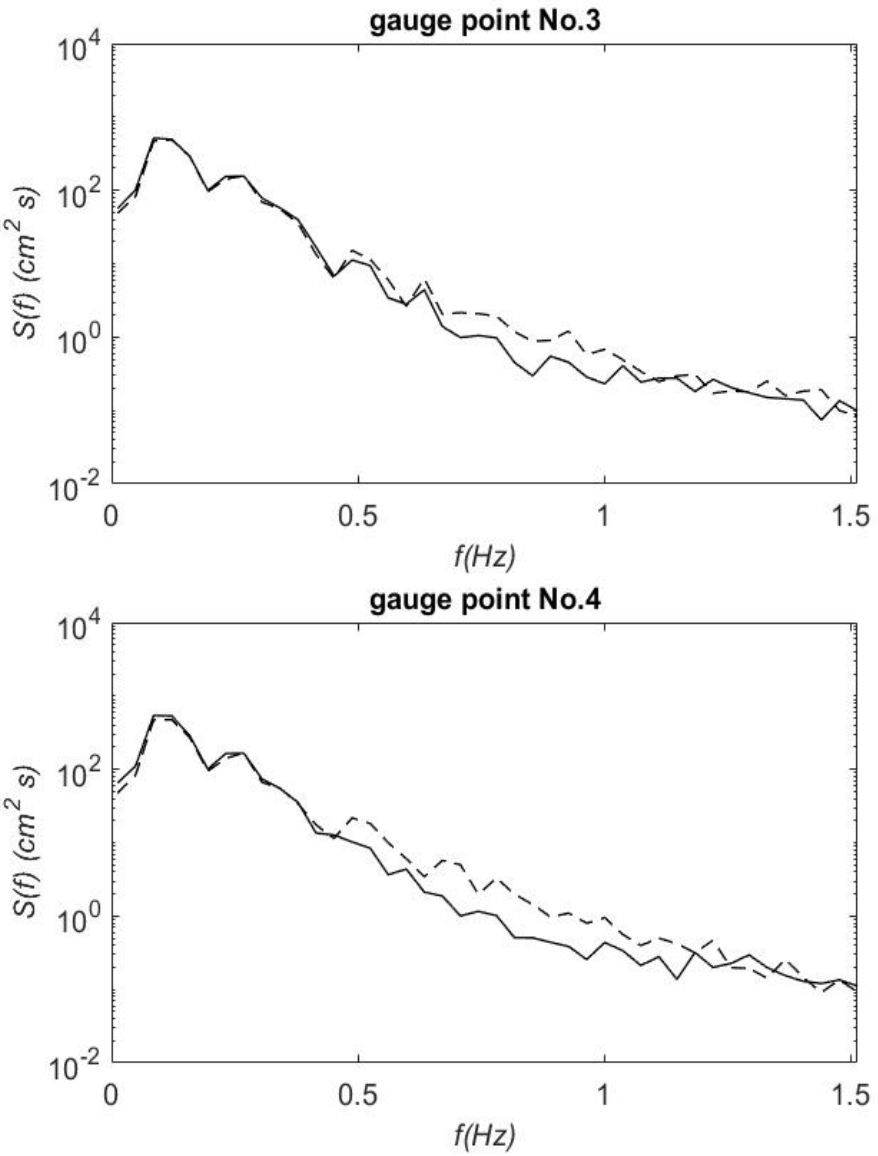

Figure 3.12: Comparison of Model Results and Experiment Data From NEES Tsunami and Swell Experiment(Soliton plus random). Experiment Data (-), Model of Kaihatu & Kirby (- -). (Top) Spectra at x=732 cm (d=2 m); (Bottom) x=1096 cm (d=2 m).

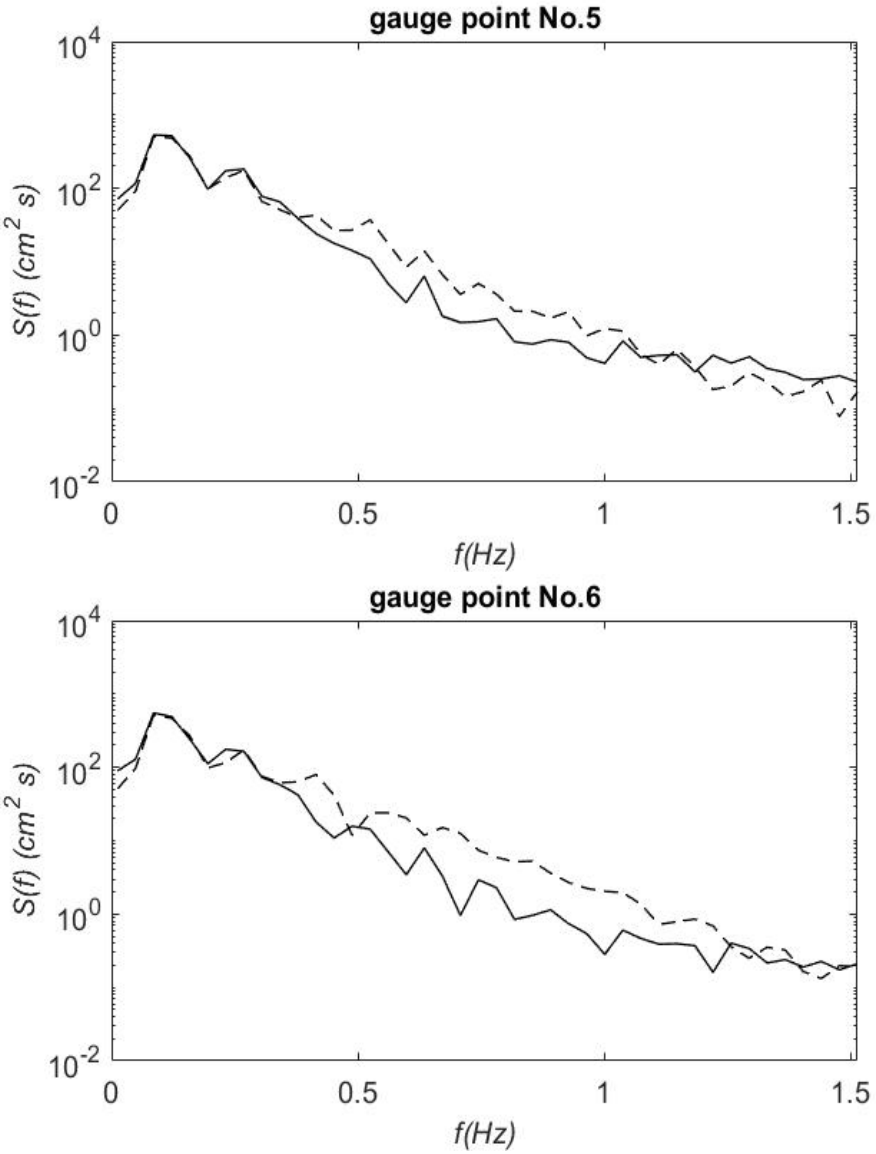

Figure 3.13: Comparison of Model Results and Experiment Data From NEES Tsunami and Swell Experiment(Soliton plus random). Experiment Data (-), Model of Kaihatu & Kirby (- -). (Top) Spectra at x=1462 cm (d=1.69 m); (Bottom) x=1828 cm (d=1.54 m).

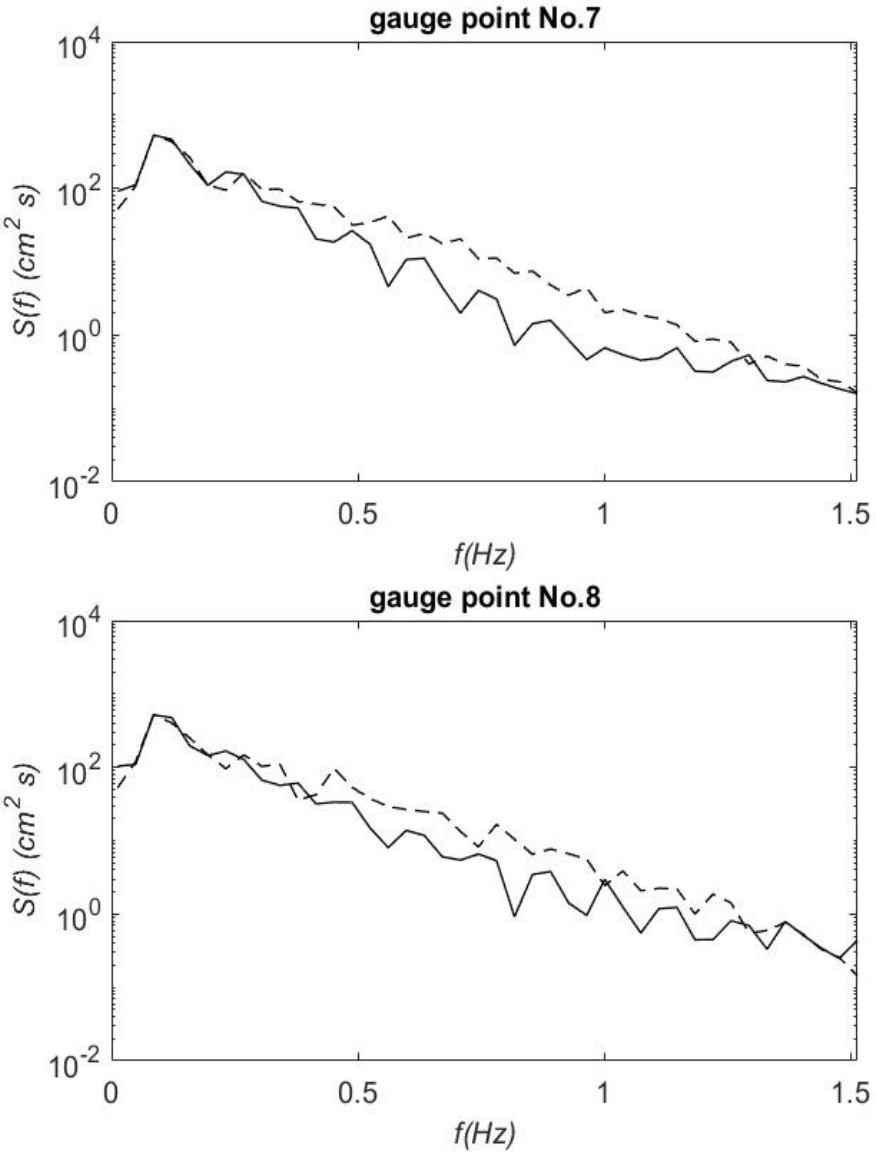

Figure 3.14: Comparison of Model Results and Experiment Data From NEES Tsunami and Swell Experiment(Soliton plus random). Experiment Data (-), Model of Kaihatu & Kirby (- -). (Top) Spectra at x=2194 cm (d=1.39 m); (Bottom) x=2570 cm (d=1.23 m).

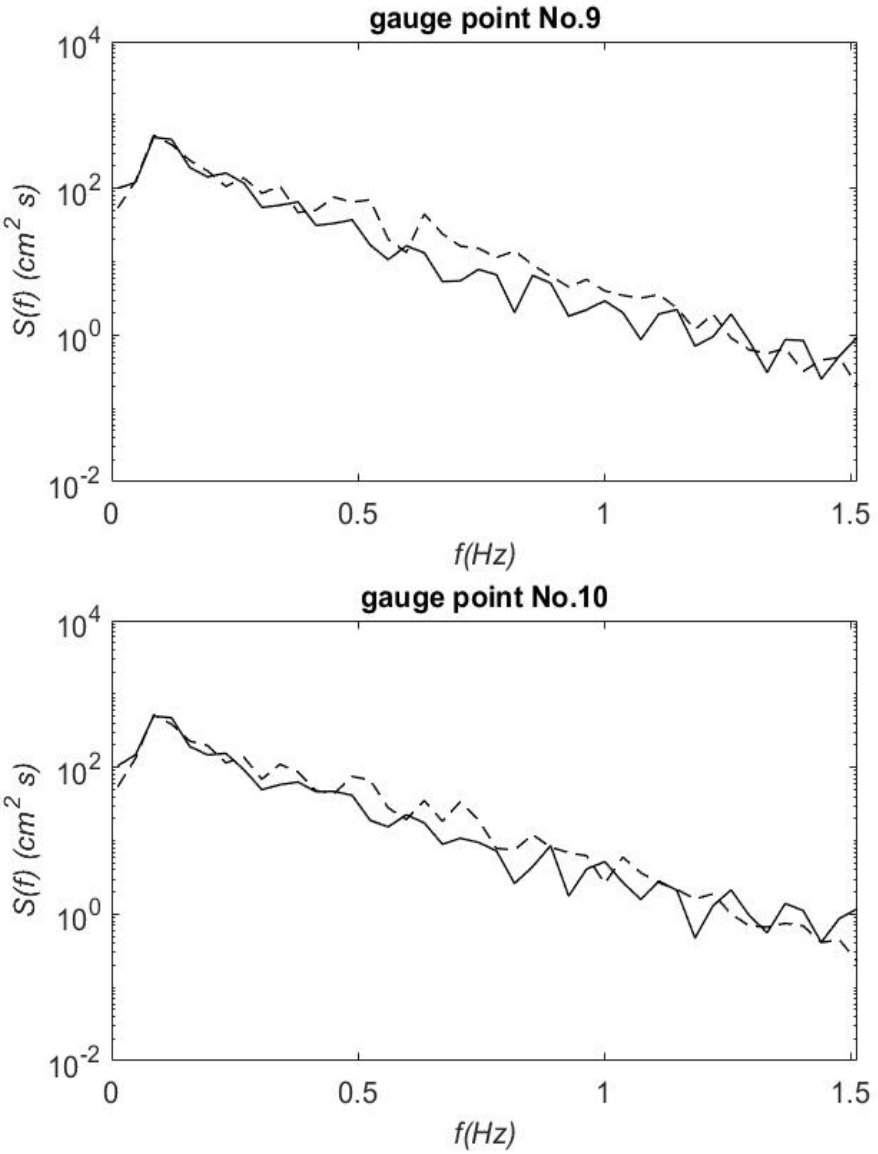

Figure 3.15: Comparison of Model Results and Experiment Data From NEES Tsunami and Swell Experiment(Soliton plus random). Experiment Data (-), Model of Kaihatu & Kirby (- -). (Top) Spectra at x=2741 cm (d=1.16 m); (Bottom) x=2934 cm (d=1.08 m).

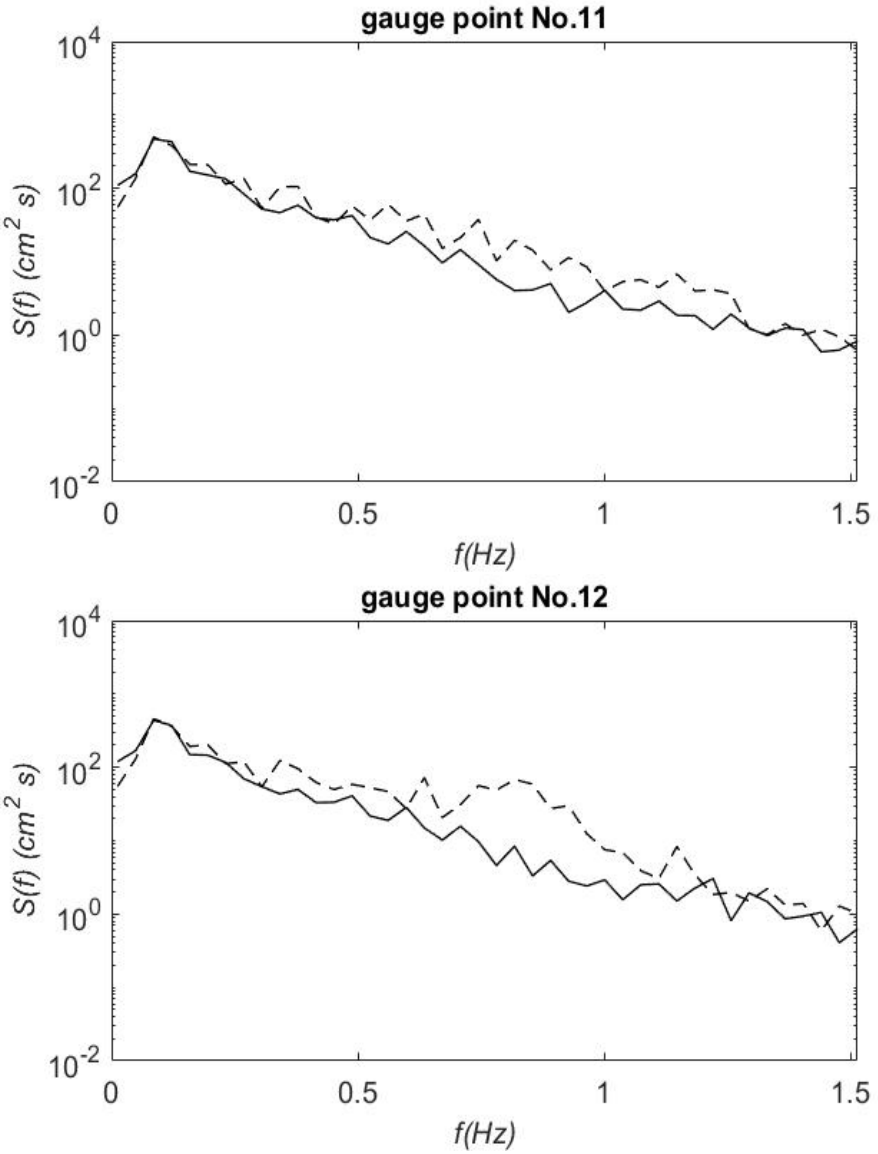

Figure 3.16: Comparison of Model Results and Experiment Data From NEES Tsunami and Swell Experiment(Soliton plus random). Experiment Data (-), Model of Kaihatu & Kirby (- -). (Top) Spectra at x=3108 cm (d=1.01 m); (Bottom) x=3300 cm (d=0.93 m).

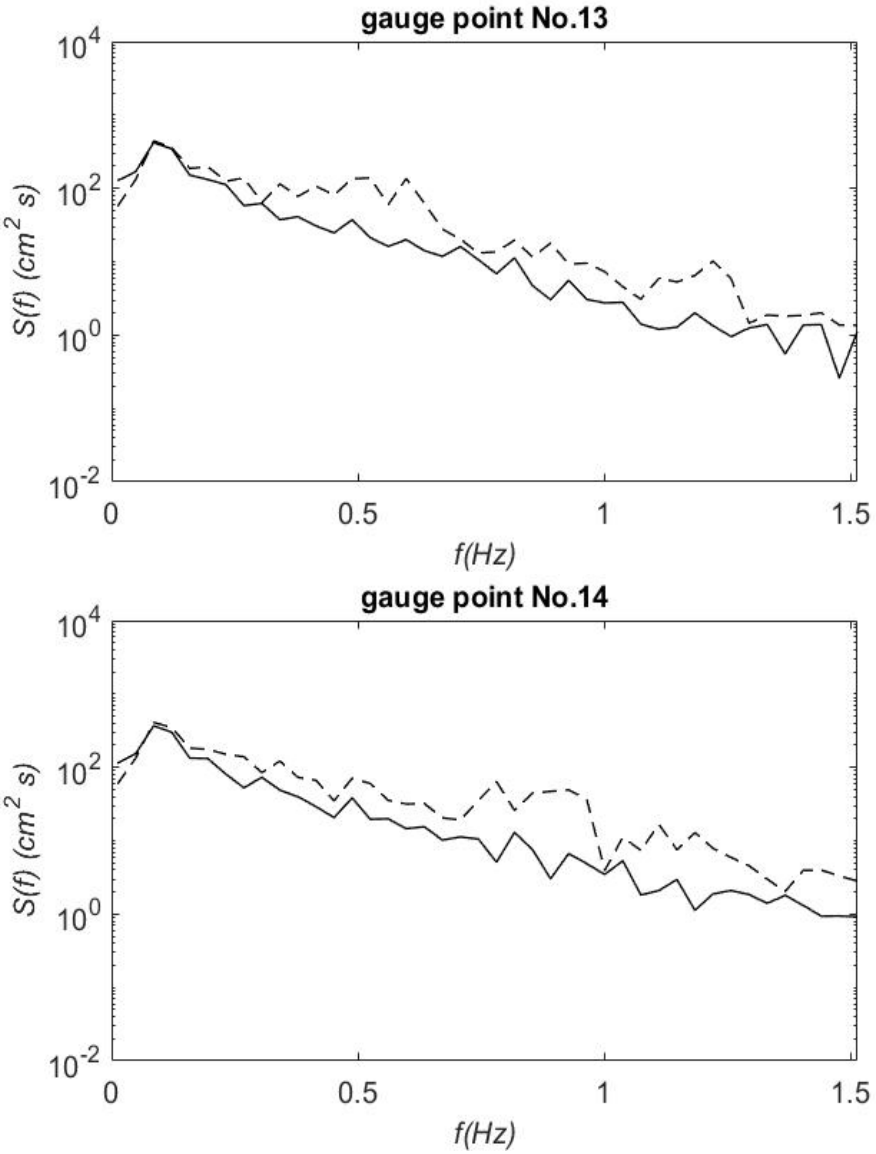

Figure 3.17: Comparison of Model Results and Experiment Data From NEES Tsunami and Swell Experiment(Soliton plus random). Experiment Data (-), Model of Kaihatu & Kirby (- -). (Top) Spectra at x=3476 cm (d=0.85 m); (Bottom) x=3657 cm (d=0.78 m).

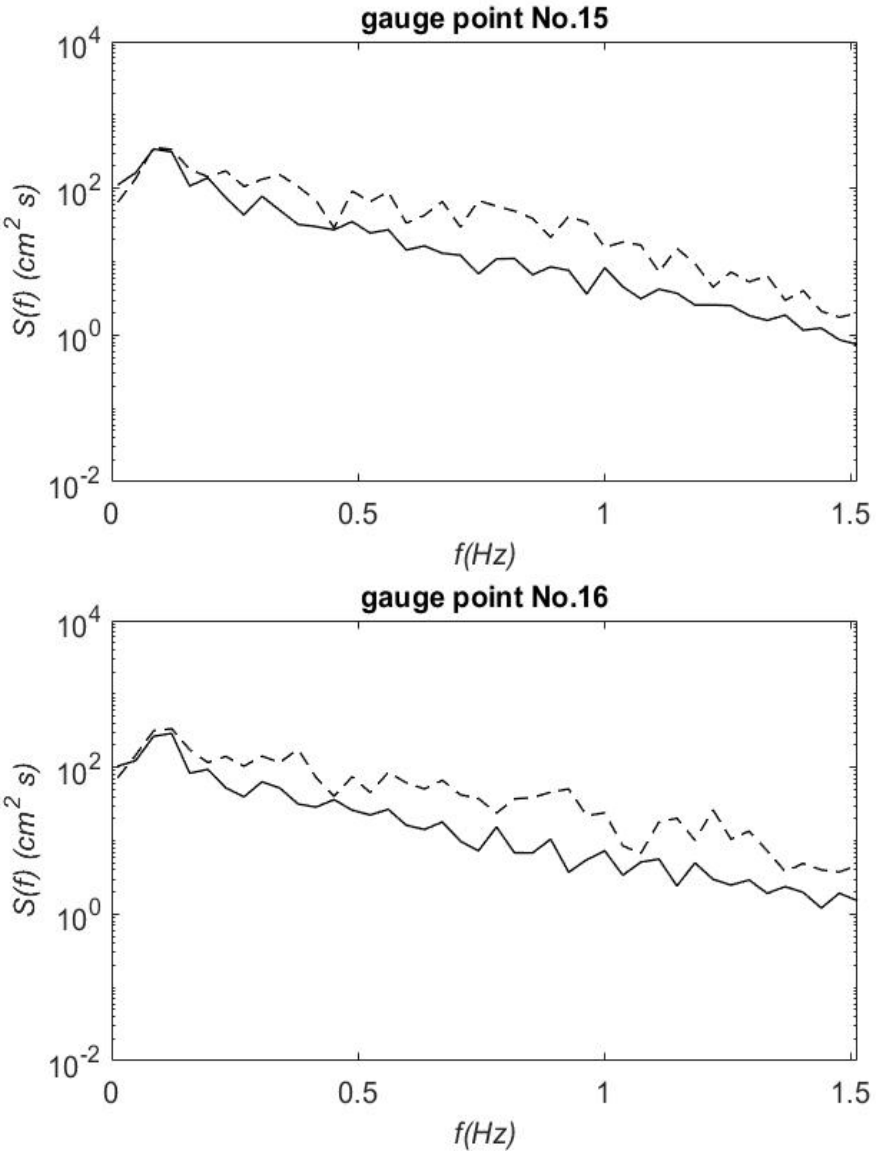

Figure 3.18: Comparison of Model Results and Experiment Data From NEES Tsunami and Swell Experiment(Soliton plus random). Experiment Data (-), Model of Kaihatu & Kirby (- -). (Top) Spectra at x=3840 cm (d=0.70 m); (Bottom) x=4035 cm (d=0.62 m).

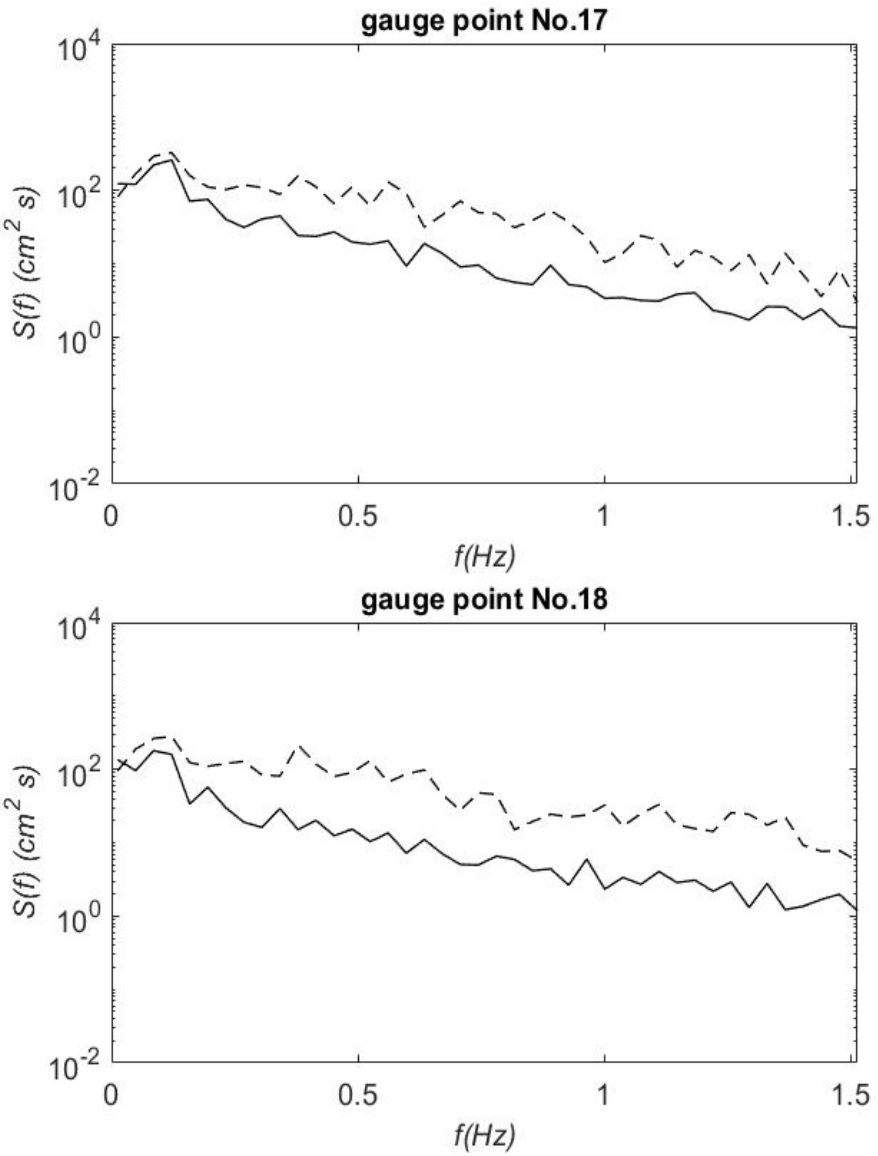

Figure 3.19: Comparison of Model Results and Experiment Data From NEES Tsunami and Swell Experiment(Soliton plus random). Experiment Data (-), Model of Kaihatu & Kirby (- -). (Top) Spectra at x=4198 cm (d=0.55 m); (Bottom) x=4399 cm (d=0.47 m).

Pure soliton was produced in Trial 2 in the Experiment 1. The sampling rate is the same as before, but the observation time is 39 seconds. Hence, there are a total of 1950 points collected at each gauge. The spectra are truncated for the lower 64 frequencies. The spectra for measurement and simulation results of Trial 2 are shown from Figure 3.20 to Figure 3.28.

The defect of the application of FFT on the soliton signal has been mentioned before. For the

soliton plus random wave, there is no means to achieve the analytical function of the signal. It is unpractical to use continuous Fourier transformation on the measurement. Hence, to make a comparison, Fast Fourier transformation is used here to handle the signal of the soliton. It might not be a correct method to get spectra for the soliton but reveals the character of the data properly.

As we can see in the figures, the most percentage of the wave energy concentrates on the lower frequencies. Theoretically, the soliton can be described as the summation of infinite Fourier series components, each of which has a frequency. In the superposition of Fourier components, the lower frequency components build the general shape of the soliton, which is similar to the 'envelope' of the group waves and higher frequencies components modify the shape of the group waves to approach the soliton. It can be also described that Fourier components with lower frequencies make the change of water level and the components at higher frequencies try to bring the curve surface rather than flat.

Though the Fast Fourier transformation greatly impacts the spectrum for a soliton, it can still reveal the general character of the data. The soliton signal is also a good test for assessment of the model. Therefore, the influence caused by Fast Fourier transformation will not be included in the following discussion.

As is shown in the spectra, the peak frequency of the soliton is around zero. The model shows surprisingly good prediction at the so-called lower frequency. However, at the higher frequency, the model's prediction does not seem to make sense. The model predicts the trend of the spectra after the peak frequency, but the prediction of the energy density is far away from accurate. The soliton is the solution of permanent form to KdV equation. A soliton has frequency components that associate with the wave shape, but frequency components themselves are not necessarily propagating waves. In the uniform water depth, a soliton does not change the wave shape during the propagation. The nonlinearity plays the role to bind the wave train together and has the intendency to make the wave steeper, while the dispersion relation makes the wave train to separate according to the different wave velocities. It is because the balance between the dispersion relation and nonlinearity that the soliton has the permanent form during the propagation. However, the model

has fully dispersion relation so that the model will take each wave component and propagate them as free waves, which are actually not. This may be the main reason for the over-prediction of the model for a pure soliton case. It might help to improve the model performance for pure soliton case that modify the dispersion relation to bind the harmonics together so that the spectra do not change during propagation above the flat bottom as a soliton does.

The spectra for the data give a general description of the soliton signal in frequency domain. This paper is not meant to analyze the nonlinear process in soliton shoaling but to make some reasonable inference for the influence brought about by soliton on the random wave field based on the characteristics shown in these spectra. As mentioned before, in the spectra for soliton plus random wave, the energy density at the lower frequencies increased compared with spectra for purely random wave but the energy at the sea wave area has not changed much. Combined with the spectra for purely soliton, it can be inferred that it happens because the most energy of soliton concentrates at lower frequency.

The dissipation model used is also not suitable for the pure soliton case. Thornton and Guza (1983) built the model based on the assumption that the wave field follows Rayleigh distribution. A soliton does not follow Rayleigh distribution apparently. It is likely to analyze the dissipation of a single wave to make the model available for a soliton. For example, Zelt (1991) built a Lagrangian finite-element Boussinesq wave model for the run-up of non-breaking and breaking solitary waves. The dissipation mechanism in the model of Zelt (1991) might be suitable to applied in the model of Kaihatu and Kirby (1995) to improve the performance of the model when dealing with solitary wave data. Further investigation should be made to know whether the prediction of the model for soliton plus random wave case can help improve the results.

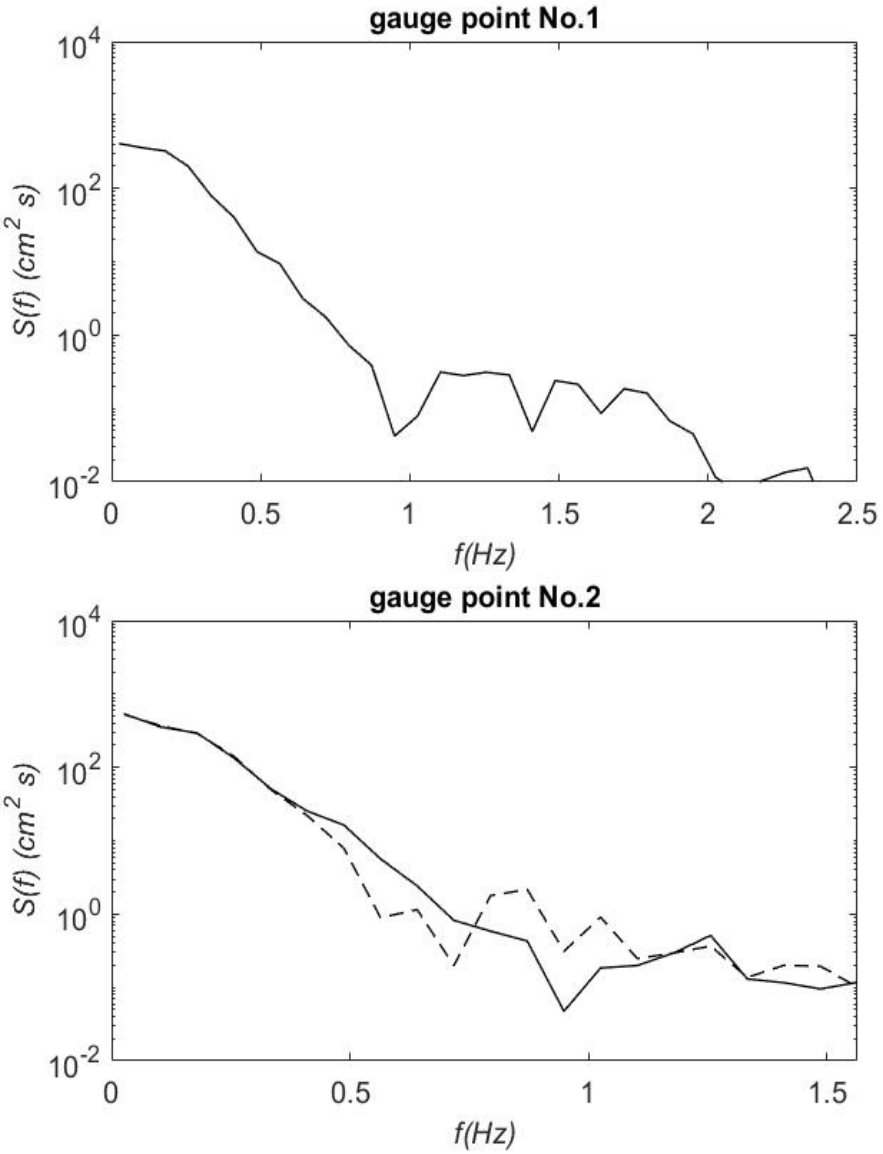

Figure 3.20: Comparison of Model Results and Experiment Data From NEES Tsunami and Swell Experiment(Soliton). Experiment Data (-), Model of Kaihatu & Kirby (- -). (Top) Input Spectra at x=0 cm (d=2 m); (Bottom) x=365 cm (d=2 m).

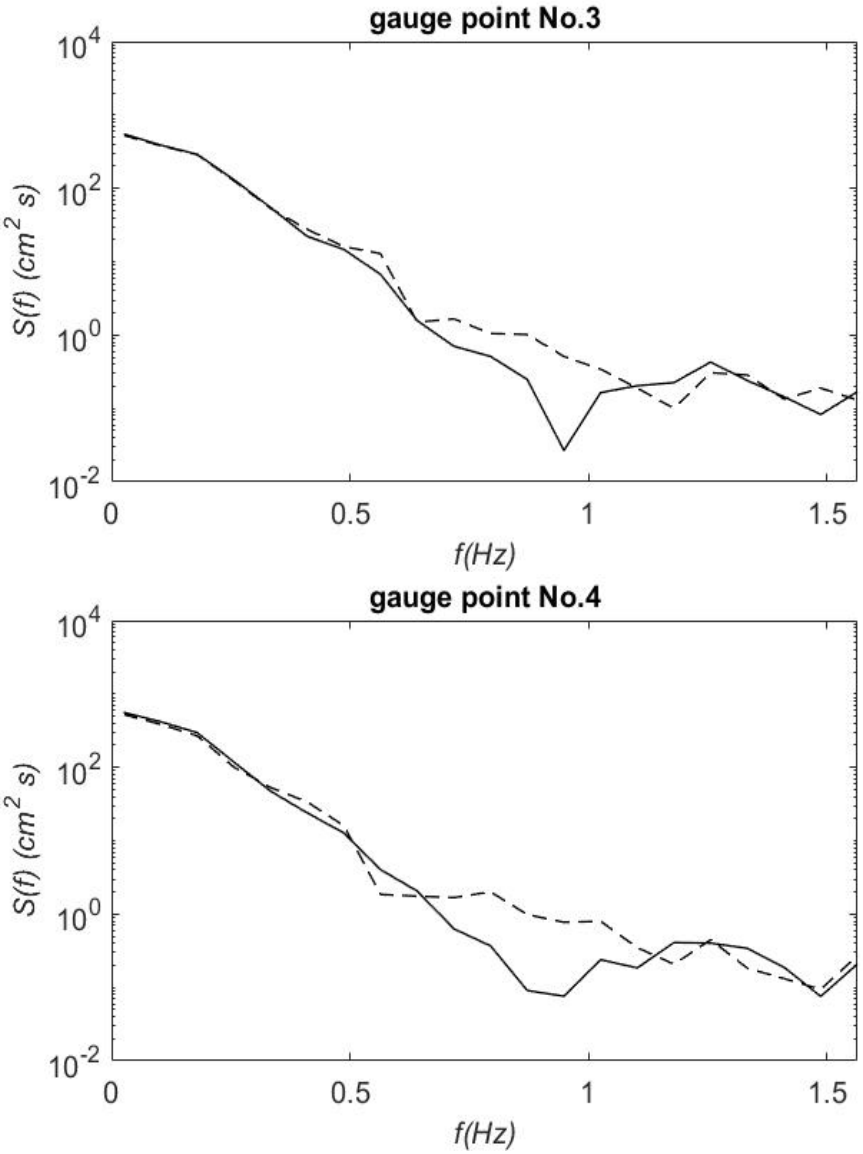

Figure 3.21: Comparison of Model Results and Experiment Data From NEES Tsunami and Swell Experiment(Soliton). Experiment Data (-), Model of Kaihatu & Kirby (- -). (Top) Spectra at x=732 cm (d=2 m); (Bottom) x=1096 cm (d=2 m).

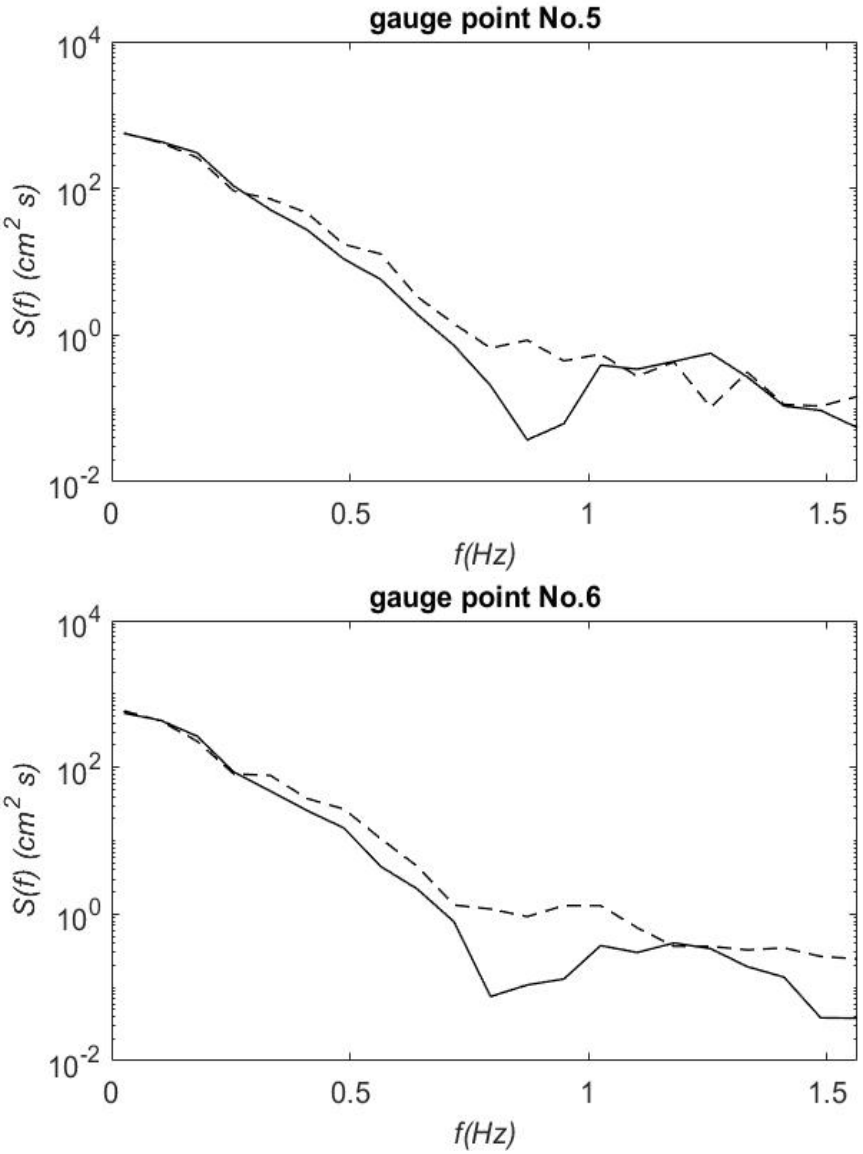

Figure 3.22: Comparison of Model Results and Experiment Data From NEES Tsunami and Swell Experiment(Soliton). Experiment Data (-), Model of Kaihatu & Kirby (- -). (Top) Spectra at x=1462 cm (d=1.69 m); (Bottom) x=1828 cm (d=1.54 m).

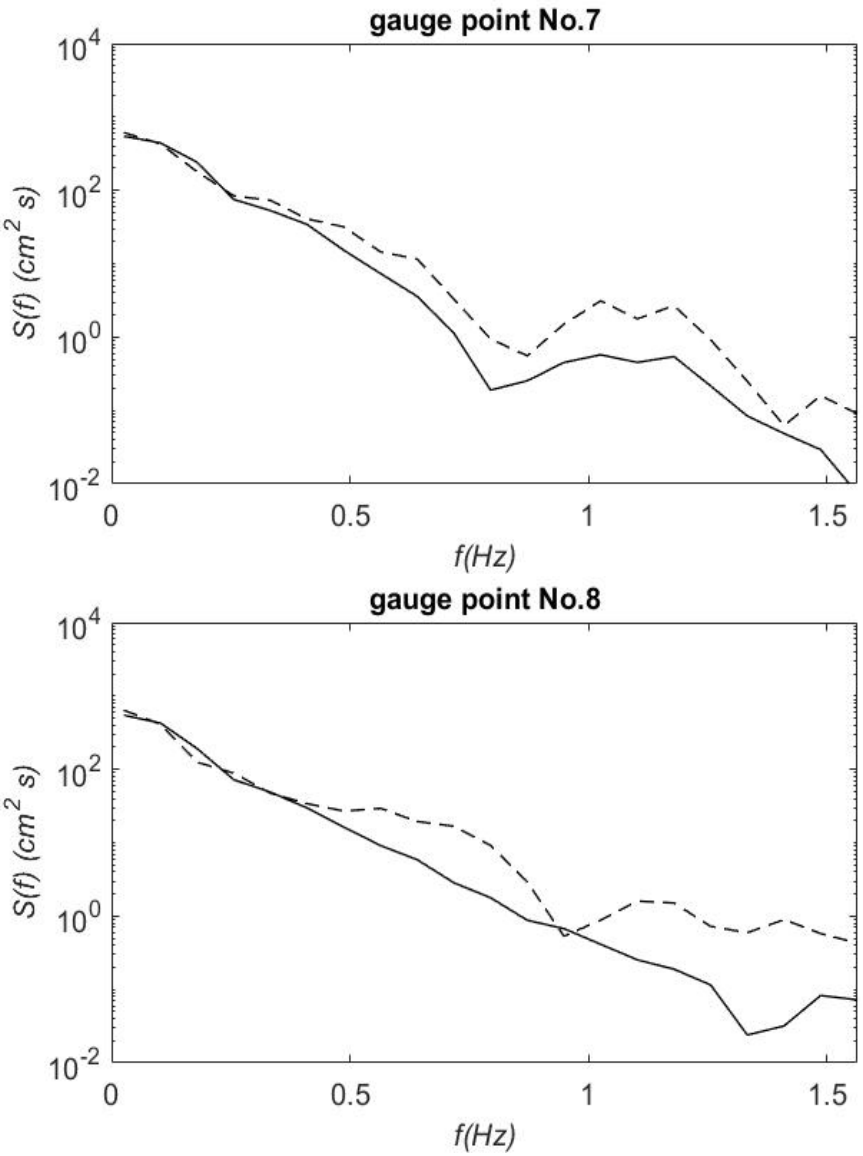

Figure 3.23: Comparison of Model Results and Experiment Data From NEES Tsunami and Swell Experiment(Soliton). Experiment Data (-), Model of Kaihatu & Kirby (- -). (Top) Spectra at x=2194 cm (d=1.39 m); (Bottom) x=2570 cm (d=1.23 m).

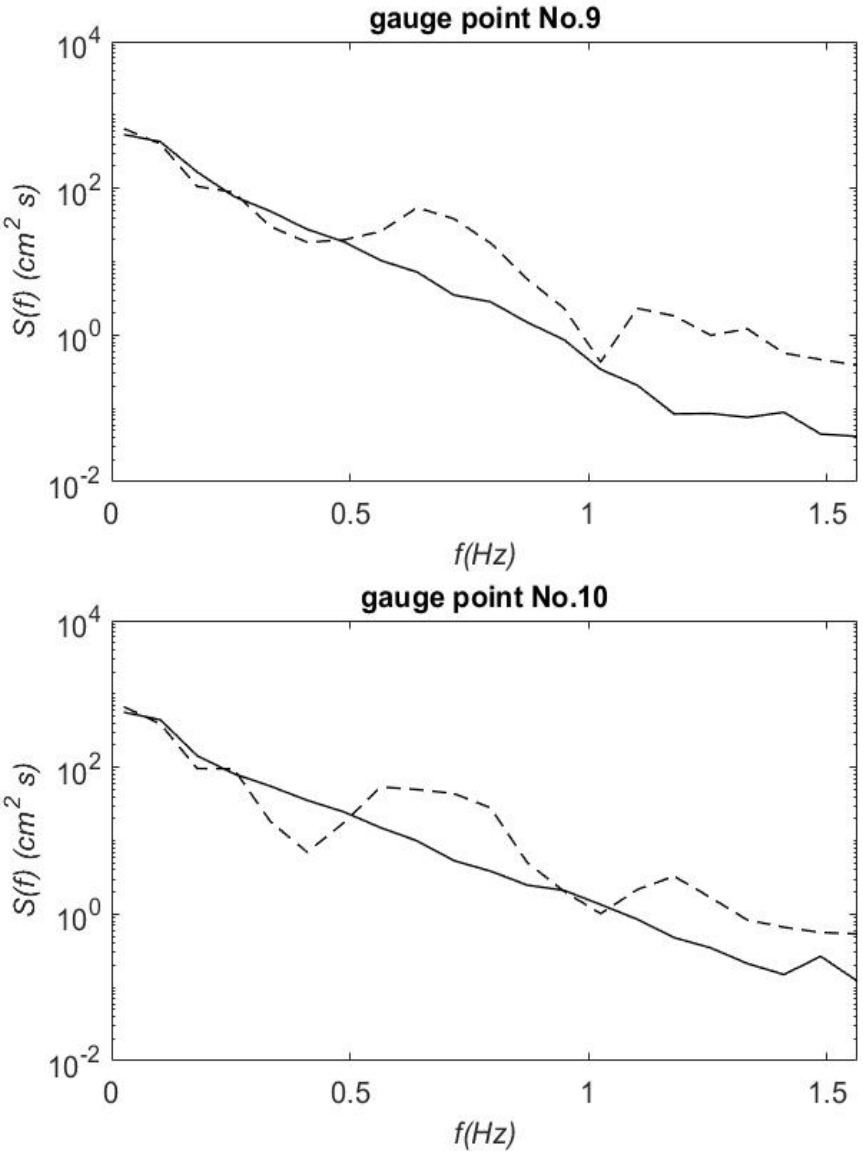

Figure 3.24: Comparison of Model Results and Experiment Data From NEES Tsunami and Swell Experiment(Soliton). Experiment Data (-), Model of Kaihatu & Kirby (- -). (Top) Spectra at x=2741 cm (d=1.16 m); (Bottom) x=2934 cm (d=1.08 m).

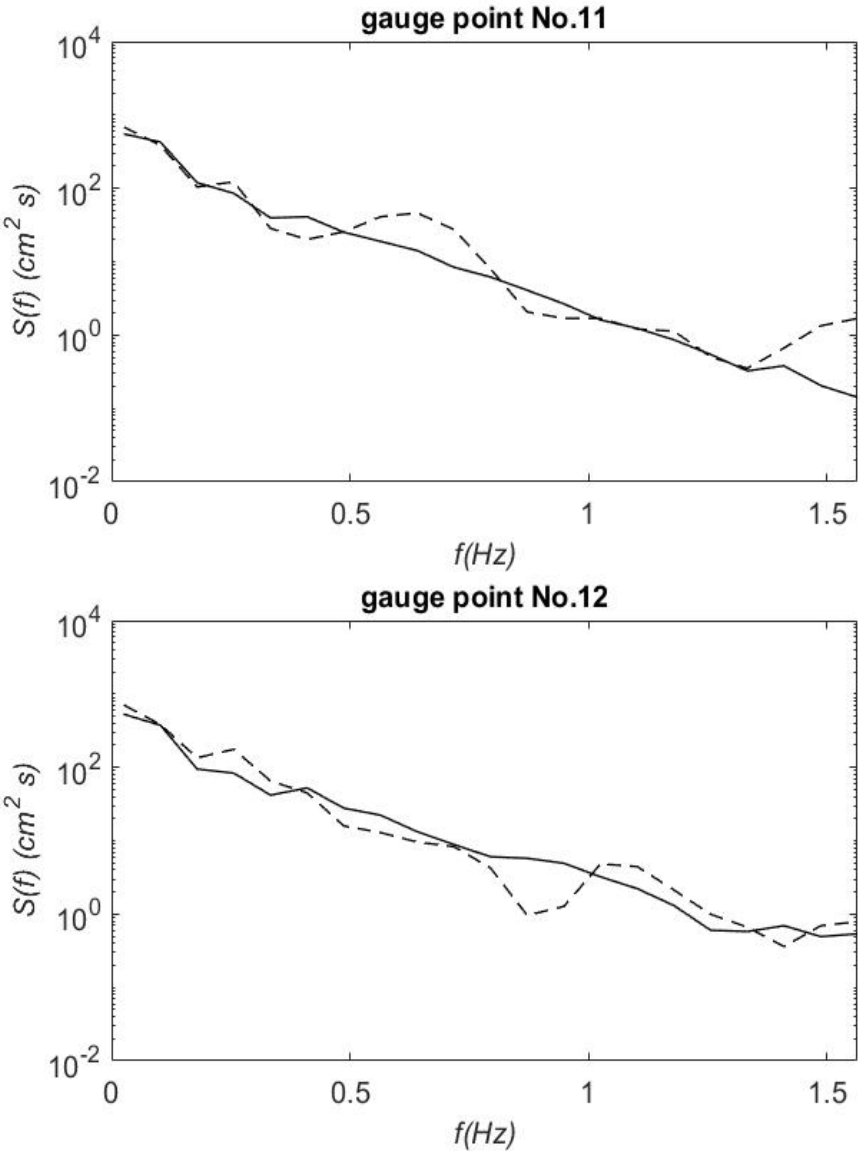

Figure 3.25: Comparison of Model Results and Experiment Data From NEES Tsunami and Swell Experiment(Soliton). Experiment Data (-), Model of Kaihatu & Kirby (- -). (Top) Spectra at x=3108 cm (d=1.01 m); (Bottom) x=3300 cm (d=0.93 m).

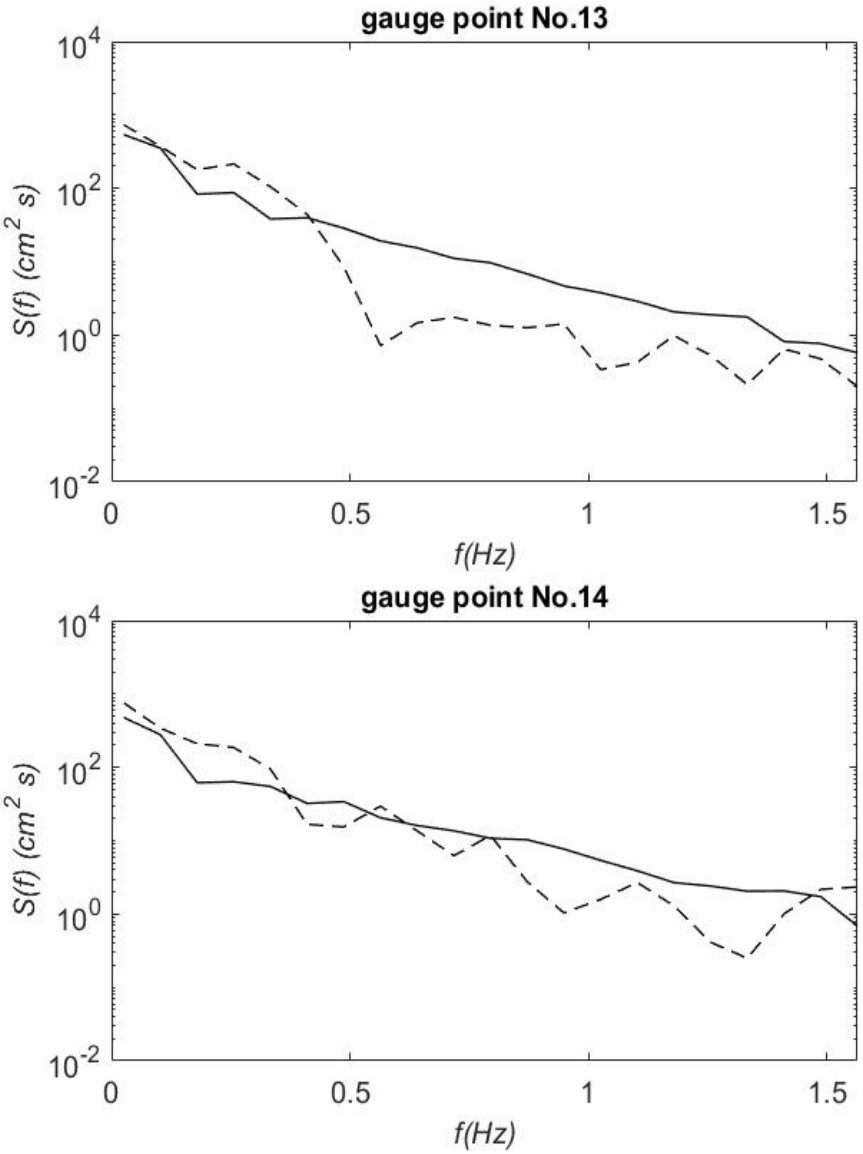

Figure 3.26: Comparison of Model Results and Experiment Data From NEES Tsunami and Swell Experiment(Soliton). Experiment Data (-), Model of Kaihatu & Kirby (- -). (Top) Spectra at x=3476 cm (d=0.85 m); (Bottom) x=3657 cm (d=0.78 m).

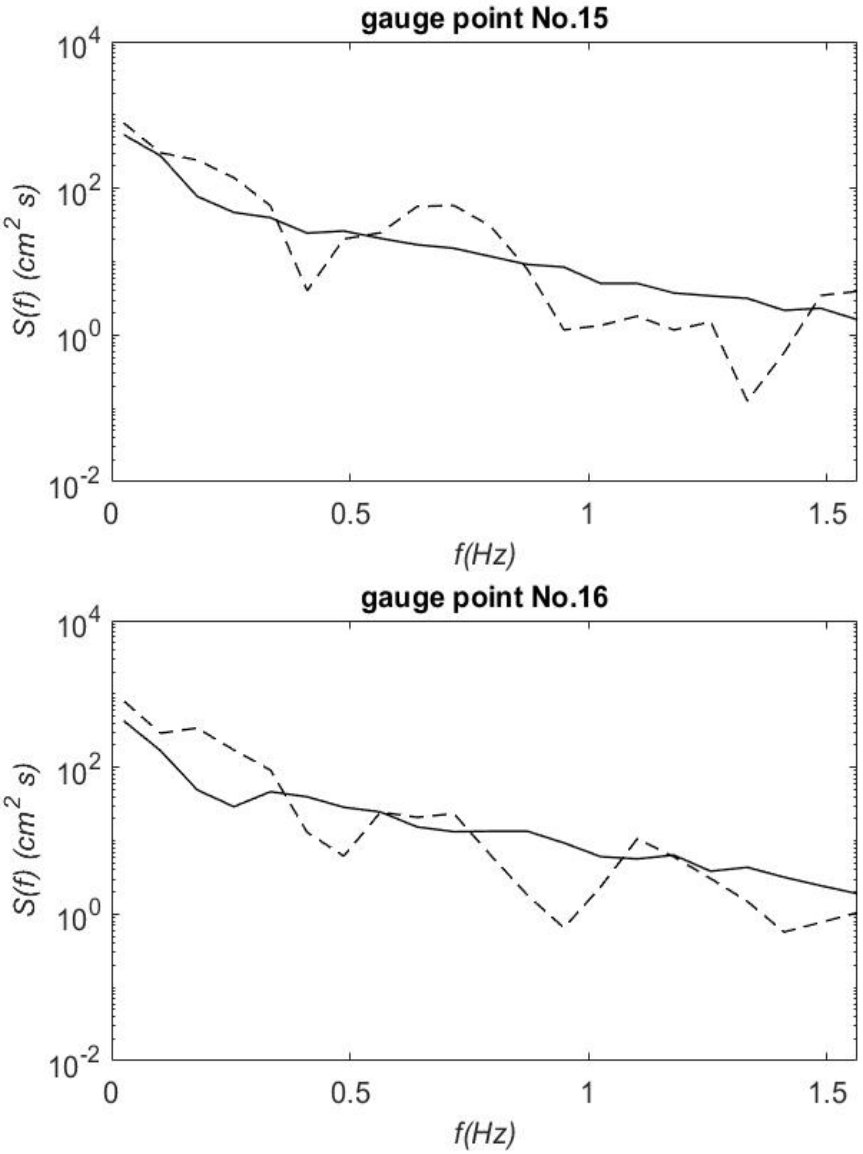

Figure 3.27: Comparison of Model Results and Experiment Data From NEES Tsunami and Swell Experiment(Soliton). Experiment Data (-), Model of Kaihatu & Kirby (- -). (Top) Spectra at x=3840 cm (d=0.70 m); (Bottom) x=4035 cm (d=0.62 m).

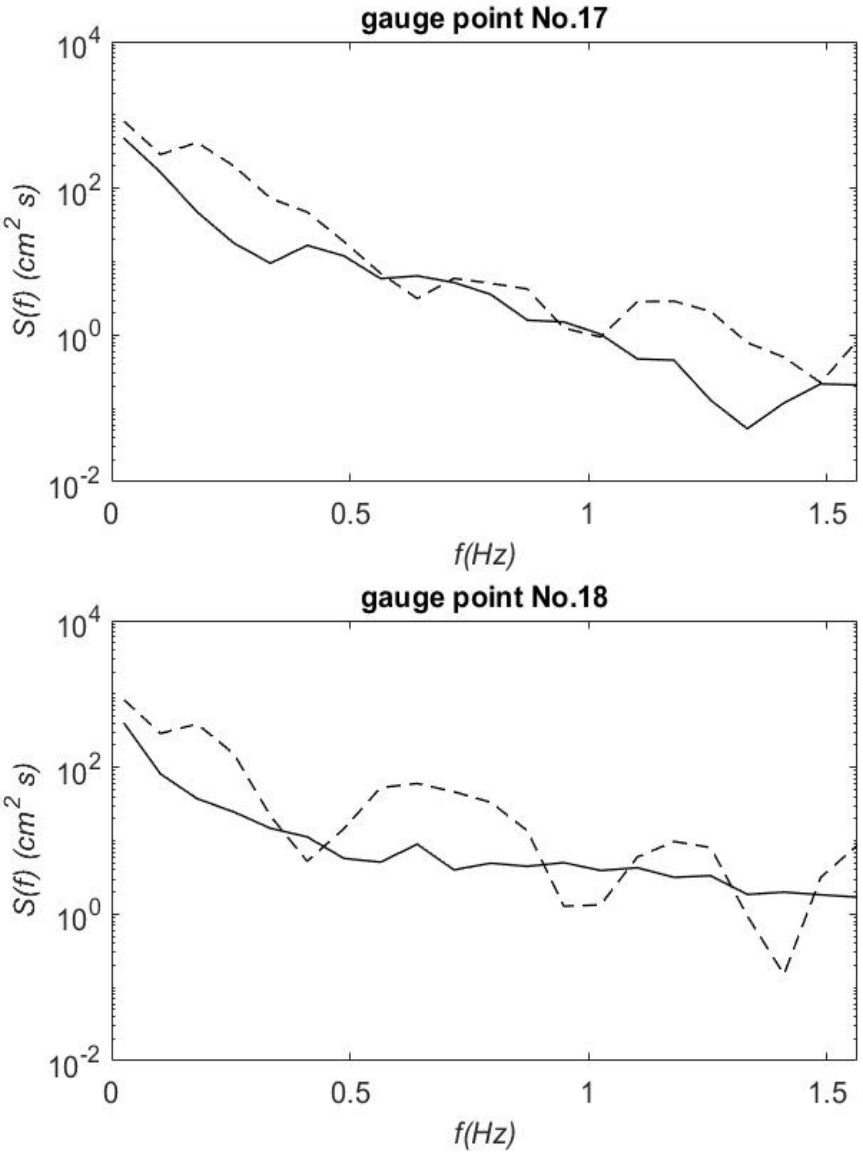

Figure 3.28: Comparison of Model Results and Experiment Data From NEES Tsunami and Swell Experiment(Soliton). Experiment Data (-), Model of Kaihatu & Kirby (- -). (Top) Spectra at x=4198 cm (d=0.55 m); (Bottom) x=4399 cm (d=0.47 m).

3.3 Experiment 2: Set The Wave Height of Soliton 0.7 m

In this section, the spectra for data obtained in the Experiment 2 and the prediction of the mild slope model are presented for comparison. There are a total of eight trials in this experiment. Trial 1 is the measurement of pure soliton, exactly the same data as that in Experiment 1. The remaining trials are the measurement of soliton plus random wave. As mentioned in the experiment intro-

duction, the only difference between Experiment 2 and Experiment 1 is that the wave amplitude of soliton in Experiment 2 is 0.7 m, which is smaller than that in Experiment 1.

As is discussed in the last section, the addition of soliton in random wave field changes the energy density distribution in frequency domain. From Figure 3.11 to Figure 3.19, the energy density in infragravity and swell area is increased. The performance of the model simulation for soliton plus random wave is not as good as that for purely random wave. It is a rational conjecture that the amplitude of the soliton is one of the reasons for the poorer performance of model. Hence, the data of Experiment 2 is simulated by the model to verify this point.

The comparisons between model results and data of Trial 2 are shown from Figure 3.29 to Figure 3.37. The spectra of the data have not changed as much as the data of Experiment 1. It is likely that the energy added to the infragravity and swell area is also not as much as that in Experiment 1 because of the smaller amplitude of soliton. It is obvious that the model does better than in Experiment 1. The model predicts energy density at the peak frequency well. The deviation has not increased until $x = 3657\ cm$. Additionally, the deviation between the model results and the data is smaller than that in Experiment 1 at the lower frequency or in the infragravity area. The error ratio of the prediction of the model in the infragravity area is around 3% in Trial 2 of Experiment 2. However, it is about 13% in Trial 6 of Experiment 1. The performance of the model will be further evaluated in the section 3.5 based on analysis of wave height root mean square and energy in different frequency areas.

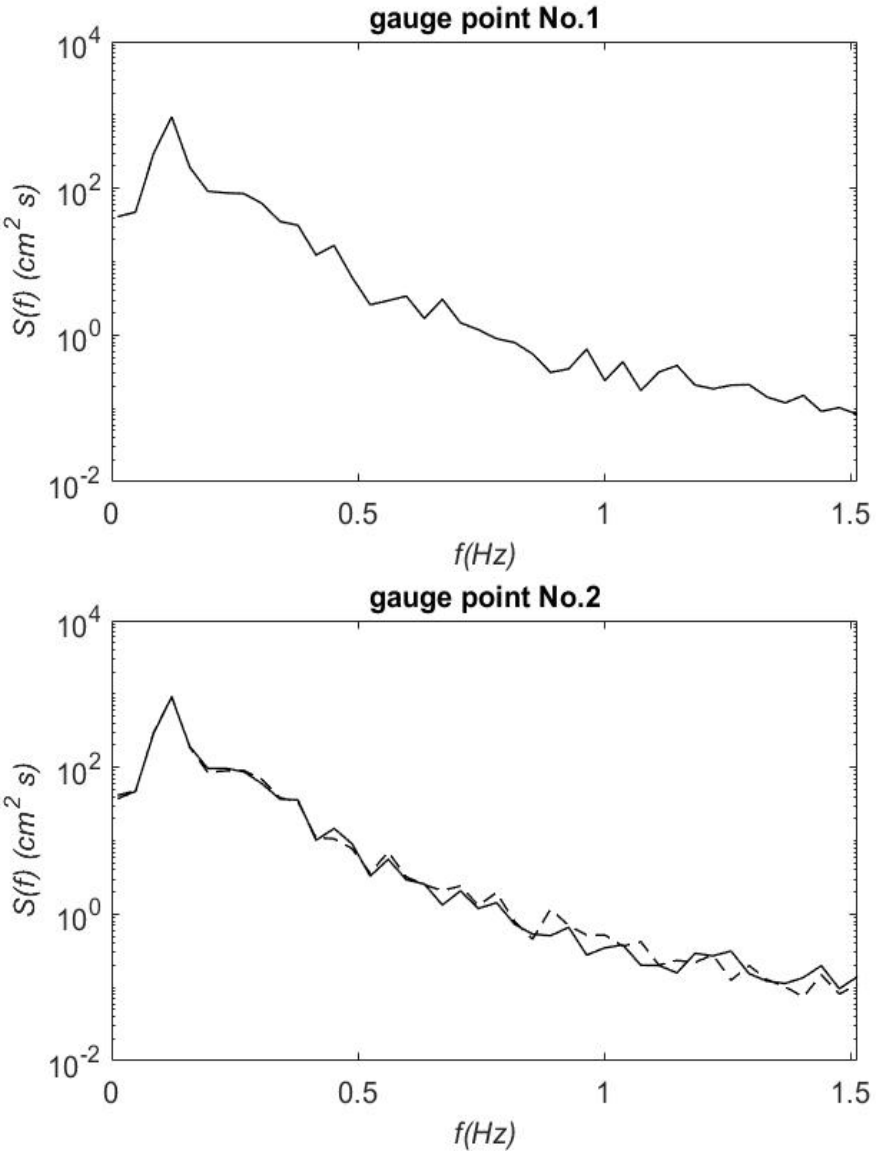

Figure 3.29: Comparison of Model Results and Experiment Data From NEES Tsunami and Swell Experiment(Soliton plus random). Experiment Data (-), Model of Kaihatu & Kirby (- -). (Top) Input Spectra at x=0 cm (d=2 m); (Bottom) x=365 cm (d=2 m).

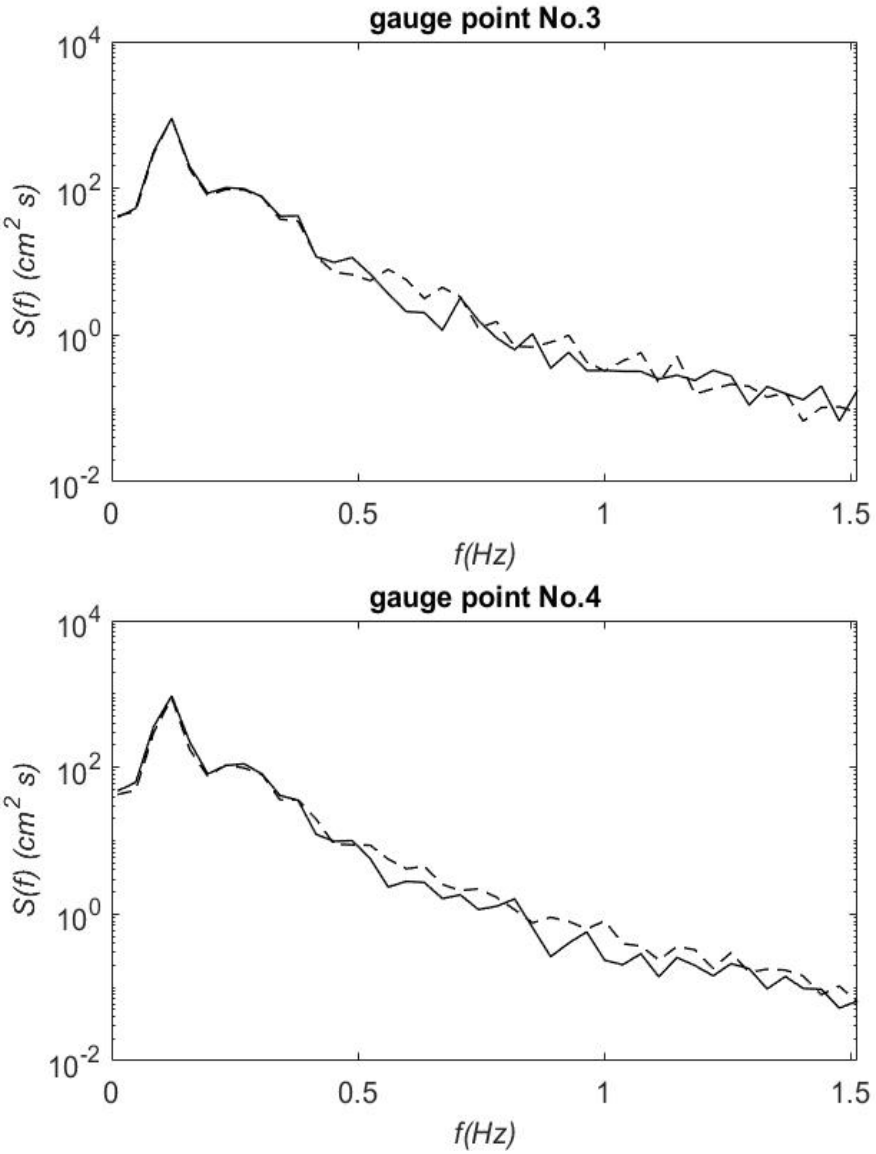

Figure 3.30: Comparison of Model Results and Experiment Data From NEES Tsunami and Swell Experiment(Soliton plus random). Experiment Data (-), Model of Kaihatu & Kirby (- -). (Top) Spectra at x=732 cm (d=2 m); (Bottom) x=1096 cm (d=2 m).

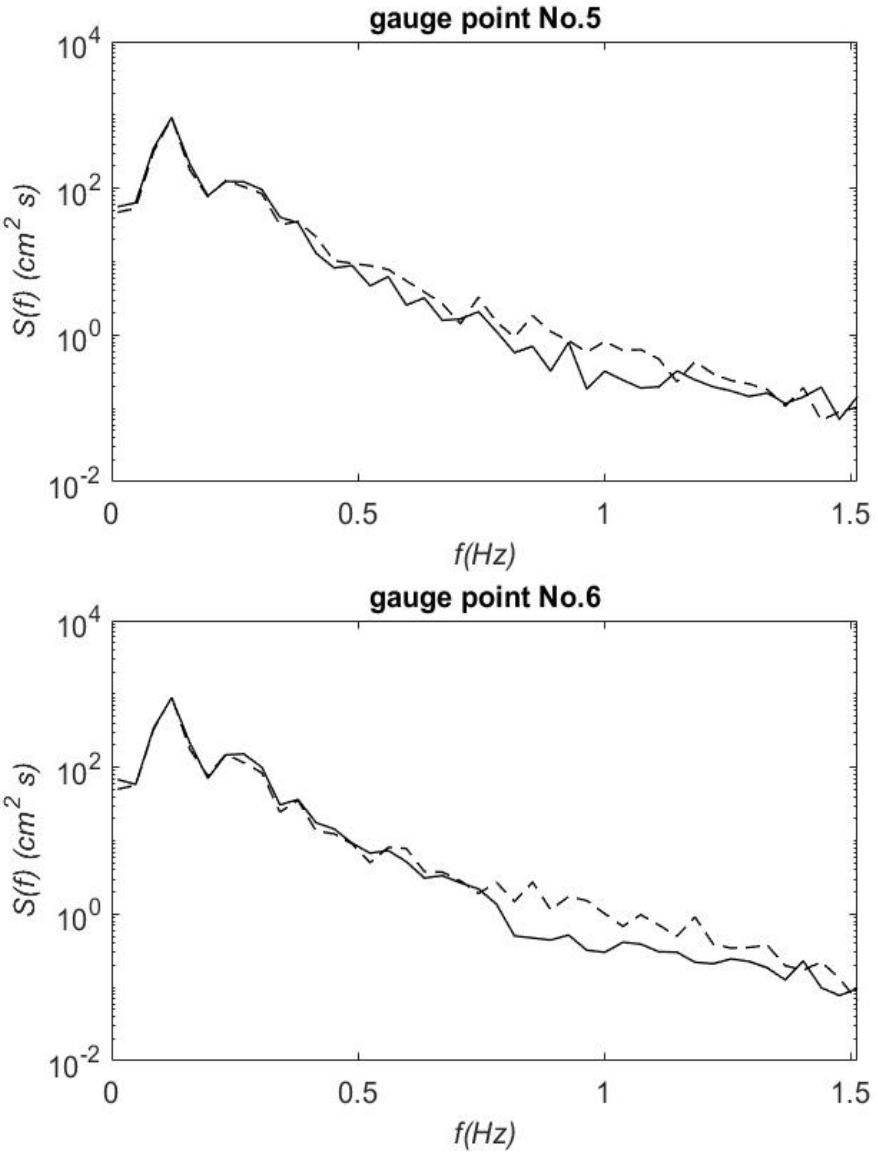

Figure 3.31: Comparison of Model Results and Experiment Data From NEES Tsunami and Swell Experiment(Soliton plus random). Experiment Data (-), Model of Kaihatu & Kirby (- -). (Top) Spectra at x=1462 cm (d=1.69 m); (Bottom) x=1828 cm (d=1.54 m).

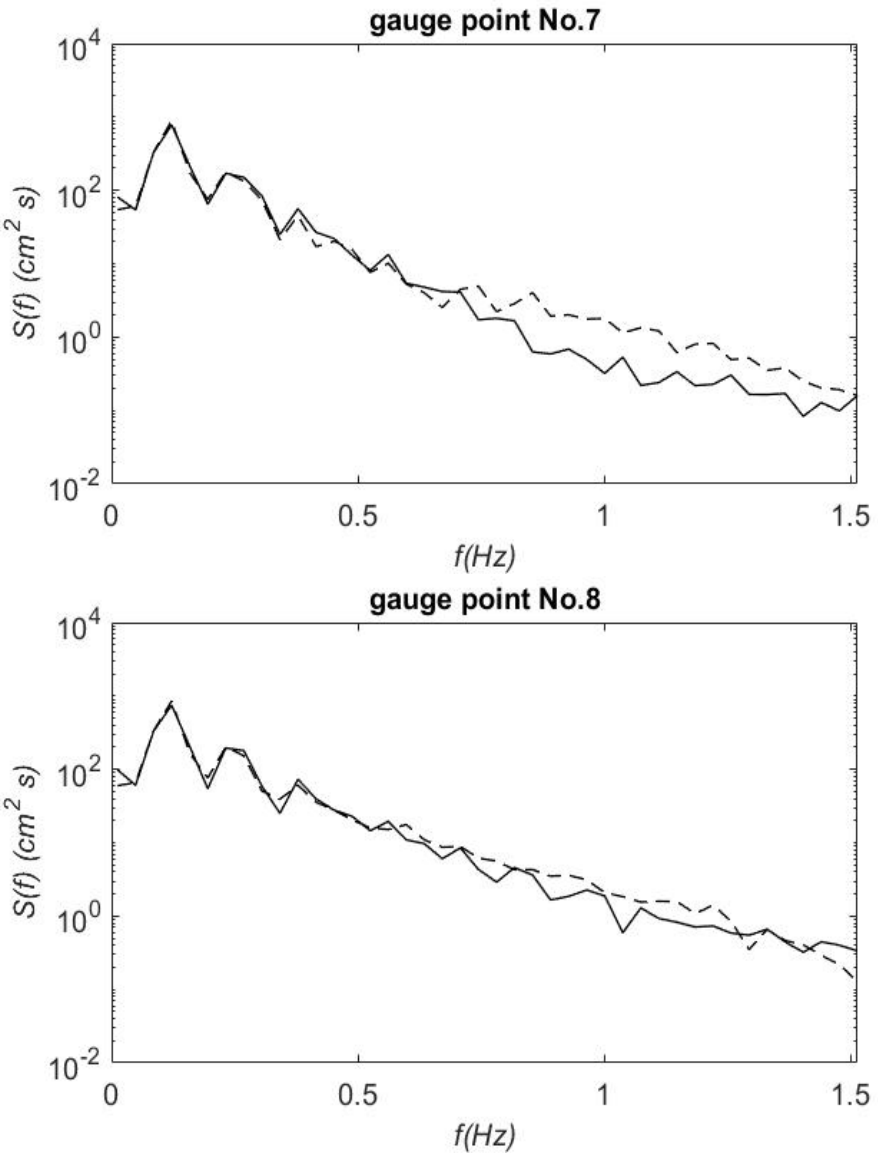

Figure 3.32: Comparison of Model Results and Experiment Data From NEES Tsunami and Swell Experiment(Soliton plus random). Experiment Data (-), Model of Kaihatu & Kirby (- -). (Top) Spectra at x=2194 cm (d=1.39 m); (Bottom) x=2570 cm (d=1.23 m).

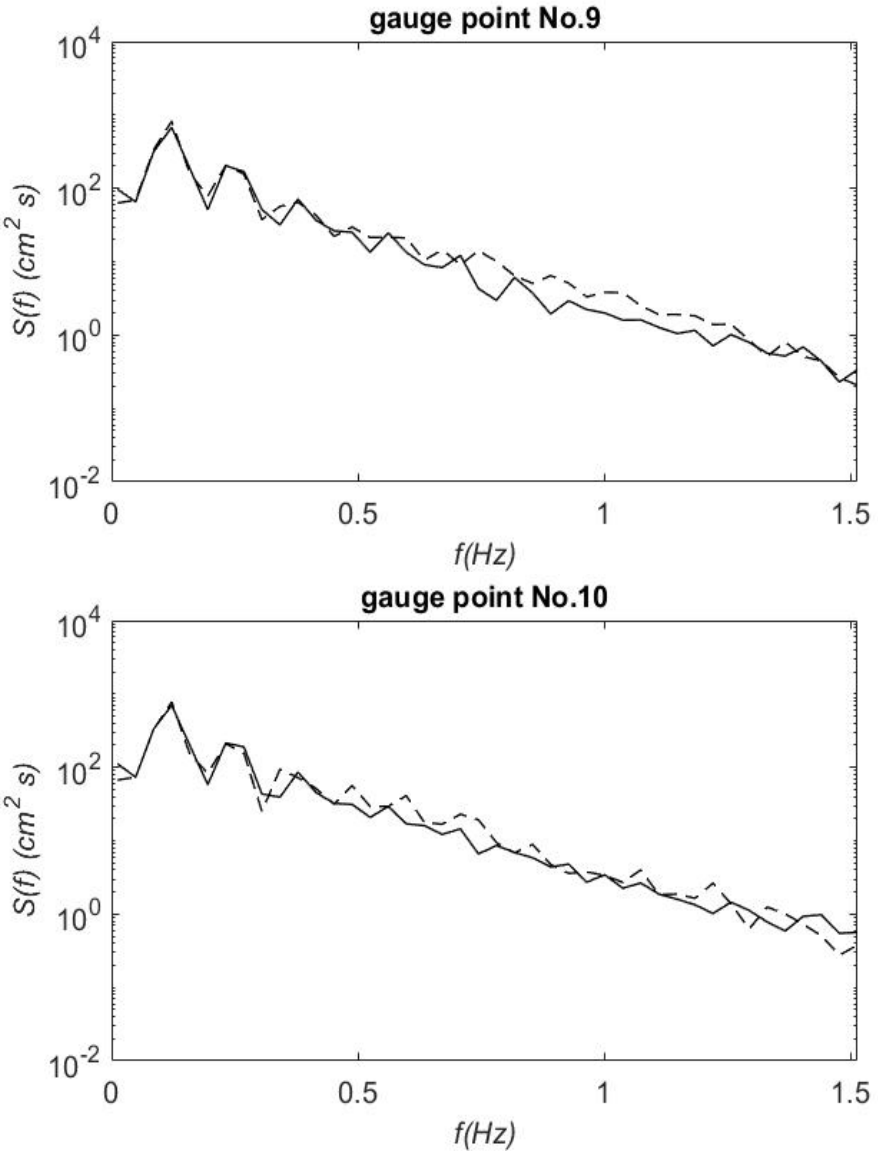

Figure 3.33: Comparison of Model Results and Experiment Data From NEES Tsunami and Swell Experiment(Soliton plus random). Experiment Data (-), Model of Kaihatu & Kirby (- -). (Top) Spectra at x=2741 cm (d=1.16 m); (Bottom) x=2934 cm (d=1.08 m).

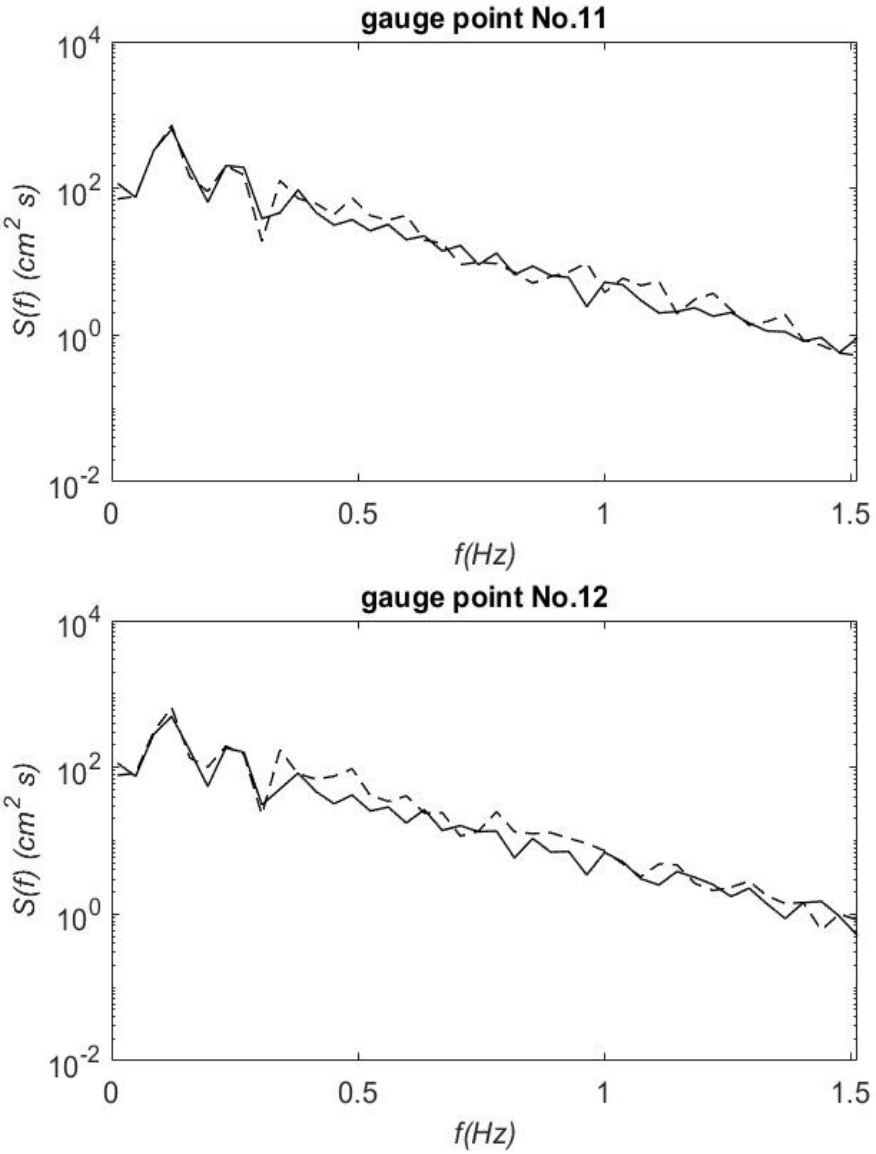

Figure 3.34: Comparison of Model Results and Experiment Data From NEES Tsunami and Swell Experiment(Soliton plus random). Experiment Data (-), Model of Kaihatu & Kirby (- -). (Top) Spectra at x=3108 cm (d=1.01 m); (Bottom) x=3300 cm (d=0.93 m).

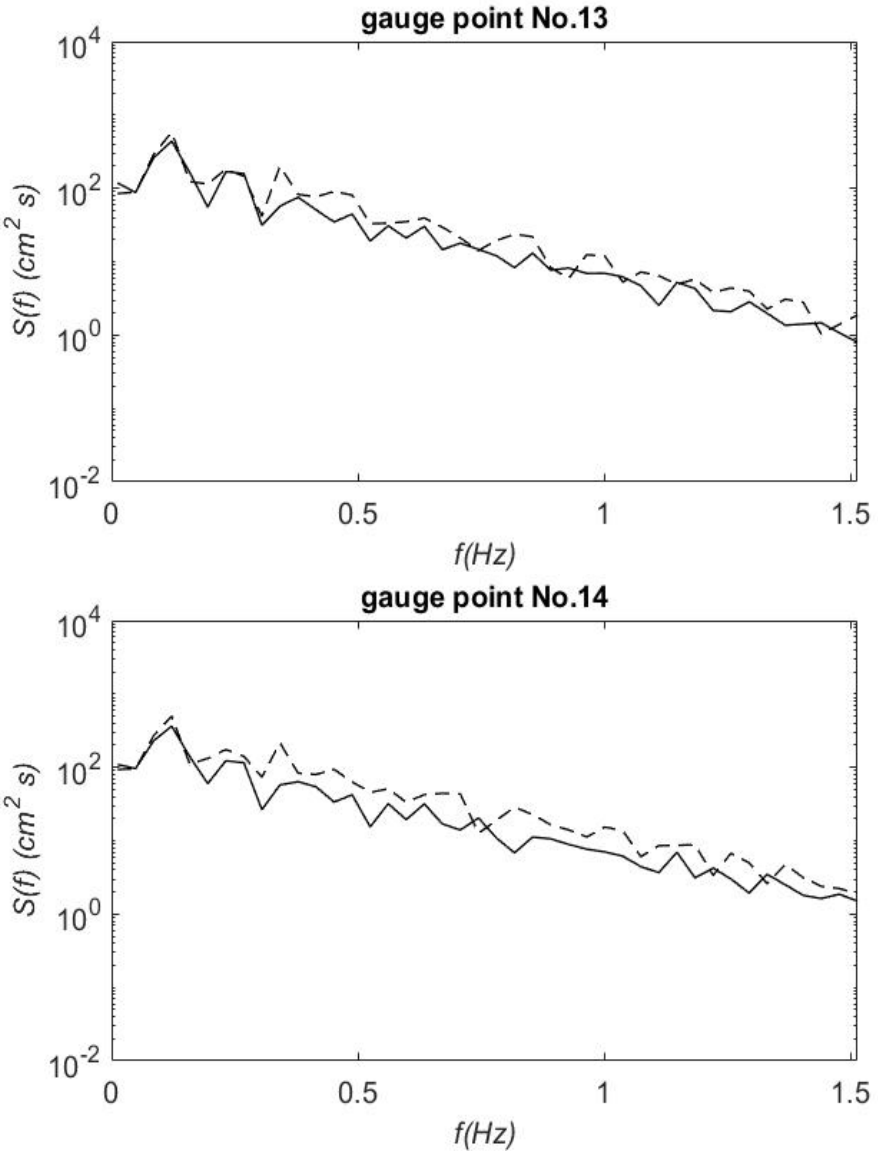

Figure 3.35: Comparison of Model Results and Experiment Data From NEES Tsunami and Swell Experiment(Soliton plus random). Experiment Data (-), Model of Kaihatu & Kirby (- -). (Top) Spectra at x=3476 cm (d=0.85 m); (Bottom) x=3657 cm (d=0.78 m).

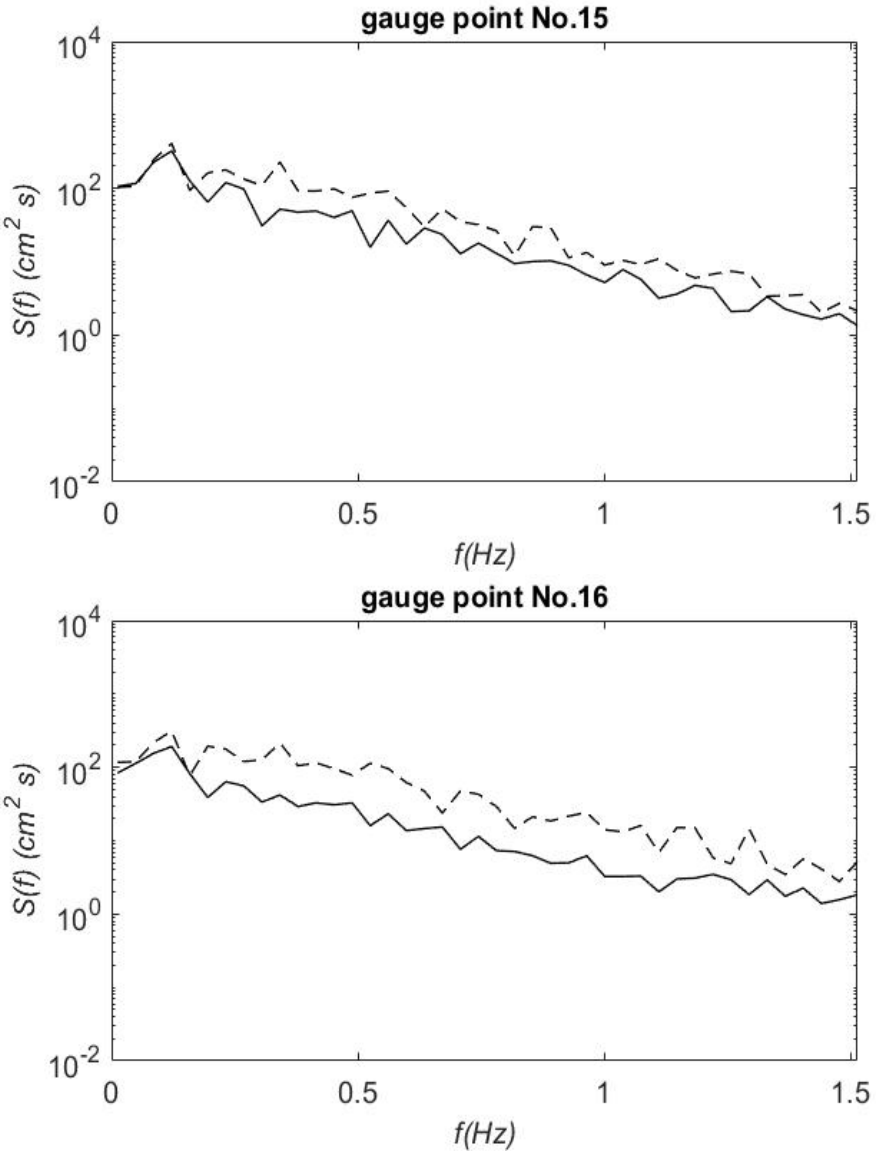

Figure 3.36: Comparison of Model Results and Experiment Data From NEES Tsunami and Swell Experiment(Soliton plus random). Experiment Data (-), Model of Kaihatu & Kirby (- -). (Top) Spectra at x=3840 cm (d=0.70 m); (Bottom) x=4035 cm (d=0.62 m).

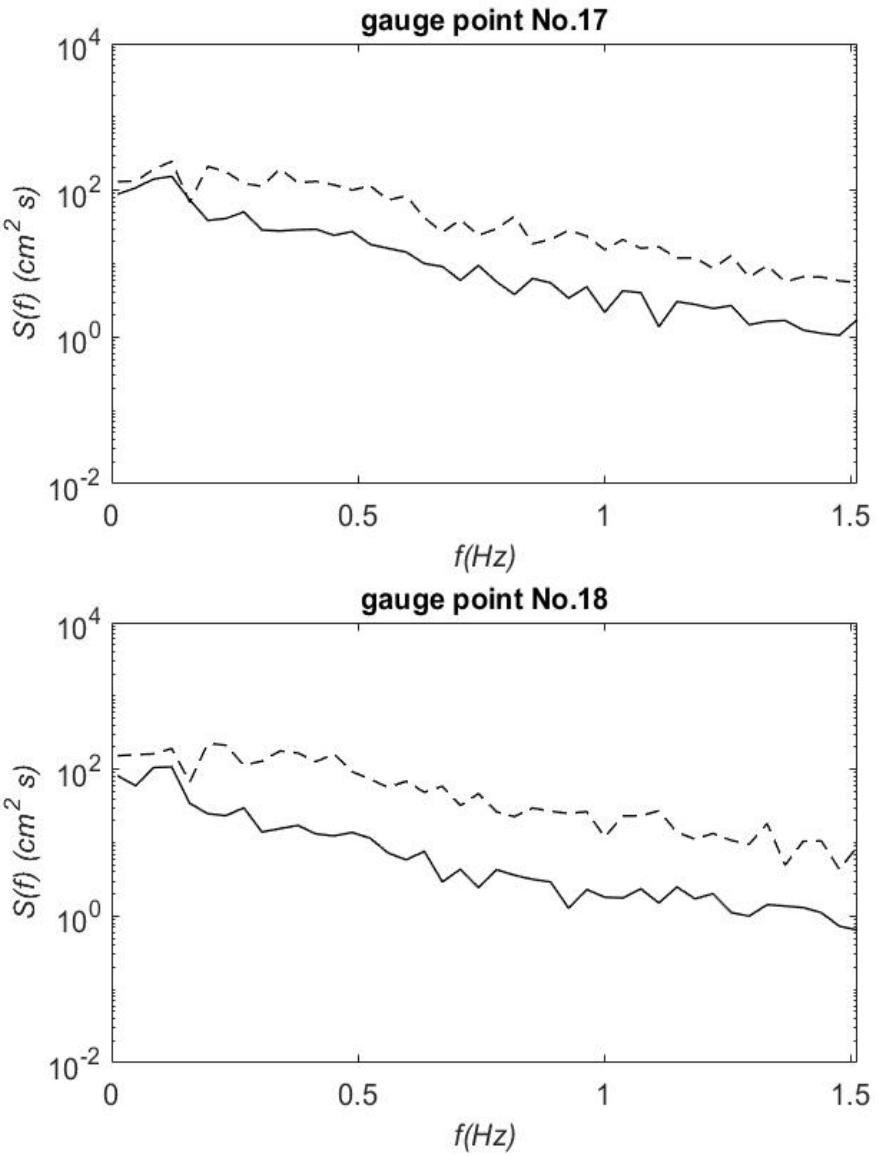

Figure 3.37: Comparison of Model Results and Experiment Data From NEES Tsunami and Swell Experiment(Soliton plus random). Experiment Data (-), Model of Kaihatu & Kirby (- -). (Top) Spectra at x=4198 cm (d=0.55 m); (Bottom) x=4399 cm (d=0.47 m).

3.4 Experiment 3: Set The Wave Height of Soliton 0.5 m

In this section, the spectra for data obtained in the Experiment 3 and the prediction of the mild slope model are presented for comparison. Again, there are eight trials in this experiment. Trial 1 is the measurement of purely soliton, exactly the same data as that in Experiment 1. The other trials are the measurement of soliton plus random wave. As mentioned in the experiment introduction,

the only difference between Experiment 3 and Experiment 1 is that the wave amplitude of soliton in Experiment 3 is 0.5 m, which is also smaller than that in Experiment 2.

The simulation results of Experiment 1 and 2 show that the amplitude of the soliton has a significant influence on the spectra of the wave field and the model performance. When the amplitude of the soliton decreases, the energy added into wave field decreases and the performance of the model becomes better. In Experiment 3, the amplitude of the soliton is reduced to 0.5 m to further verify the influence of the soliton amplitude.

The comparisons between model results and data of Trial 2 are shown from Figure 3.38 to Figure 3.46. From the prediction of energy density at the peak frequency, it is hard to say whether the performance of the model becomes better in general merely from the spectra. The influence of soliton amplitude will be further discussed in the section 3.5.

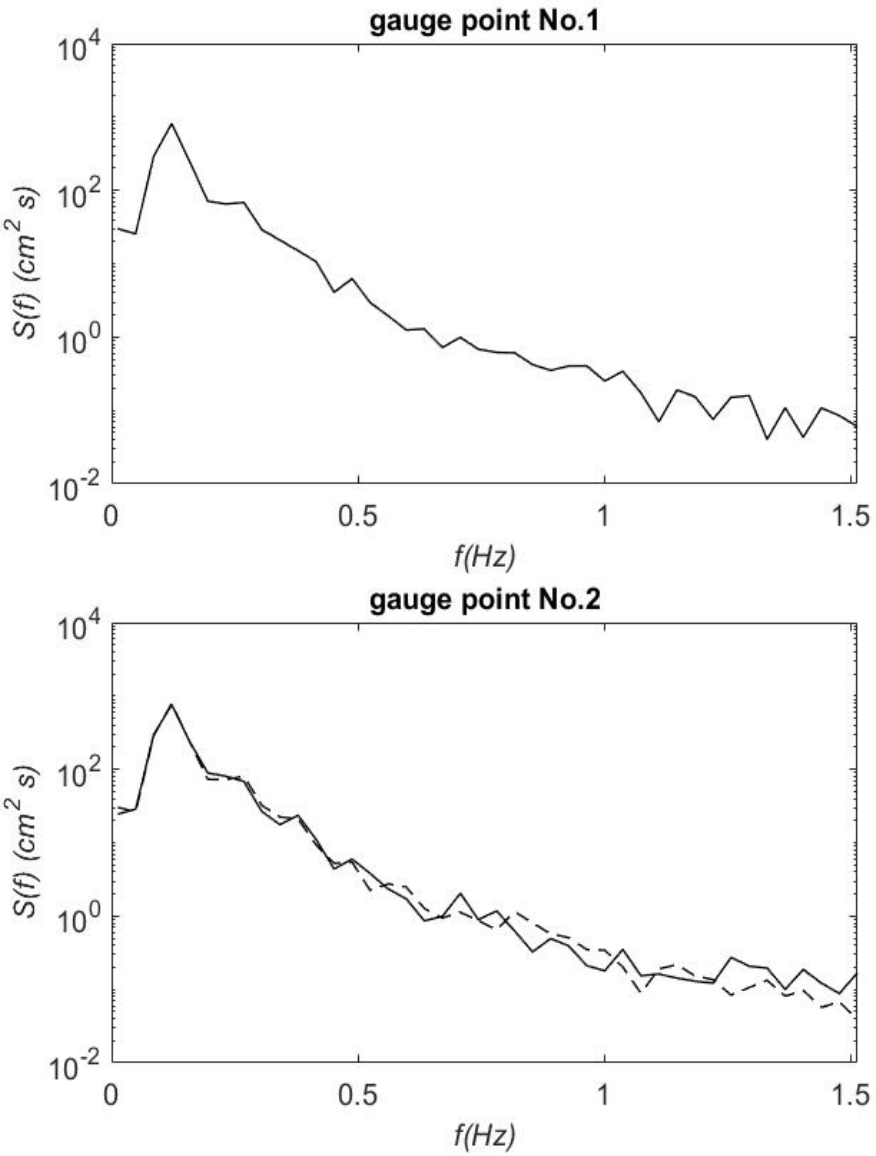

Figure 3.38: Comparison of Model Results and Experiment Data From NEES Tsunami and Swell Experiment(Soliton plus random). Experiment Data (-), Model of Kaihatu & Kirby (- -). (Top) Input Spectra at x=0 cm (d=2 m); (Bottom) x=365 cm (d=2 m).

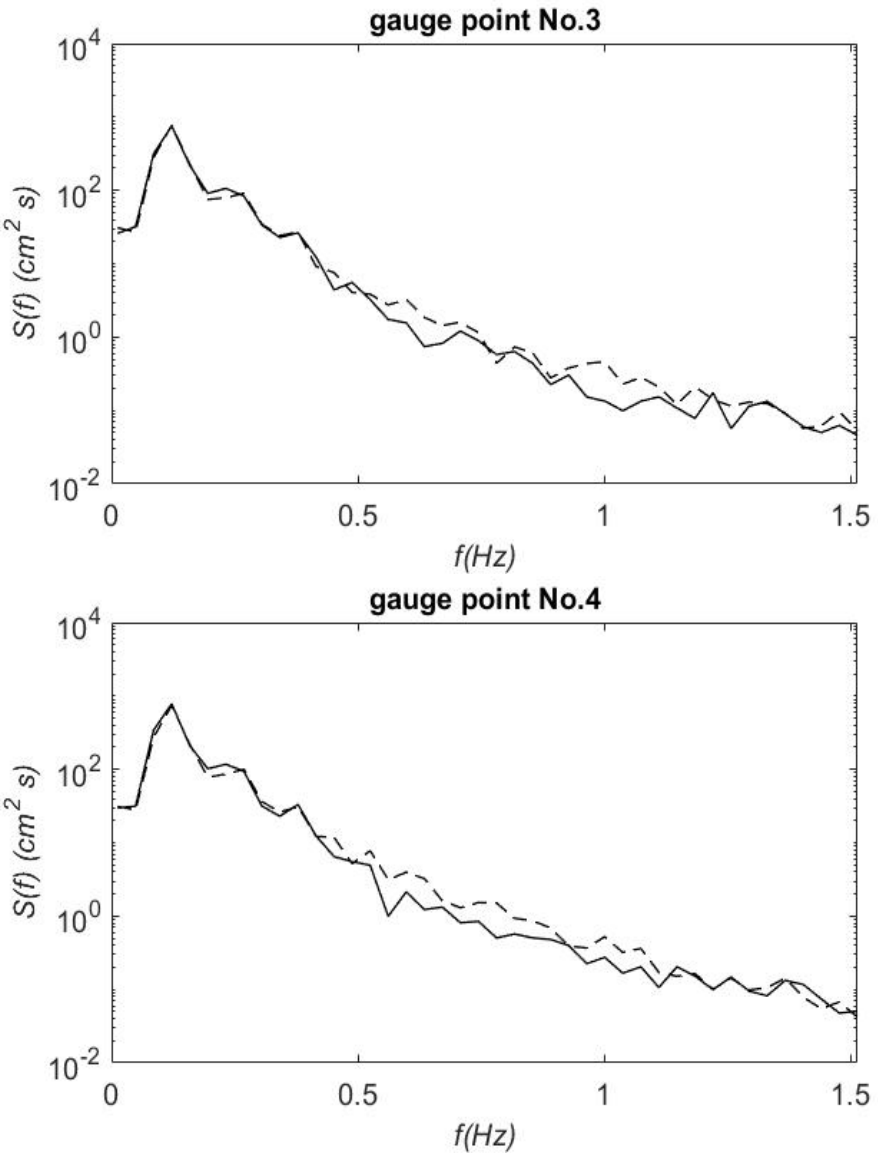

Figure 3.39: Comparison of Model Results and Experiment Data From NEES Tsunami and Swell Experiment(Soliton plus random). Experiment Data (-), Model of Kaihatu & Kirby (- -). (Top) Spectra at x=732 cm (d=2 m); (Bottom) x=1096 cm (d=2 m).

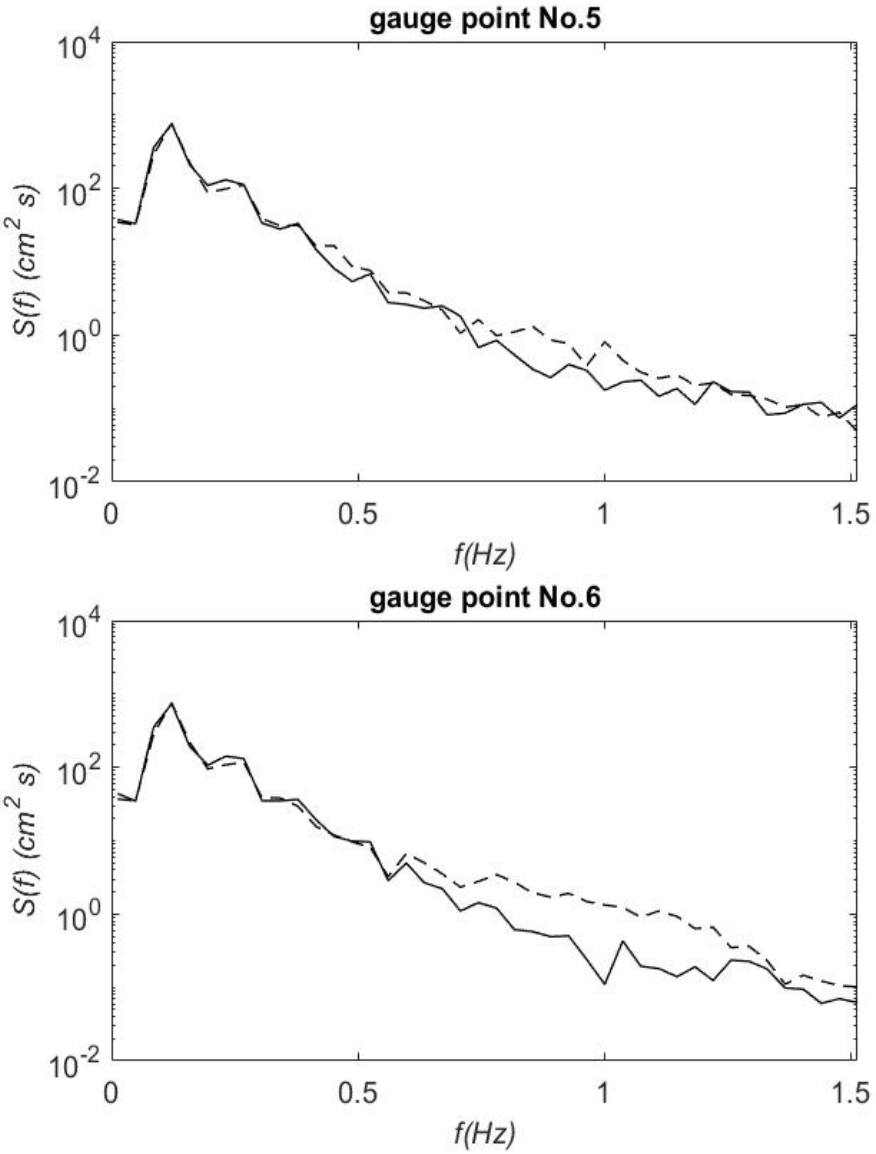

Figure 3.40: Comparison of Model Results and Experiment Data From NEES Tsunami and Swell Experiment(Soliton plus random). Experiment Data (-), Model of Kaihatu & Kirby (- -). (Top) Spectra at x=1462 cm (d=1.69 m); (Bottom) x=1828 cm (d=1.54 m).

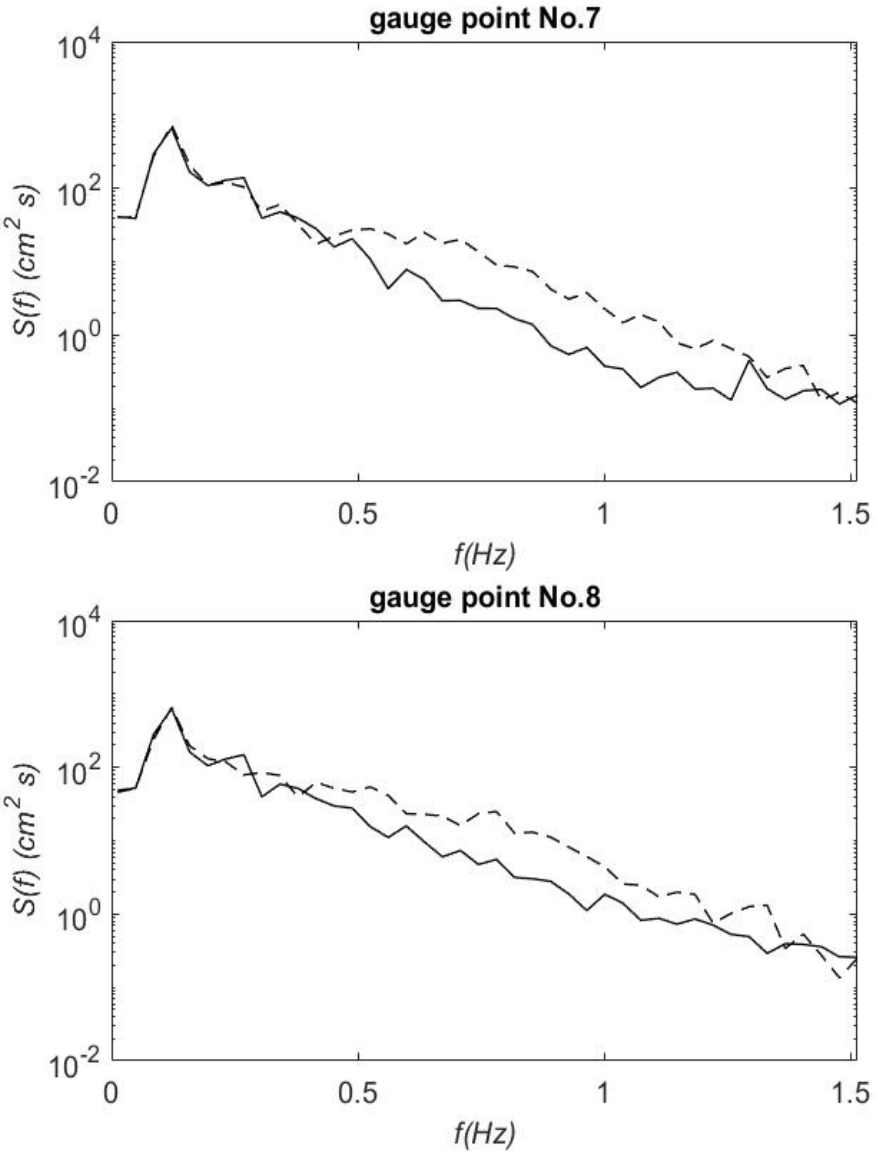

Figure 3.41: Comparison of Model Results and Experiment Data From NEES Tsunami and Swell Experiment(Soliton plus random). Experiment Data (-), Model of Kaihatu & Kirby (- -). (Top) Spectra at x=2194 cm (d=1.39 m); (Bottom) x=2570 cm (d=1.23 m).

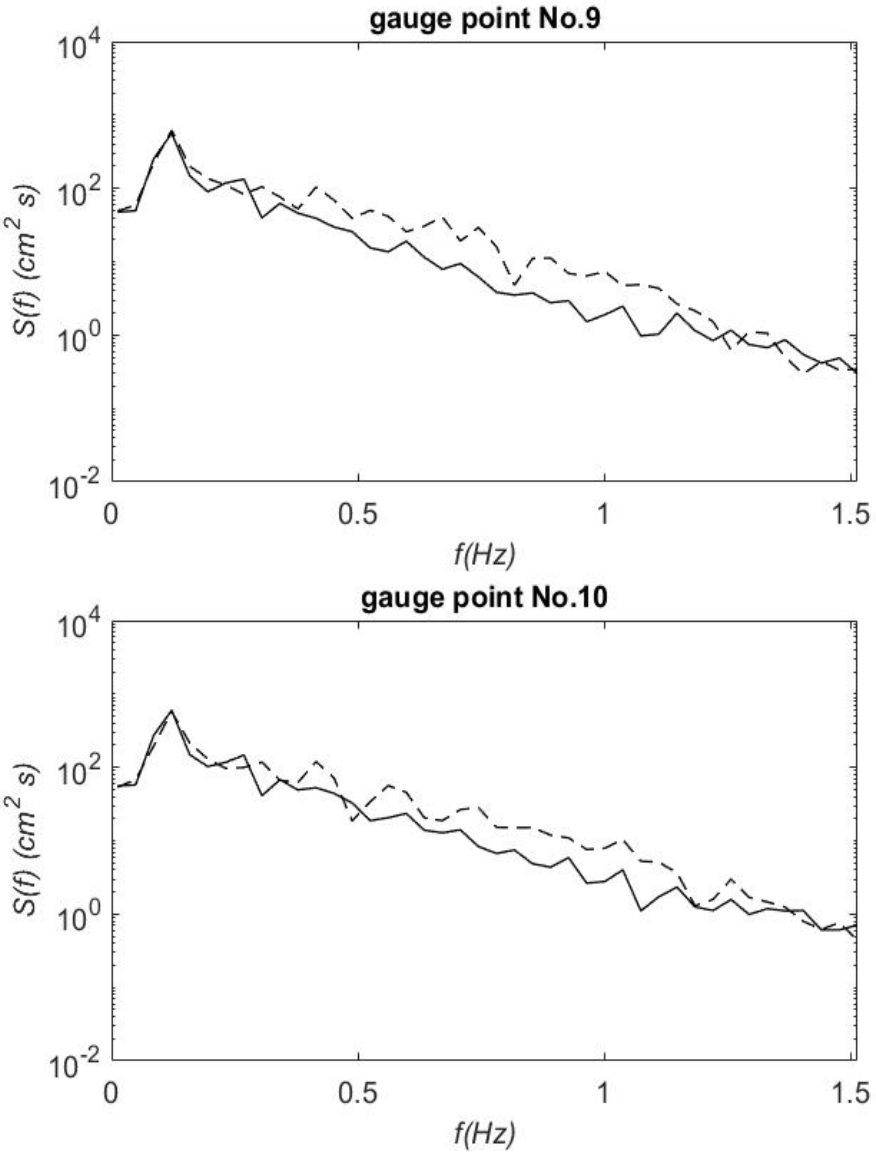

Figure 3.42: Comparison of Model Results and Experiment Data From NEES Tsunami and Swell Experiment(Soliton plus random). Experiment Data (-), Model of Kaihatu & Kirby (- -). (Top) Spectra at x=2741 cm (d=1.16 m); (Bottom) x=2934 cm (d=1.08 m).

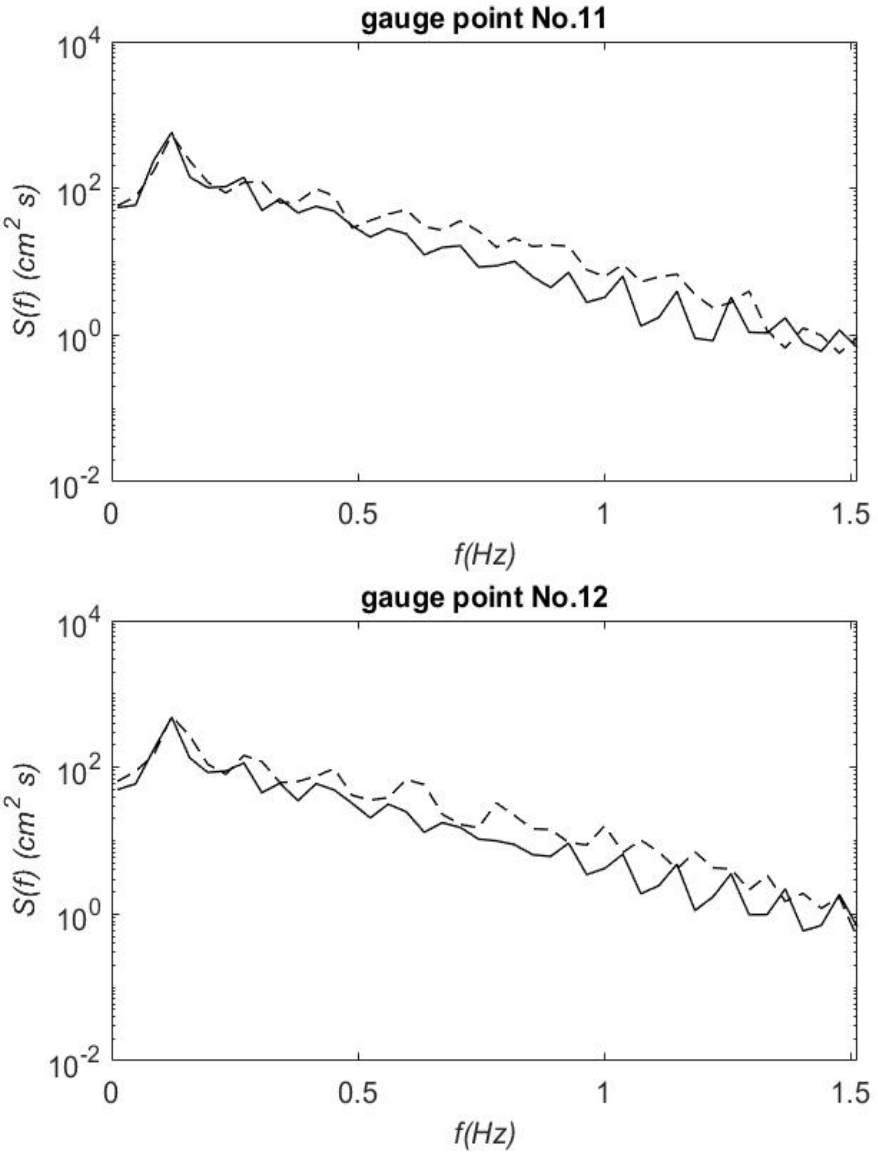

Figure 3.43: Comparison of Model Results and Experiment Data From NEES Tsunami and Swell Experiment(Soliton plus random). Experiment Data (-), Model of Kaihatu & Kirby (- -). (Top) Spectra at x=3108 cm (d=1.01 m); (Bottom) x=3300 cm (d=0.93 m).

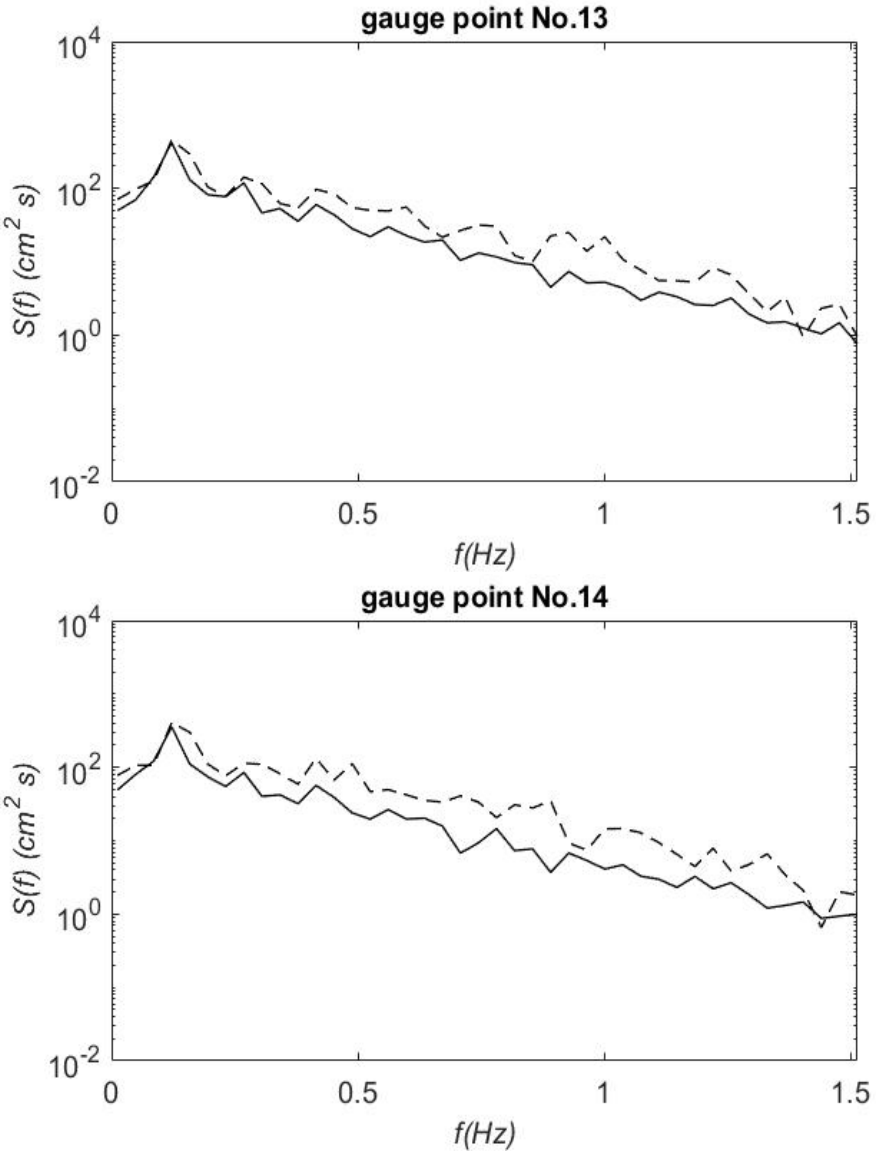

Figure 3.44: Comparison of Model Results and Experiment Data From NEES Tsunami and Swell Experiment(Soliton plus random). Experiment Data (-), Model of Kaihatu & Kirby (- -). (Top) Spectra at x=3476 cm (d=0.85 m); (Bottom) x=3657 cm (d=0.78 m).

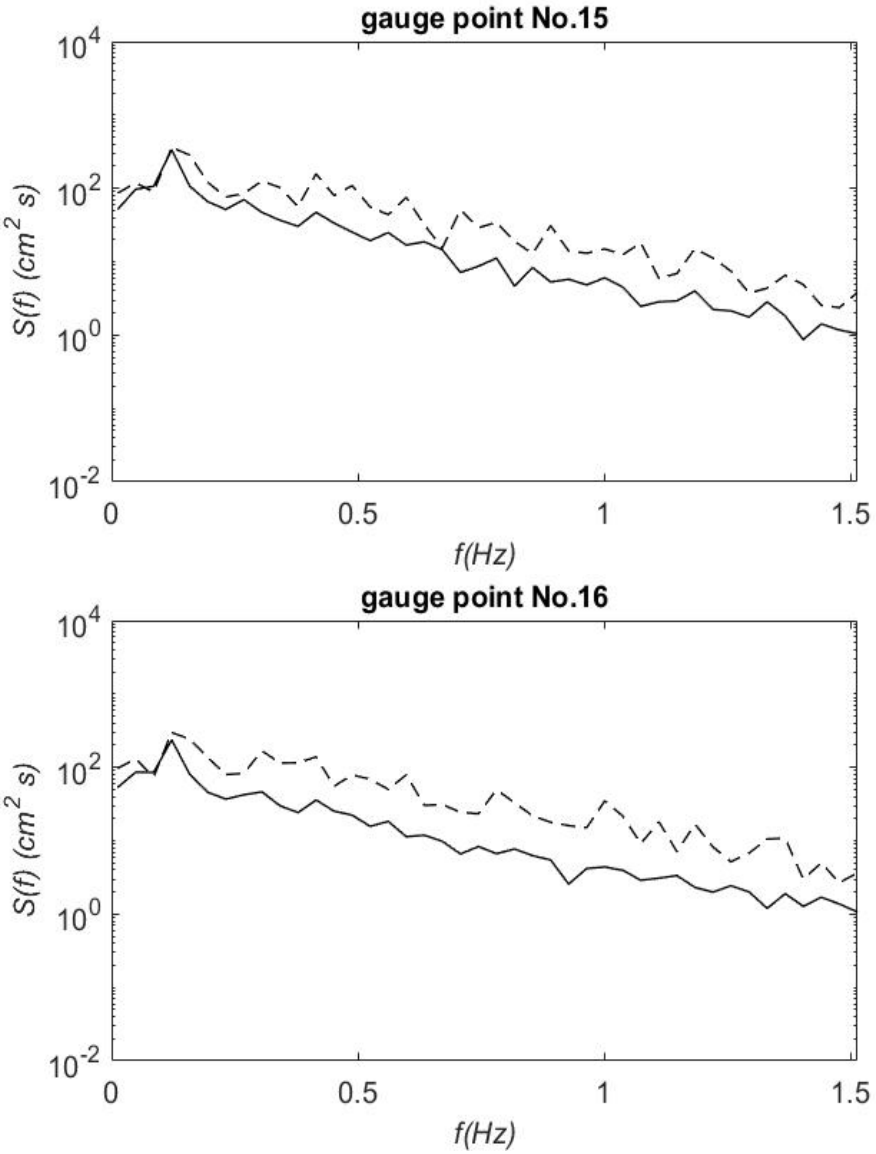

Figure 3.45: Comparison of Model Results and Experiment Data From NEES Tsunami and Swell Experiment(Soliton plus random). Experiment Data (-), Model of Kaihatu & Kirby (- -). (Top) Spectra at x=3840 cm (d=0.70 m); (Bottom) x=4035 cm (d=0.62 m).

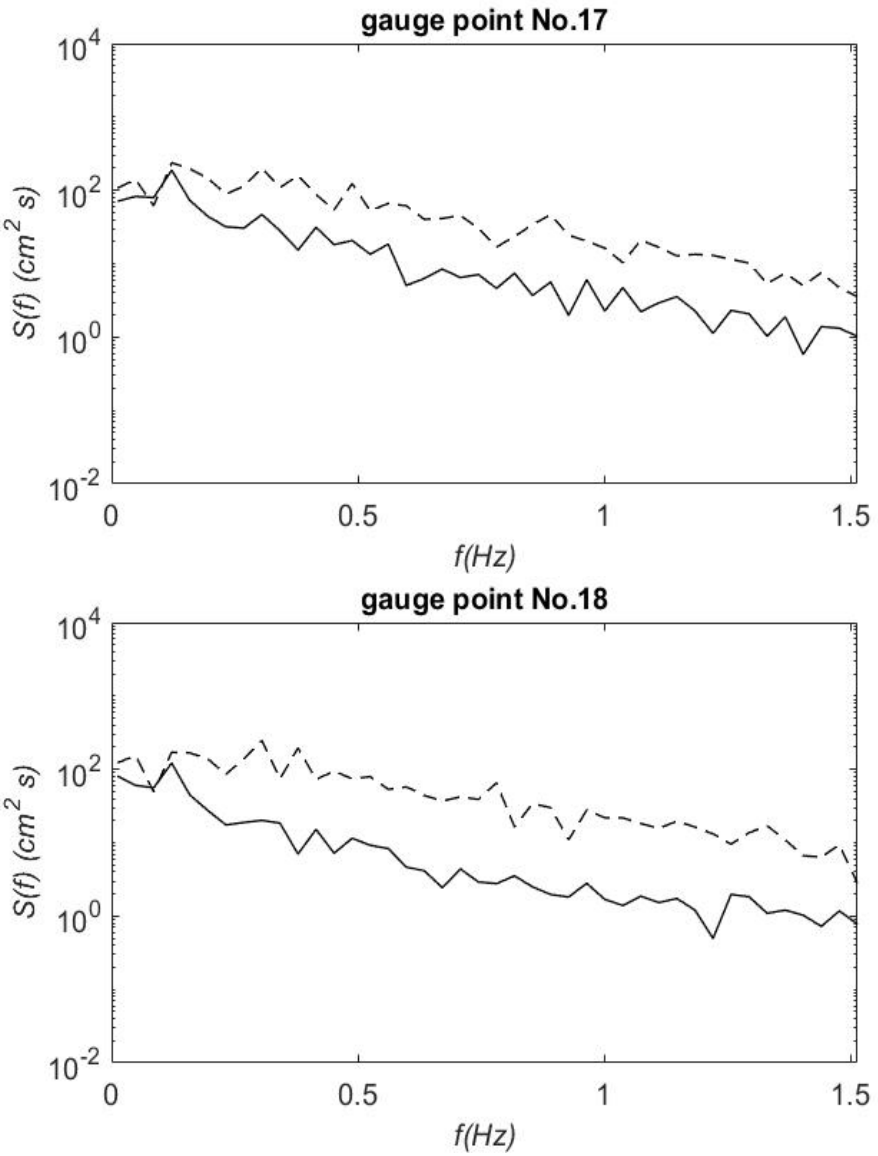

Figure 3.46: Comparison of Model Results and Experiment Data From NEES Tsunami and Swell Experiment(Soliton plus random). Experiment Data (-), Model of Kaihatu & Kirby (- -). (Top) Spectra at x=4198 cm (d=0.55 m); (Bottom) x=4399 cm (d=0.47 m).

3.5 H_{rms}, Skewness and Asymmetry and Wave Energy in Three Areas

In the sections before, the spectra for the experiments data and model simulation have been present and compared. It is found that the amplitude of the soliton has a significant influence on the spectra for wave field and the model simulation. However, statistical parameters from experiment data and model prediction should be compared to verify the influence of the soliton amplitude and

to evaluate the performance of the model.

In this section, the root mean squares of wave heights (H_{rms}), skewness and asymmetry of measurement and simulation results are calculated and compared based on the first 128 frequency components in each trial. The frequency scale is divided into three areas, infragravity area ($0 \leq f \leq \frac{f_{peak}}{2}$), swell area ($\frac{f_{peak}}{2} \leq f \leq \frac{3f_{peak}}{2}$) and sea area ($\frac{3f_{peak}}{2} \leq f$), and the energy in each area is calculated for both experiment data and model results. In order to show the performance of the model, the x axis is set to be the energy of data and the y axis is set to be the energy of model result. The better the model performs, the points will be closer to the line $y = x$.

As is shown in the top of Figure 3.47, the model does predict the H_{rms} of the wave field well for the purely random wave field. The shoaling process is described by the model correctly. However, the model over-predicts the root-mean-square of the wave height in shallow water depths. There is a possibility that the dissipation is not enough. Additionally, the truncation of the data could account for some over-prediction. Combined with the energy scatter diagrams (Figure 3.51), the model over-predicts the energy in the sea area, but under-predicts the energy in the infragravity area and performs highly accurate in the swell area.

From Figure 3.47 to Figure 3.50, the prediction of H_{rms} for the soliton plus random wave is also not good in shallow water depths. Around the 1.40 m water depth, the model results continue to grow up, which performs as shoaling. The dissipation mechanism seems to lose validation. From the plots of H_{rms} for the model results, it can be inspected that the dissipation mechanism used in the model actually is unable to predict the breaking of the soliton plus random wave. From Figure 3.53 to Figure 3.56, the plots of H_{rms} for the Experiment 2 are presented. Figure 3.58 to Figure 3.61 are the plots for the Experiment 3. The deviation between the model results and the data about root-mean-square of wave height starts to increase from about 1.40 m of the water depth in Experiment 1. Respectively, it starts from about 1.01 m of the water depth in Experiment 2 and Experiment 3. The performance of the model seems to be improved when the wave height of the soliton is decreased.

According to Thornton and Guza (1983), their dissipation model is built based on the assump-

tion that the spectrum of the wave field follows Raleigh distribution. They created a distribution of breaking wave heights which is expressed as a weighting of the Rayleigh distribution for all waves. Waves with higher amplitudes have higher possibility to break. However, for the soliton, which is a single wave, the Raleigh distribution and breaking possibility distribution do not make sense. That may be the main reason for the under-prediction of H_{rms}.

The energy scatter diagrams are meant to show the general performance of the model in the infragravity area, swell area and sea area, respectively. In the Figure 3.51, the plots are based on the simulation result and data for Trial 1 in Experiment 1, where the wave field is purely random. In the infragravity area, the points are mostly close to the line with slope one, but the model under-predicts the energy in this area at most gauges. In the swell area, where energy evolution happens more evidently, the model performs good and the points distribute around the line with slope one. In the sea area, the energy is over-predicted at most points.

There are seven trials for soliton plus random wave in each experiment. The energy of infragravity, swell and sea area are calculated and put into the diagram for each experiment respectively. Therefore, the model performance in each area for each experiment can be showed clearly.

Figure 3.52 shows the energy scatter diagram for soliton plus random wave in Experiment 1. In the infragravity area, the model predicts the data well when the energy is less than $5cm^2$, but the points are more divergent when the infragravity energy is larger than $5cm^2$. The performance of model is not optimistic. In the swell area, the points are concentrated around the line with slope one. It can be said that the model performance in the swell area for soliton plus random wave is quite similar to that for purely random wave. In the sea area, the points are over the $y = x$ line. Compared with the diagrams for purely random wave, the model performance in the infragravity area and sea area is influenced by the soliton and the accuracy of prediction decreases significantly. However, the model still performs well in the swell area. This also agrees with the conclusion reached from the inspection of spectra.

Figure 3.57 shows the simulation performance for Experiment 2. In the diagram for infragravity energy, the points are closer to the line $y = x$ than that in the infragravity energy for

Experiment 1 and the points are less divergent than that in Experiment 1. The infragravity energy in most gauges of Experiment 2 is less than $5cm^2$. In the swell area, the model performance is quite similar to that for Experiment 1. Figure 3.62 shows the energy scatter diagrams for Experiment 3. The performance of the model in the infragravity area is improved and the points lump around the line with slope 1. The infragravity energy of every gauge is less than $5cm^2$ in Experiment 3. The points in the sea area also lump together. It can be concluded from the analysis above that the as the amplitude of the soliton increases, the influence on the wave field will be aggravated and the model performance will get worse, especially in the infragravity area and sea area.

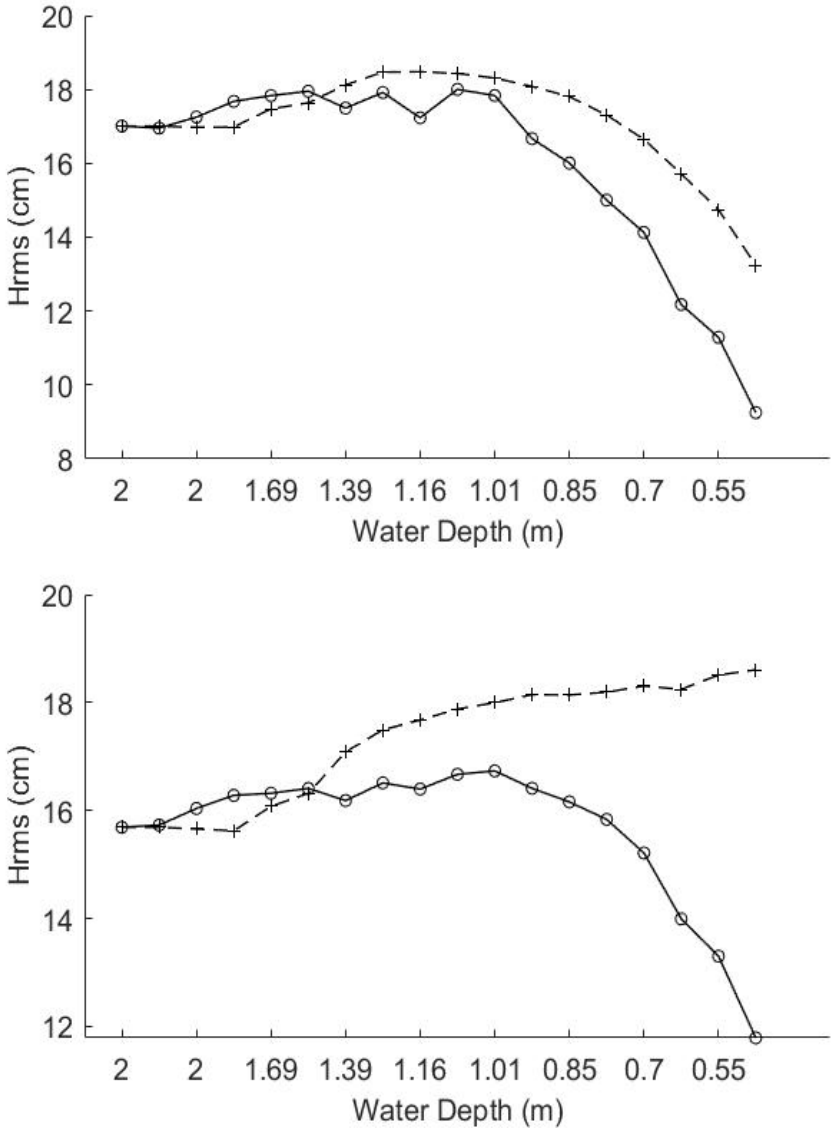

Figure 3.47: Variation of H_{rms} of Model Results and Experiment Data From NEES Tsunami and Swell Experiment with Depth. Experiment Data (○), Model of Kaihatu & Kirby (+). (Top) Purely Random; (Bottom) Solitan plus Random (Experiment 1, Trial 3).

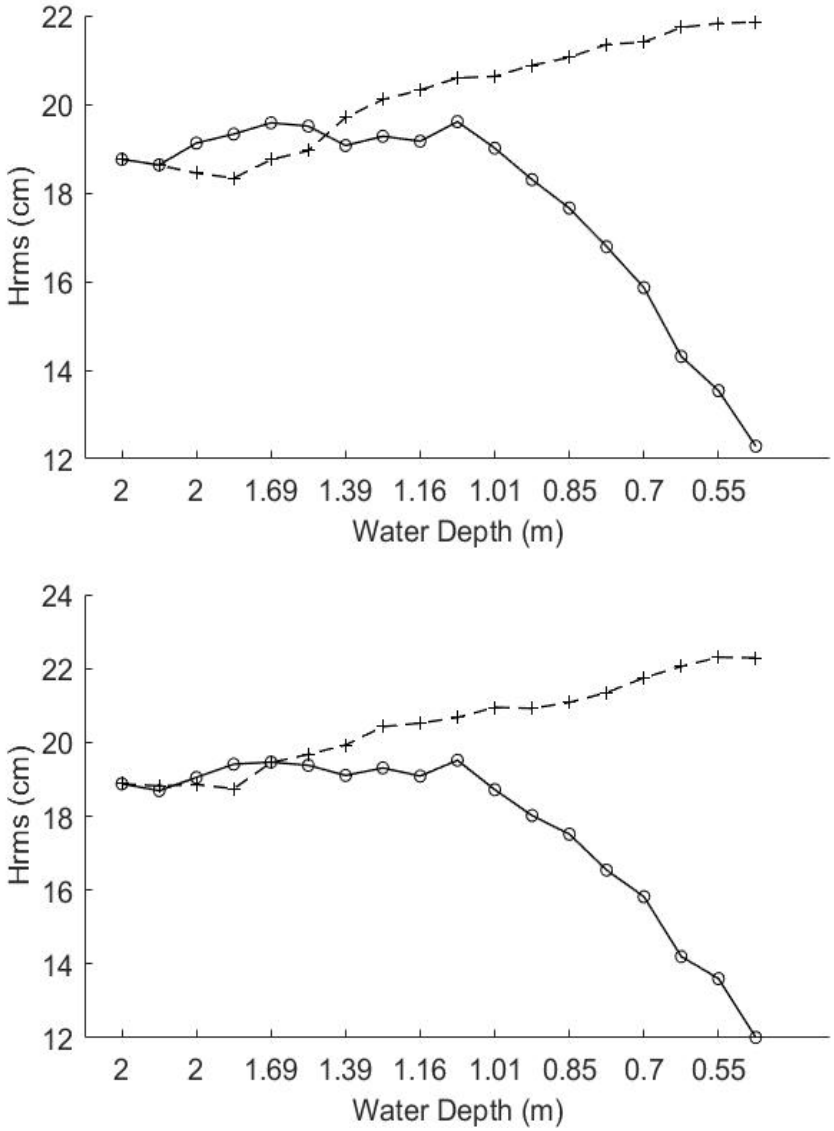

Figure 3.48: Variation of H_{rms} of Model Results and Experiment Data From NEES Tsunami and Swell Experiment with Depth. Experiment Data (○), Model of Kaihatu & Kirby (+). (Top) Soliton plus Random (Experiment 1, Trial 4); (Bottom) Solitan plus Random (Experiment 1, Trial 5).

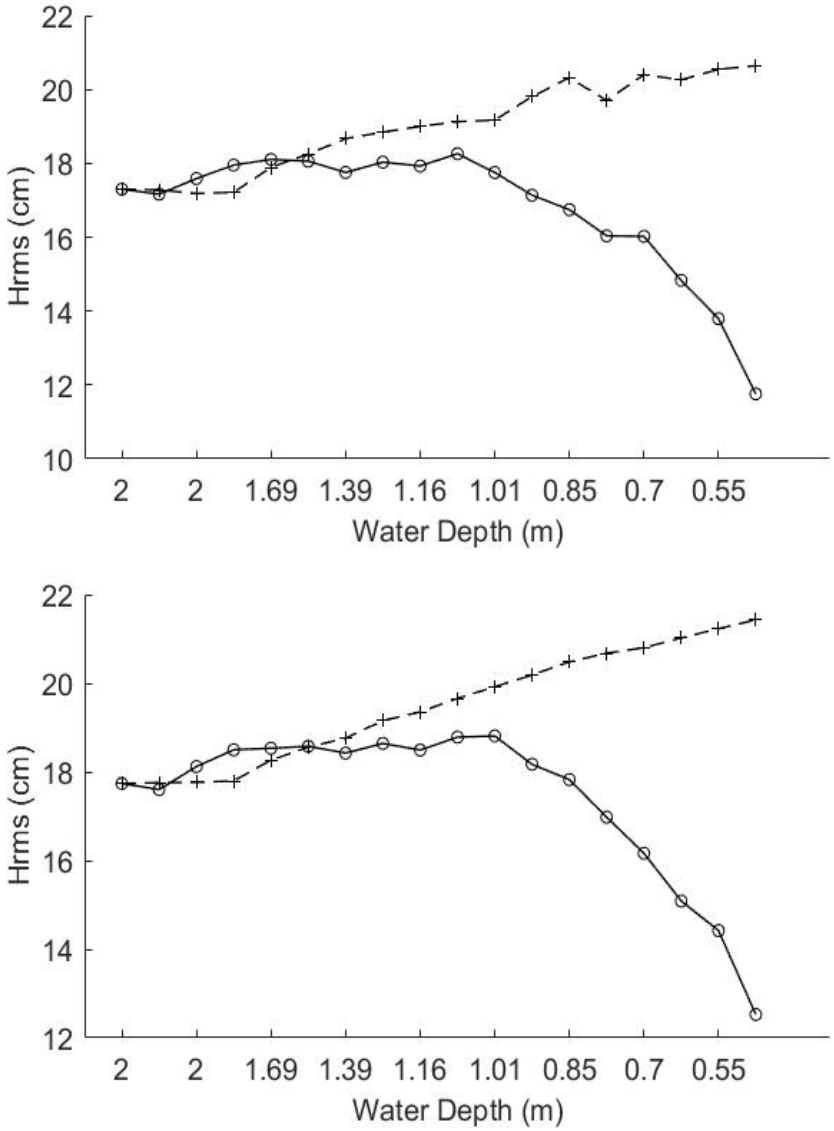

Figure 3.49: Variation of H_{rms} of Model Results and Experiment Data From NEES Tsunami and Swell Experiment with Depth. Experiment Data (○), Model of Kaihatu & Kirby (+). (Top) Soliton plus Random (Experiment 1, Trial 6); (Bottom) Solitan plus Random (Experiment 1, Trial 7).

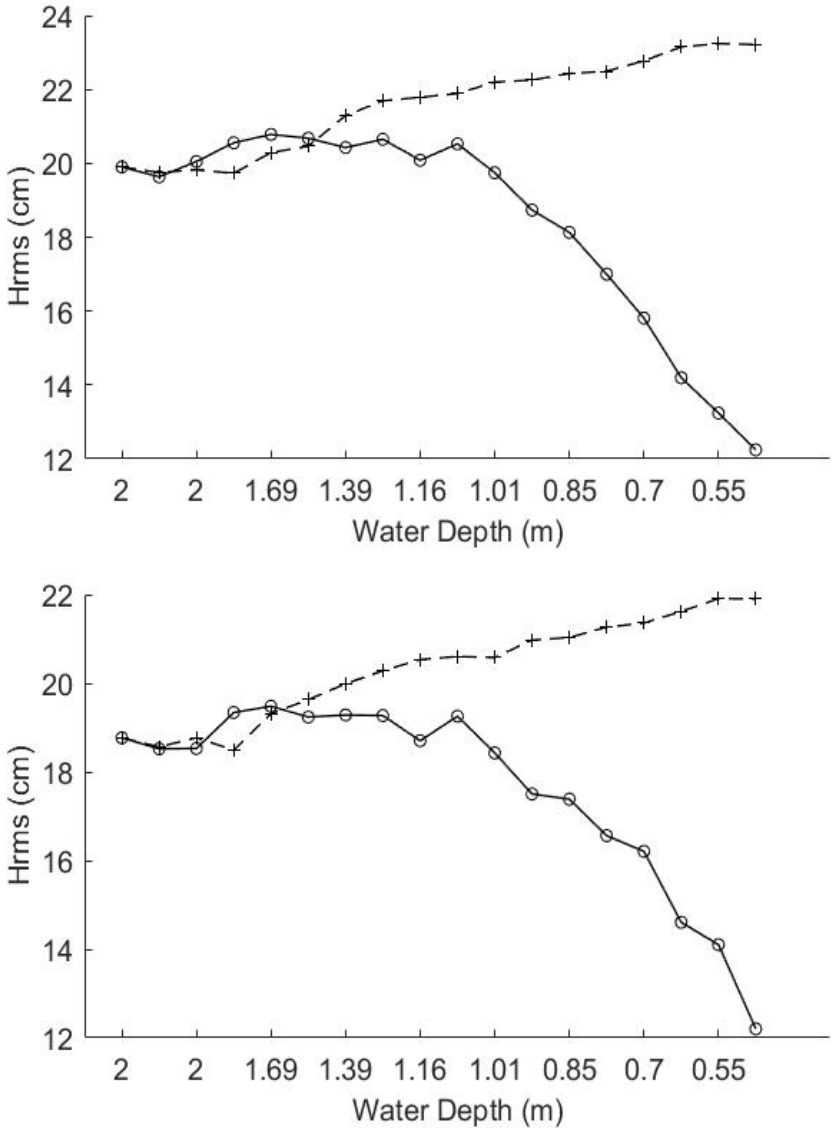

Figure 3.50: Variation of H_{rms} of Model Results and Experiment Data From NEES Tsunami and Swell Experiment with Depth. Experiment Data (○), Model of Kaihatu & Kirby (+). (Top) Soliton plus Random (Experiment 1, Trial 8); (Bottom) Solitan plus Random (Experiment 1, Trial 9).

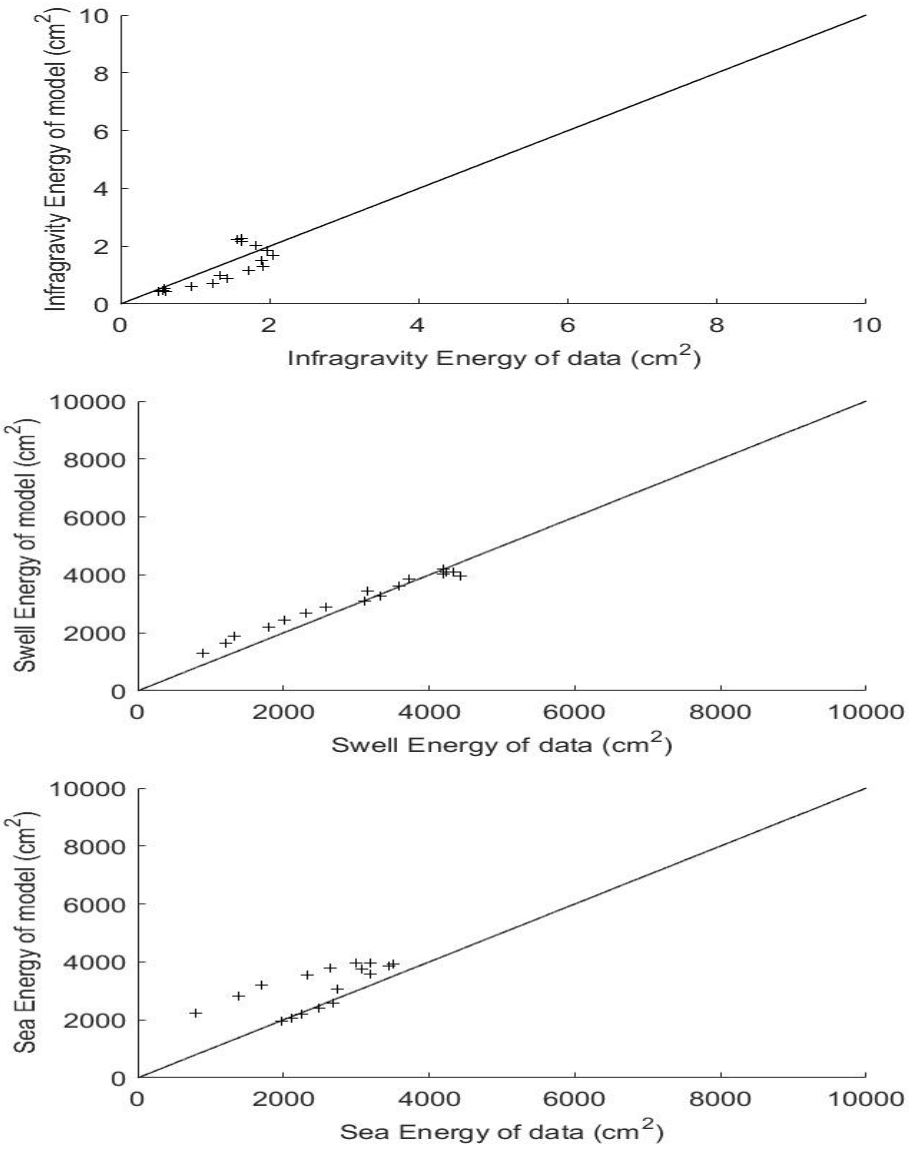

Figure 3.51: Energy Scatter Diagram For Data and Simulation From NEES Tsunami and Swell Experiment(Experiment 1, Trial 1, Purely Random Wave). Line: $y = x$. (Top) Infragravity Energy, $0 \leq f \leq \frac{f_{peak}}{2}$; (Middle) Swell Energy, $\frac{f_{peak}}{2} \leq f \leq \frac{3f_{peak}}{2}$; (Bottom) Sea Energy, $\frac{3f_{peak}}{2} \leq f$.

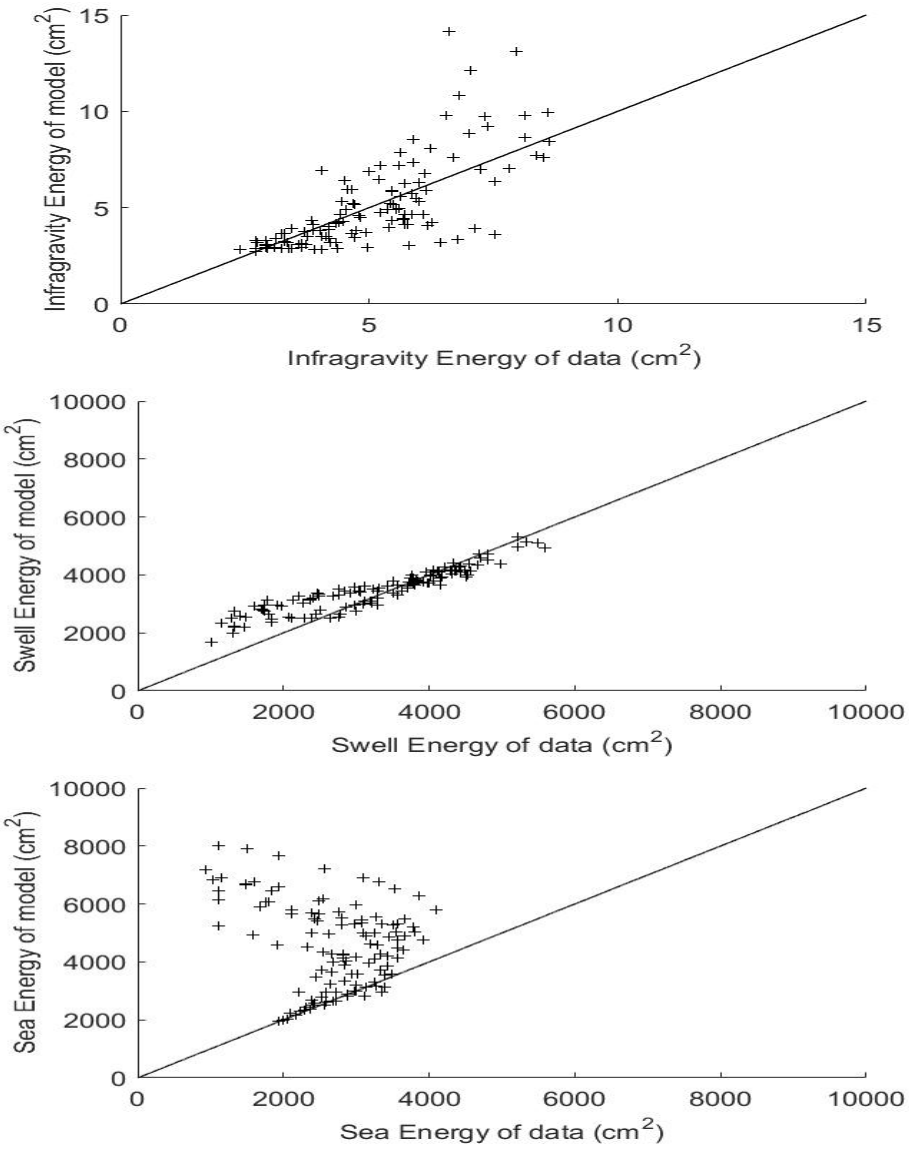

Figure 3.52: Energy Scatter Diagram For Data and Simulation From NEES Tsunami and Swell Experiment(Experiment 1, Soliton Plus Random Wave). Line: $y = x$. (Top) Infragravity Energy, $0 \leq f \leq \frac{f_{peak}}{2}$; (Middle) Swell Energy, $\frac{f_{peak}}{2} \leq f \leq \frac{3f_{peak}}{2}$; (Bottom) Sea Energy, $\frac{3f_{peak}}{2} \leq f$.

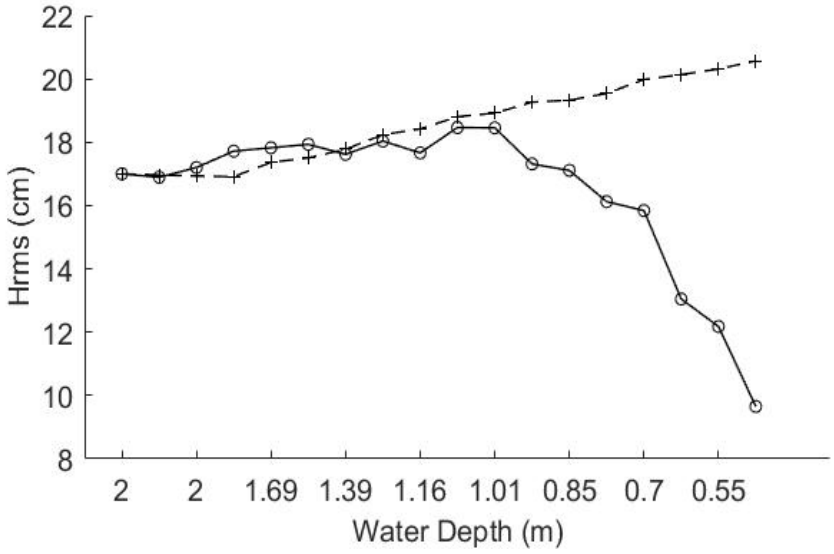

Figure 3.53: Variation of H_{rms} of Model Results and Experiment Data From NEES Tsunami and Swell Experiment with Depth. Experiment Data (○), Model of Kaihatu & Kirby (+). Solitan plus Random (Experiment 2, Trial 2).

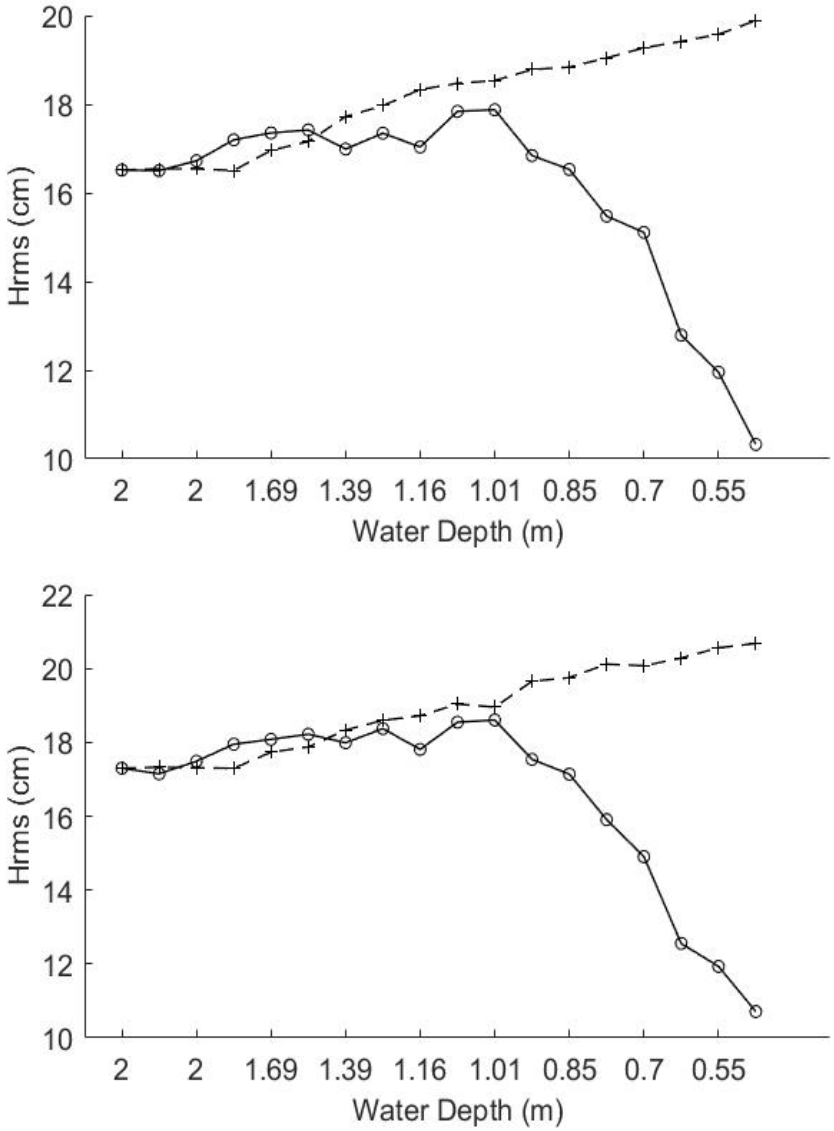

Figure 3.54: Variation of H_{rms} of Model Results and Experiment Data From NEES Tsunami and Swell Experiment with Depth. Experiment Data (○), Model of Kaihatu & Kirby (+). (Top) Soliton plus Random (Experiment 2,Trial 3); (Bottom) Solitan plus Random (Experiment 2, Trial 4).

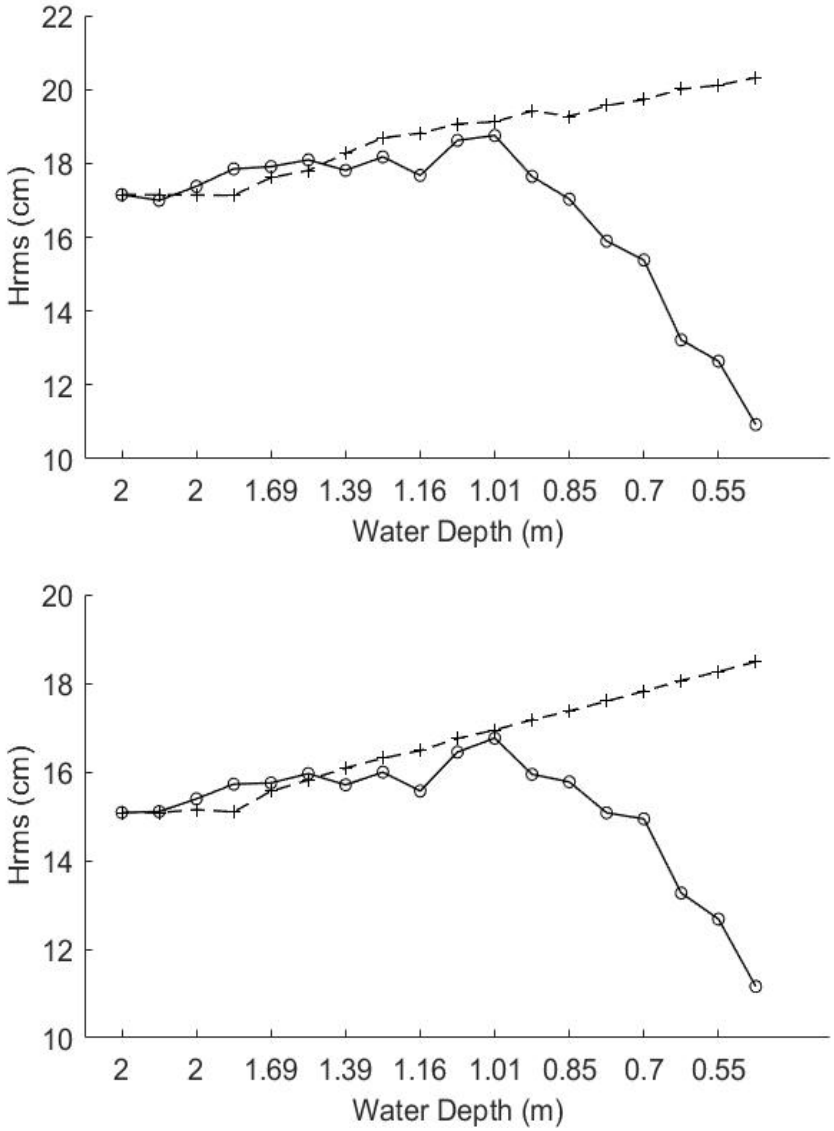

Figure 3.55: Variation of H_{rms} of Model Results and Experiment Data From NEES Tsunami and Swell Experiment with Depth. Experiment Data (○), Model of Kaihatu & Kirby (+). (Top) Soliton plus Random (Experiment 2,Trial 5); (Bottom) Solitan plus Random (Experiment 2, Trial 6).

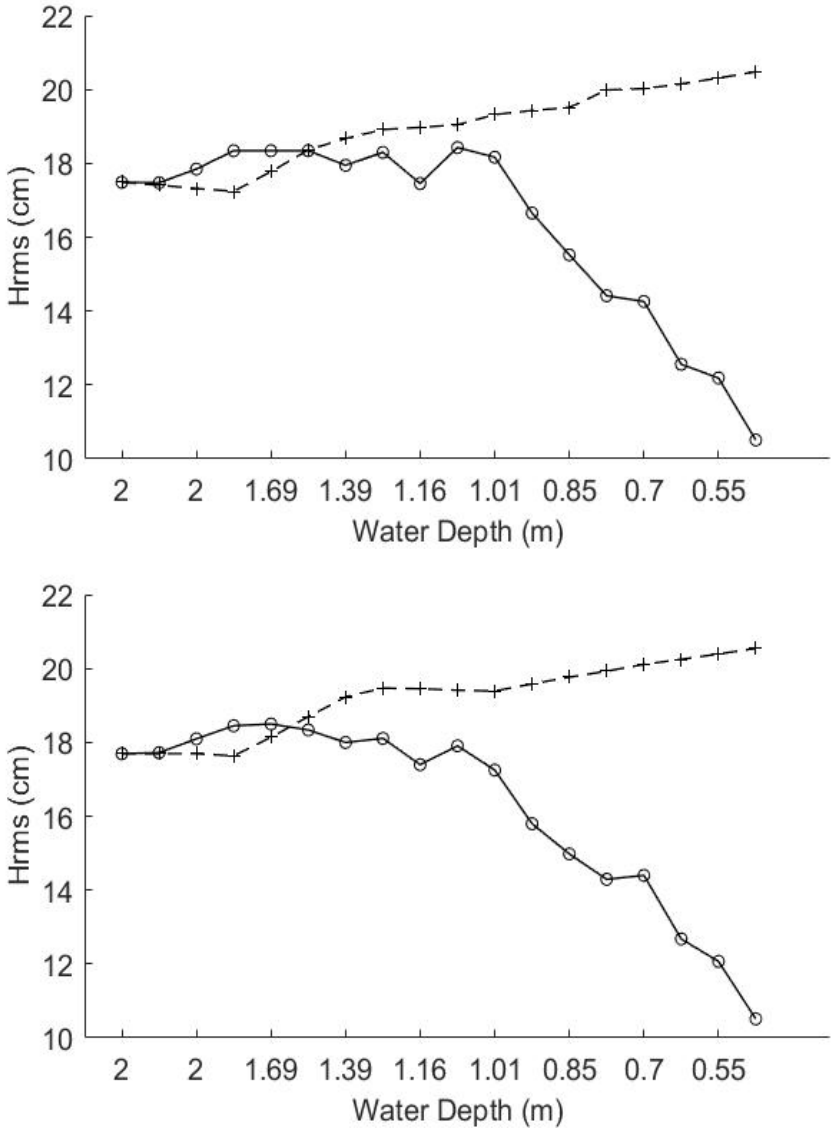

Figure 3.56: Variation of H_{rms} of Model Results and Experiment Data From NEES Tsunami and Swell Experiment with Depth. Experiment Data (○), Model of Kaihatu & Kirby (+). (Top) Soliton plus Random (Experiment 2, Trial 7); (Bottom) Solitan plus Random (Experiment 2, Trial 8).

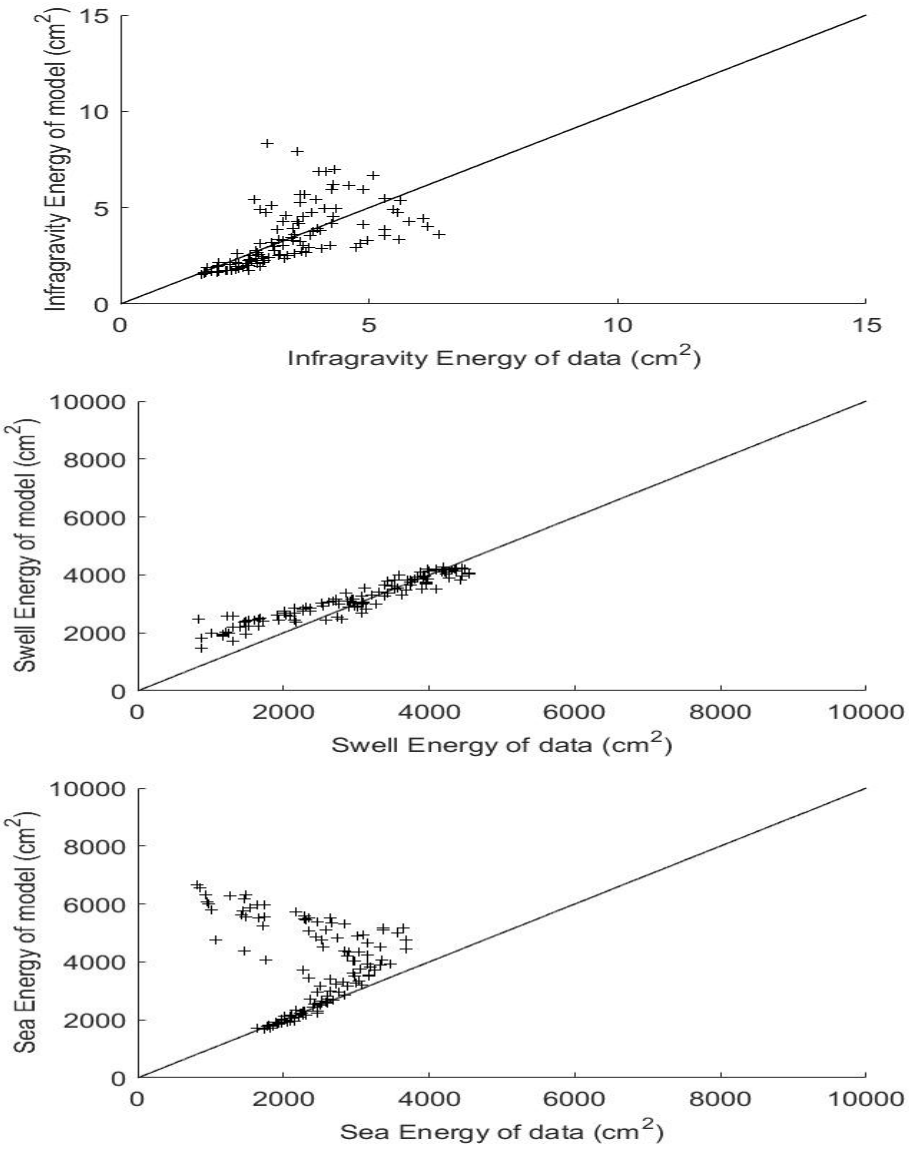

Figure 3.57: Energy Scatter Diagram For Data and Simulation From NEES Tsunami and Swell Experiment(Experiment 2, Soliton Plus Random Wave). Line: $y = x$. (Top) Infragravity Energy, $0 \leq f \leq \frac{f_{peak}}{2}$; (Middle) Swell Energy, $\frac{f_{peak}}{2} \leq f \leq \frac{3f_{peak}}{2}$; Sea Energy, $\frac{3f_{peak}}{2} \leq f$.

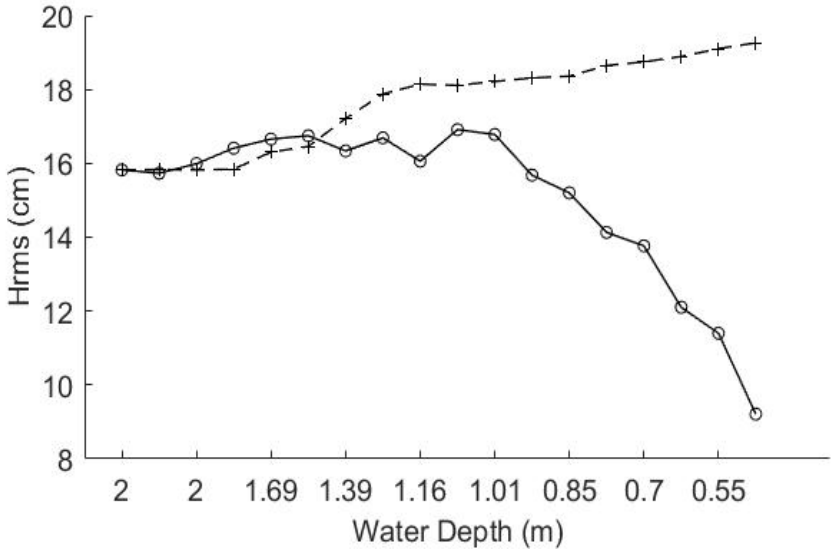

Figure 3.58: Variation of H_{rms} of Model Results and Experiment Data From NEES Tsunami and Swell Experiment with Depth. Experiment Data (○), Model of Kaihatu & Kirby (+). Solitan plus Random (Experiment 3, Trial 2).

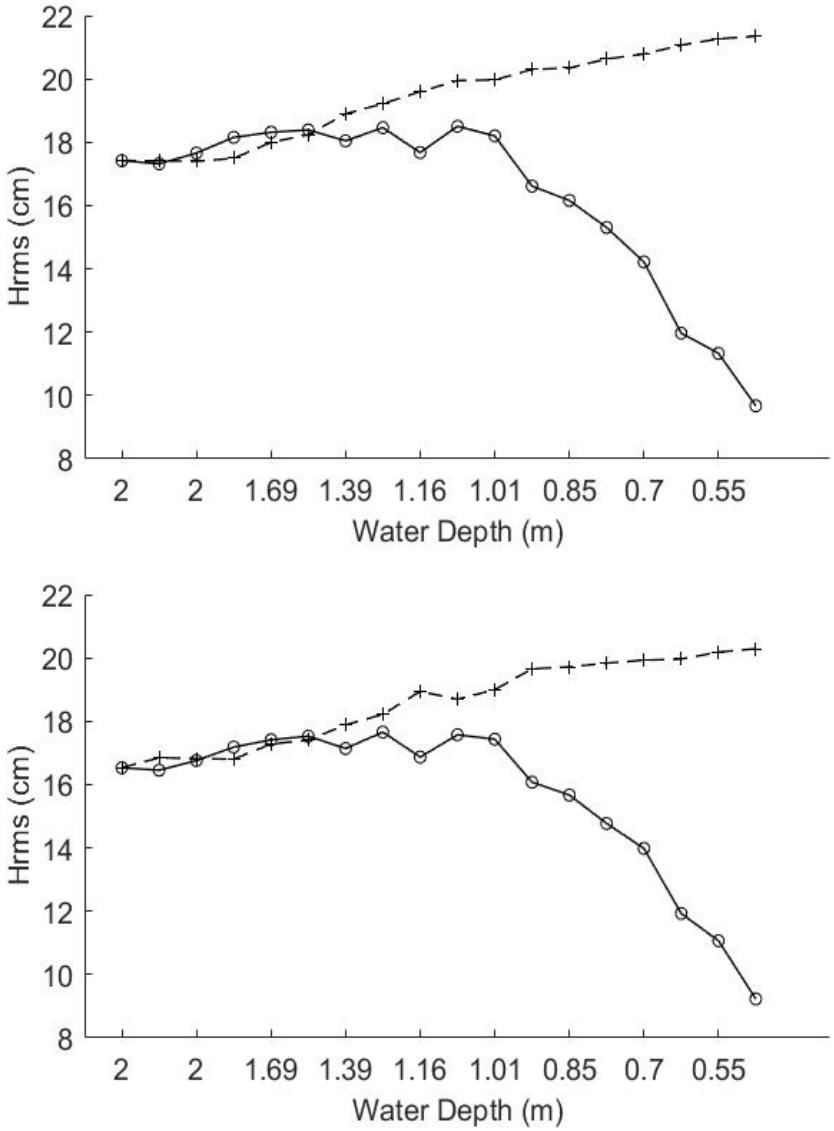

Figure 3.59: Variation of H_{rms} of Model Results and Experiment Data From NEES Tsunami and Swell Experiment with Depth. Experiment Data (○), Model of Kaihatu & Kirby (+). (Top) Soliton plus Random (Experiment 3, Trial 3); (Bottom) Solitan plus Random (Experiment 3, Trial 4).

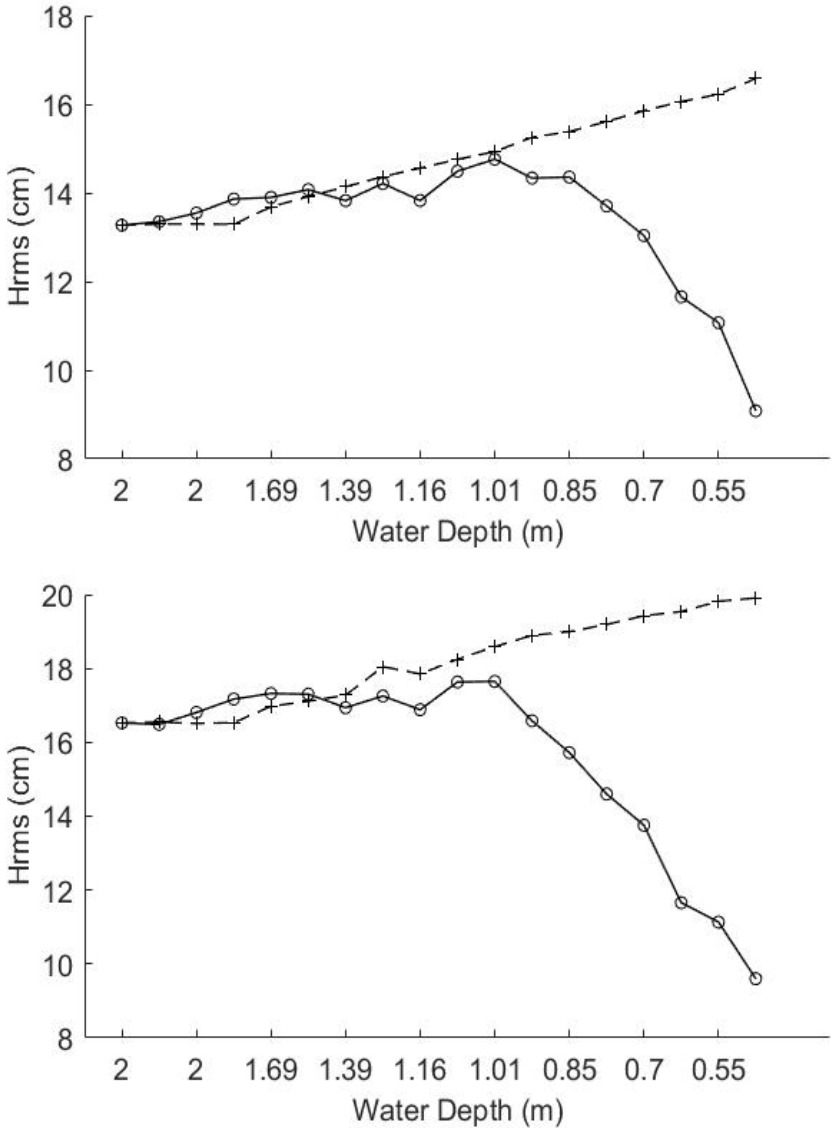

Figure 3.60: Variation of H_{rms} of Model Results and Experiment Data From NEES Tsunami and Swell Experiment with Depth. Experiment Data (○), Model of Kaihatu & Kirby (+). (Top) Soliton plus Random (Experiment 3, Trial 5); (Bottom) Solitan plus Random (Experiment 3, Trial 6).

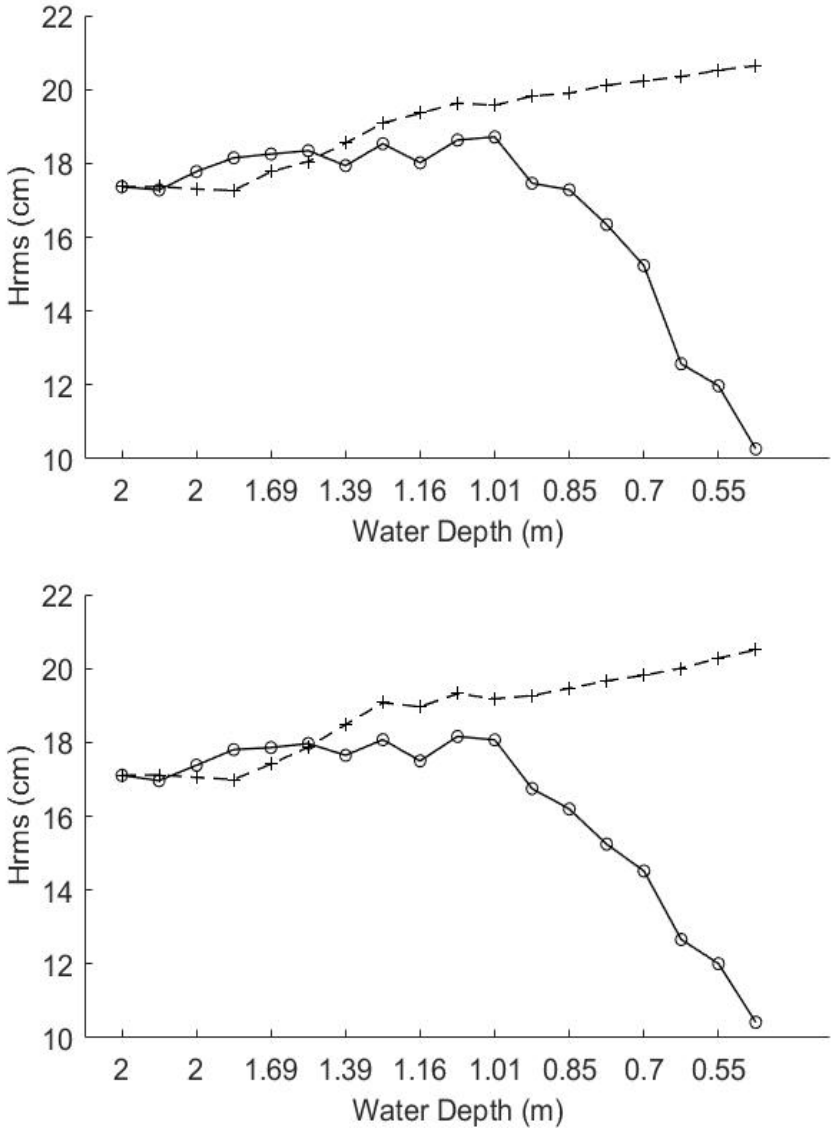

Figure 3.61: Variation of H_{rms} of Model Results and Experiment Data From NEES Tsunami and Swell Experiment with Depth. Experiment Data (○), Model of Kaihatu & Kirby (+). (Top) Soliton plus Random (Experiment 3, Trial 7); (Bottom) Solitan plus Random (Experiment 3, Trial 8).

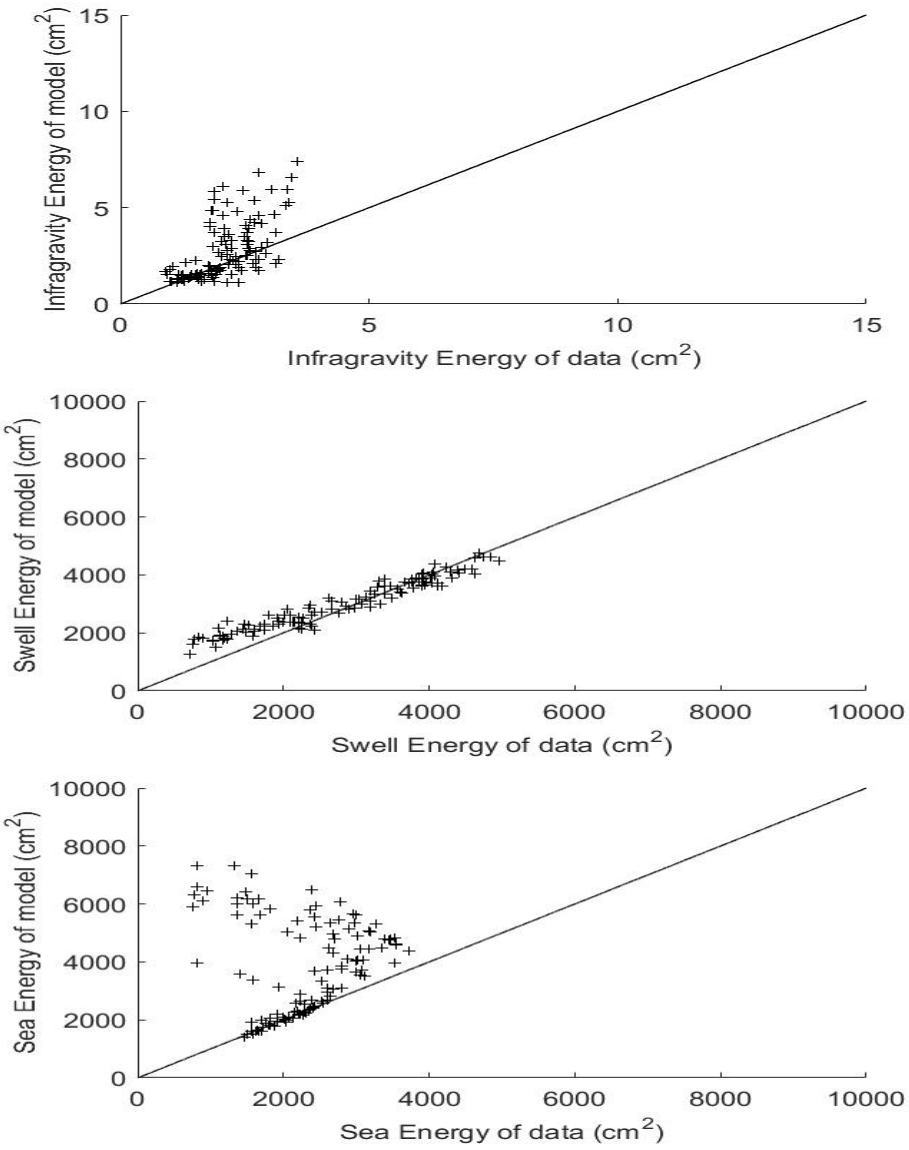

Figure 3.62: Energy Scatter Diagram For Data and Simulation From NEES Tsunami and Swell Experiment(Experiment 3, Soliton Plus Random Wave). Line: $y = x$. (Top) Infragravity Energy, $0 \leq f \leq \frac{f_{peak}}{2}$; (Middle) Swell Energy, $\frac{f_{peak}}{2} \leq f \leq \frac{3f_{peak}}{2}$; (Bottom) Sea Energy, $\frac{3f_{peak}}{2} \leq f$.

The energy scatter diagram in different areas and the comparison between the H_{rms} of model and measurement give a quantitative evaluation of the model's performance about energy. They also give further analysis of the spectra comparisons shown in section 3.2, 3.3 and 3.4. In this section, skewness and asymmetry are calculated to evaluate the model's performance in the prediction of the wave shape.

Skewness is calculated by :

$$Skewness = \frac{\langle \eta^3 \rangle}{\langle \eta^2 \rangle^{\frac{3}{2}}} \tag{3.1}$$

where η is the wave surface and the brackets $\langle\rangle$ denote an average. Asymmetry is calculated by:

$$Asymmetry = \frac{\langle (\mathcal{H}(\eta))^3 \rangle}{\langle \eta^2 \rangle^{\frac{3}{2}}} \tag{3.2}$$

where $\mathcal{H}(\eta)$ denotes the Hilbert transform of the signal η.

To make comparisons, each of the four realizations in each trial was transformed into time domain with inverse Fast Fourier Transform. Then, skewness and asymmetry were calculated and averaged over all four realizations at each gauge. As mentioned before, the first 128 frequency components were retained to input the parabolic model for simulation. Hence, the experimental data at each gauge were processed by Fast Fourier Transform and then only the first 128 frequency components were transformed by inverse Fast Fourier Transform to obtain a time series. Then, skewness and asymmetry were calculated based on the time series signal based on the first 128 frequency components.

According to Kaihatu (1994), the truncation of the frequency components does not affect H_{rms} much since the first 128 frequency components account for about 80% of the wave energy. However, the skewness and asymmetry are less stable statistical parameters than H_{rms}. Kaihatu (1994) compared the skewness between the truncated and full data spectra and showed that the truncation had a significant influence on the skewness and asymmetry. Bowen (1994) also maintained that the calculation of higher order moments could be affected by the truncation.

It should be noted here that strict comparison of skewness and asymmetry between model and

measurement is misleading. For the data, even though the spectra were truncated, each frequency component has engaged into all possible nonlinear interactions. However, for the simulation result, the data which was input the model was truncated. Hence, the nonlinear interaction only happened among the frequency components retained. The true comparison of skewness and asymmetry between model and measurement can be achieved only if all the frequency components are input into the model, which is not economic.

There are seven trials for soliton plus random wave in each experiments. In this section, the performance of the model in the wave shape prediction is evaluated generally. It does not lose the generality to choose the data and model results of Trial 5 in each experiment as a representation for ensemble. The average skewness and asymmetry of data and model at each gauge in all of the trials are calculated and plotted as scatter diagram to show the general performance of the model.

In the Figure 3.63, the comparisons of average skewness for trial 5 in each experiment are shown. Generally, the model results have the correct prediction of the trend. In the uniform depth, the model really performs well in each experiment. Especially in Experiment 3, from $2m$ to $0.85m$ water depth, the model has a good prediction of the skewness of the measurement. It is clearly that the model performs better in the prediction of skewness when the wave height of the soliton is decreased.

Take a close inspection on the skewness of measurement along the wave propagation, the larger amplitude of the soliton is, the larger skewness is at the initial gauge. (The amplitudes of the soliton in Experiment 1, 2 and 3 are $0.85m$, $0.7m$ and $0.5m$ respectively.) Skewness describes the top-to-bottom asymmetry. The skewness of sinusoidal wave is zero. The addition of the soliton makes the crests sharper and the troughs flatter than sinusoidal waves.

The skewness of the data increases during the shoaling. It describes the increase of the wave amplitude and the narrower the crests are during the shoaling. Around the last gauge, the skewness starts to decrease. It is likely caused by the dissipation. During the shoaling, the energy at lower frequencies is transformed to the higher frequencies and the crest becomes sharper because of that. However, the wave breaking dissipated large amount of the energy and the wave amplitude

decreases dramatically, which may make the wave shape more smooth.

The model over-predicts the skewness during shoaling. It might be caused by the truncation of the frequency components, since the nonlinear process transforms the energy at lower frequencies to higher frequencies. It can be a reason that the addition of the soliton adds energy at the lower frequencies, which has not had complete nonlinear interaction due to the truncation. It can be also seen in the spectra for the last gauge like Figure 3.46 that the model over-predicts the energy in the swell and sea area. This extra energy can be the reason for the over-prediction of the skewness.

The similar evaluation method in energy scatter diagrams is used here to show the general performance of the model in each experiments. According to Figure 3.64, the model generally over-predicts the skewness of the data. It is hard to say difference between the performance of the model for each experiments generally. However, it is obvious that more points are in the area where skewness is smaller than one and lump around the line with slope one as the wave height of the soliton decrease.

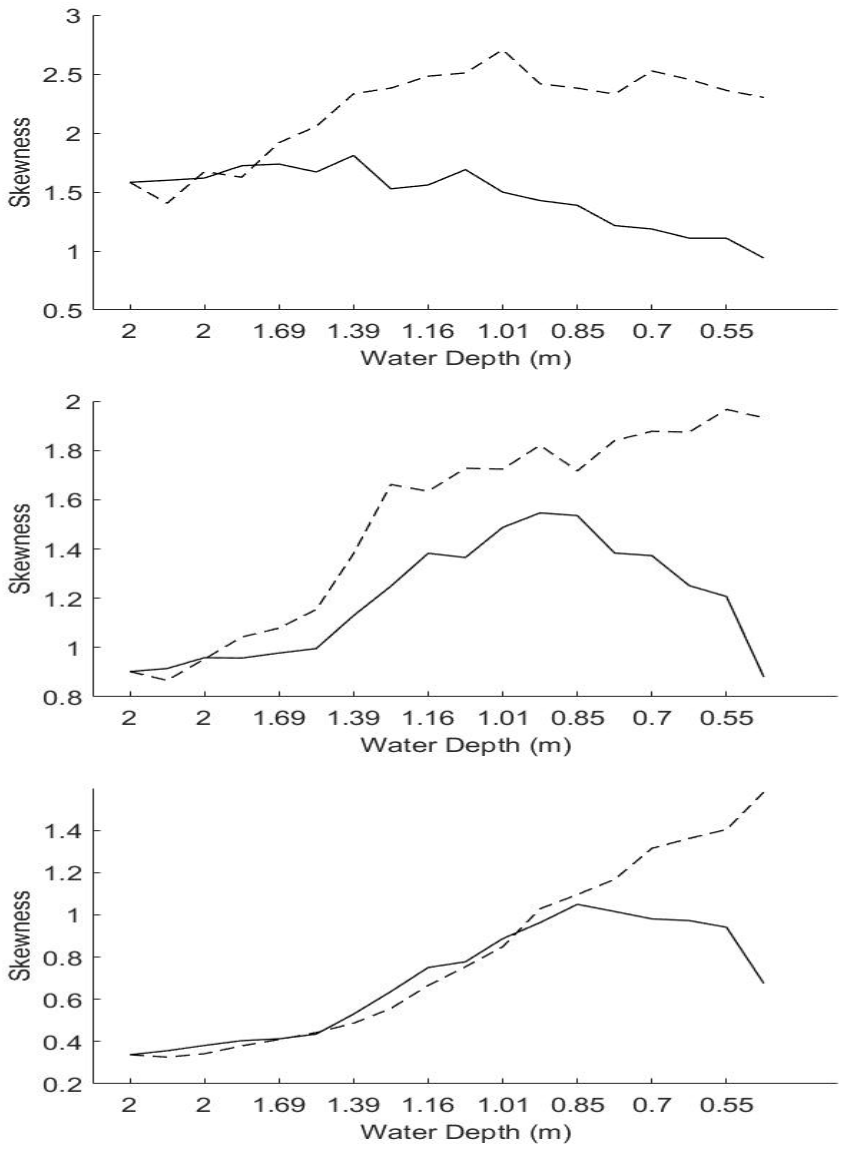

Figure 3.63: Comparison of Average Skewness. (Soliton Plus Random Wave) Experiment Data (-), Model of Kaihatu & Kirby (- -). (Top) Trial 5, Experiment 1 ; (Middle) Trial 5, Experiment 2; (Bottom) Trial 5, Experiment 3.

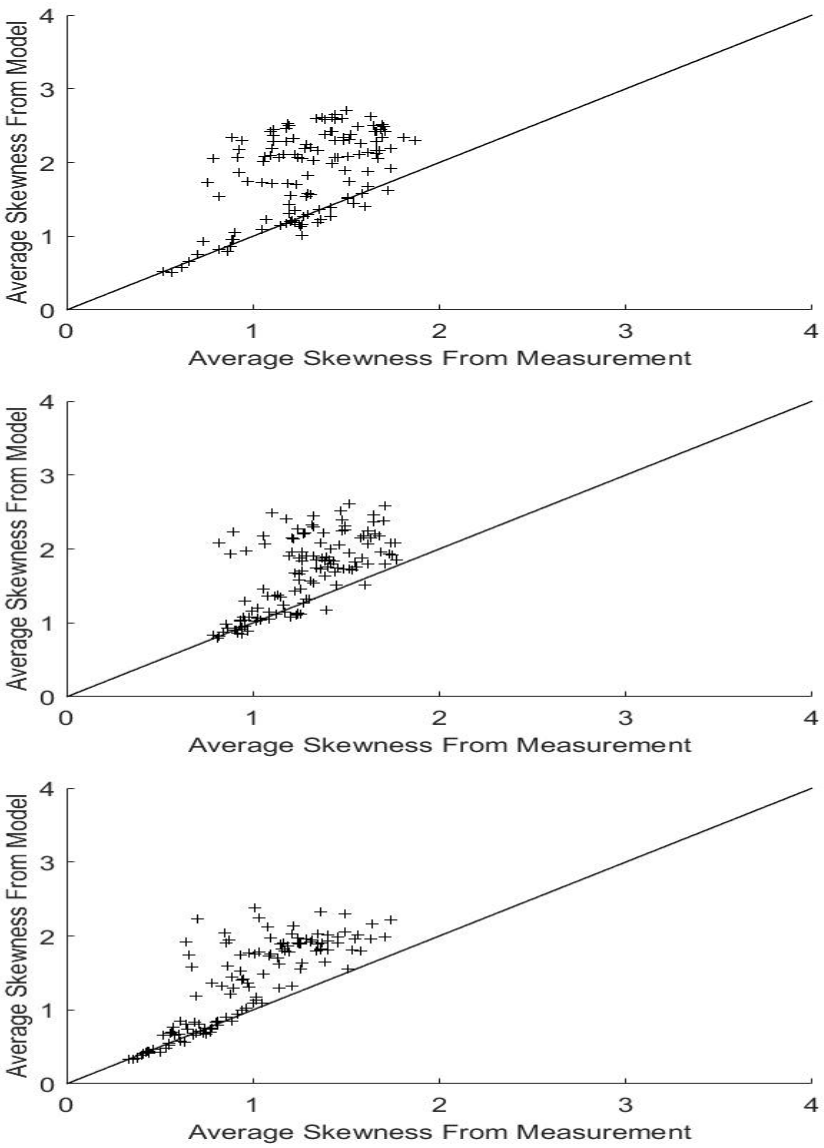

Figure 3.64: Scatter Diagram for Average Skewness(Soliton Plus Random Wave). Line: $y = x$. Experiment Data (-), Model of Kaihatu & Kirby (- -). (Top) Experiment 1 ; (Middle) Experiment 2; (Bottom) Experiment 3.

In Figure 3.65, the comparisons of average asymmetry for trial 5 in each experiment are present. The performance of the model varies significantly in different experiments. For Experiment 3, where the wave amplitude of the soliton is $0.5m$, the model performs well generally. However, for Experiment 1 and 2, the model has a wrong prediction of the trend around 1.20 m of the water depth. Figure 3.66 shows the general performance of model in asymmetry preditcion in each experiment. The difference of the performance is not that evident. However, it is similar to the case about skewness. More points distribute from -1 to 0 and concentrate around the line with slope one as the wave height of the soliton decreases.

The asymmetry describes the front-to-back asymmetry. The asymmetry of the sinusoidal wave is zero. When the wave intends to break, the asymmetry is negative and the wave has sawtooth-like shape. Between the last two gauges, the asymmetry of the measurement has a positive trend, which indicates that the wave front had the tendency to turn backward . It is actually unnatural for the run-up of the waves because the wave breaking happens when the slope of the wave front face tends to be zero and even positive. According to the description of the experiment operator, it is possible to be one reason that the gauge equipment is dragged backward by the run-down of the water.

Kaihatu (1994) compared the asymmetry of the complete data between the data with truncation and the average asymmetry with one standard deviation added or subtracted. The standard deviation band for asymmetry is fairly wide. It is unclear why the asymmetry of the model simulation increases along shoaling and why the model performs poor during the shoaling. Since only 128 frequencies are retained, the stability of the asymmetry might be the reason.

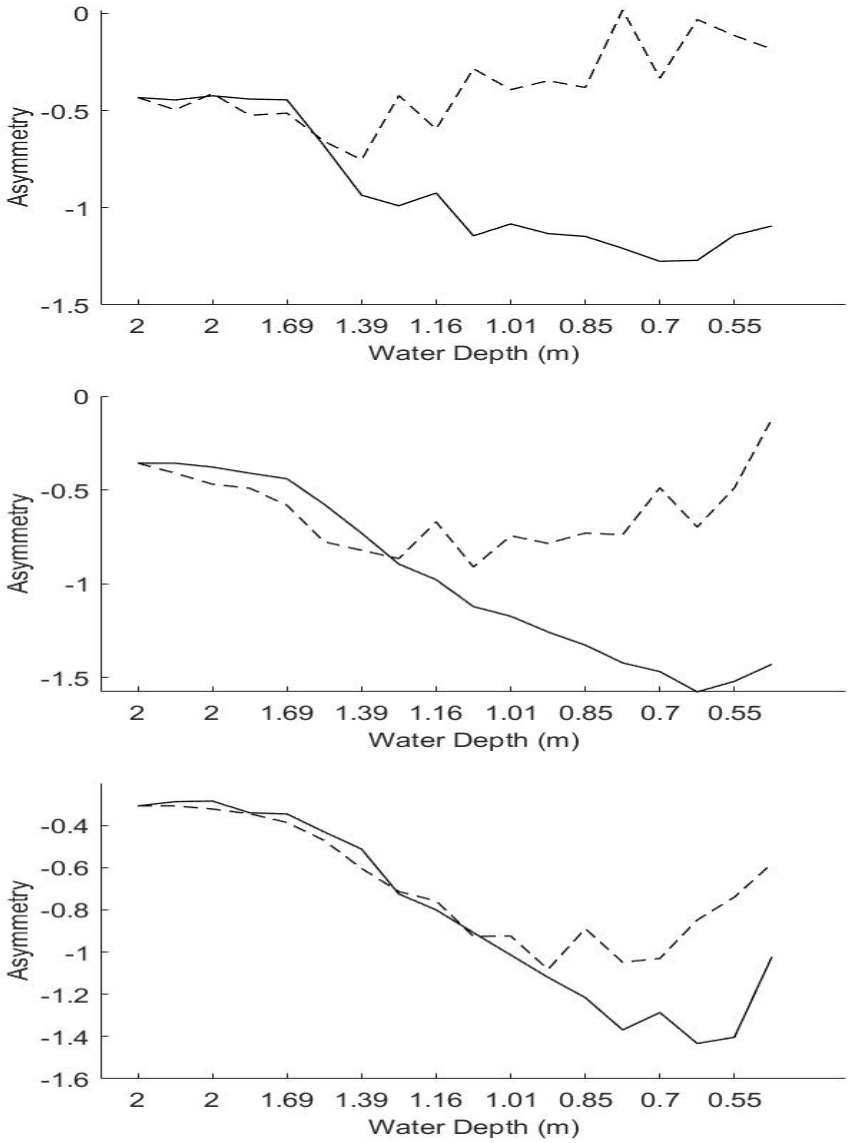

Figure 3.65: Comparison of Average Asymmetry. (Soliton Plus Random Wave) Experiment Data (-), Model of Kaihatu & Kirby (- -). (Top) Trial 5, Experiment 1 ; (Middle) Trial 5, Experiment 2; (Bottom) Trial 5, Experiment 3.

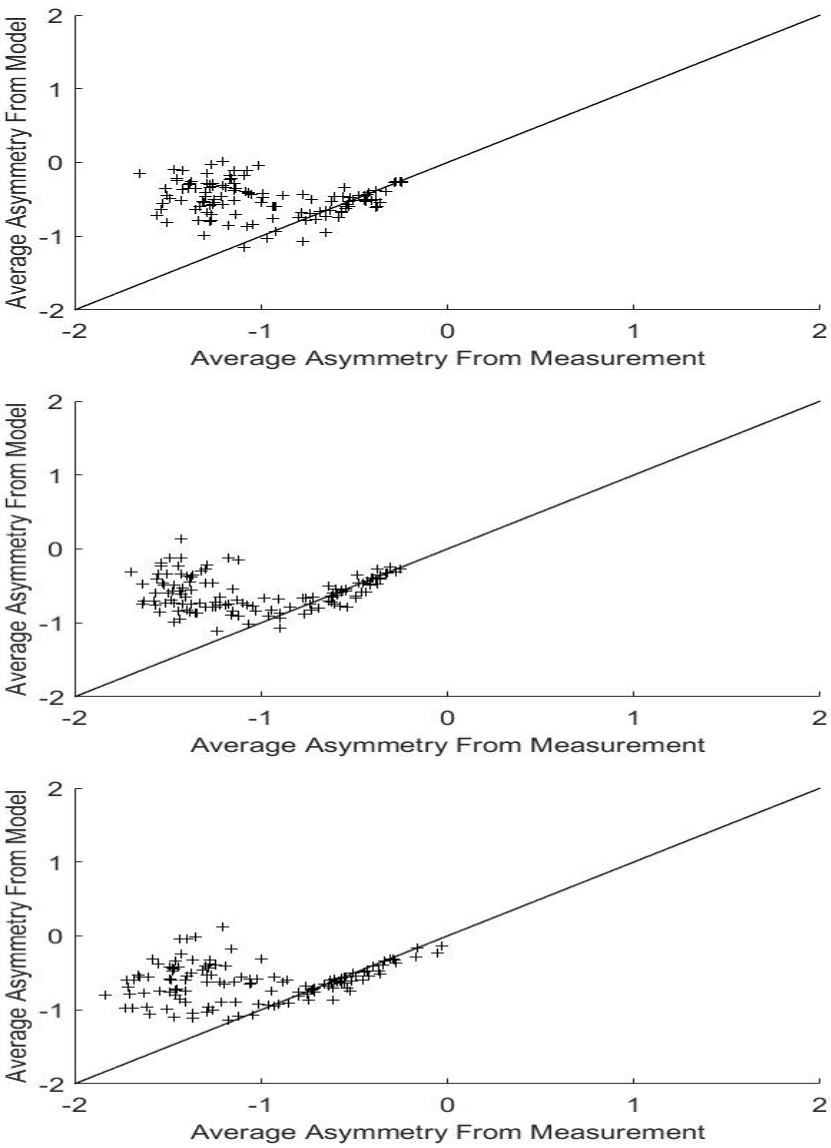

Figure 3.66: Scatter Diagram for Average Asymmetry (Soliton Plus Random Wave). Line: $y = x$. (Top) Experiment 1 ; (Middle) Experiment 2; (Bottom) Experiment 3.

4. CONCLUSIONS AND SUGGESTIONS FOR FUTURE WORK

In this work, we review two general frequency domain methodologies to model the nonlinear wave propagation during shoaling that extend the limit of Boussinesq equations in shallow water, extended Boussinesq equations and weakly nonlinear mild-slope equation. The weakly nonlinear frequency domain parabolic mild-slope model from Kaihatu and Kirby (1995) is rederived in this work. The model of Kaihatu and Kirby (1995) has the same dispersion relation and shoaling properties as linear theory and weakly nonlinearity which enables the model to have the same order of accuracy in nonlinearity with weakly nonlinear extended Boussinesq equation model.

The nonlinear mild-slope model is built for periodic wave fields since the Fourier series is applied in the derivation of the model, where every mode has a specific period. However, the wave signals in any given wave record can be mixed up with some aperiodic signals like soliton and cnoidal wave. It is meaningful to test the performance of the model when dealing with periodic signals interacted by aperiodic signals. Therefore, we make use of the data from the experiments conducted at Oregon State University on combining Tsunami and Swell to evaluate the model performance.

Three different cases of data from the experiments are processed through the model, purely random wave, purely soliton and soliton plus random wave. The model performs well for purely random wave field. However, when the soliton with 0.85 m amplitude is added into the wave field, the performance of the model is influenced significantly. Though the model predicts the general trend of the spectra well, the energy of the wave field in the infragravity and swell area is remarkably increased compared with the purely random wave field. Therefore, the deviation in the infragravity and swell area keeps growing. When it comes to the root mean square of wave height, the model does not simulate well because of the under-prediction of the energy in the infragravity and swell area. The energy scatter diagrams give an qualitative view of the performance of the model in the infragravity, swell and sea area respectively.

It is hard to identify the factors affecting the performance of the model through derivation since

the analytical expression of the soliton is unknown in the experiment. According to the results mentioned above, it is reasonable to assume that the amplitude of the soliton accounts for the effect on the nonlinear process of the random waves and the performance of the model. Therefore, in Experiment 2, the amplitude of the soliton is reduced to 0.7 m, and the shapes of the spectra are less influenced by the addition of the soliton. It is still hard to say whether the performance of the model is improved through the plots of H_{rms}. However, from the energy scatter diagrams, the performance of the model is significantly improved, especially in the infragravity and swell area.

To further verify the influence of the soliton, in Experiment 3, the amplitude of the soliton is set as 0.5 m. From the comparisons between spectra for data and simulation results, the prediction of the model is better than that for Experiment 2. The prediction of H_{rms} is similar, but the model performs better in the energy scatter diagrams.

In conclusion, the addition of the soliton increases the energy density of the wave field in the infragravity and swell area. The larger the amplitude of the soliton, the larger the effect of the soliton on the nonlinear processes in random waves, and with that the poorer the performance of the model.

Then, two higher order statistical parameters, skewness and asymmetry, are calculated to evaluate the performance of the model in predicting the wave shape. Because of the sensitivity of these two parameters to the frequency truncation, the performance of the model can only be estimated generally. The model over-predicts the skewness during the shoaling. Even though the data and model results are both retained to 128 frequencies, the 128 frequencies in data have experienced all possible nonlinear interactions during propagation, while the nonlinear process only happens among the retained frequency components in the model. The addition of the soliton, which adds most energy at lower frequencies, might exaggerate the deviation. It is evident that the model has some limits in the prediction of asymmetry. The dissipation mechanism might be a reason for the problem since the model results fail to show the wave breaking effect clearly. The model performance in predicting the skewness and asymmetry is generally evaluated in each experiment. The increase of the amplitude of the soliton had a significant influence on the performance of the

model. The model performs better as the amplitude of the soliton decreases.

There are several reasons for the poor performance of the model. Firstly, during the derivation of the model, the discrete Fourier transformation is applied, which is actually an assumption that the wave signal is periodic. Hence, the deviation of the model simulation for soliton plus random wave is as expected. This drawback is hard to solve or avoid. The right way to convert the soliton into frequency domain is to use the continuous Fourier transformation on the analytical expression of the soliton. However, it is unpractical to achieve the expression of the soliton in any situations. From the analysis in this work, the addition of the soliton increases the energy density of the wave field in the infragravity and swell area. There might be a way to add some nonlinear term into the model to describe the interaction between soliton and random waves.

Secondly, the model uses the model of Thornton and Guza (1983) as the dissipation mechanism. The dissipation model of Thornton and Guza (1983) is applicable for the random wave field, which is assumed to follow the Rayleigh distribution. However, the soliton does not follow the Rayleigh distribution and the method used by Thornton and Guza (1983) does not make sense for the soliton. Zelt (1991)[28] built a Lagrangian finite-element Boussinesq wave model, where wave breaking and bore propagation is modeled with an artificial viscosity technique for the soliton. The performance can be improved if the dissipation model of Zelt (1991) is used in the model of Kaihatu and Kirby (1995). However, the model of Zelt (1991) is a time-series model. Some modification might need to be made on the model of Zelt (1991) to be useful.

REFERENCES

[1] M. Freilich and R. Guza, "Nonlinear effects on shoaling surface gravity waves," *Philosophical Transactions of the Royal Society of London. Series A, Mathematical and Physical Sciences*, vol. 311, no. 1515, pp. 1–41, 1984.

[2] C. C. Mei, M. Stiassnie, and D. K.-P. Yue, *Theory and applications of ocean surface waves: nonlinear aspects*, vol. 23. World scientific, 2005.

[3] F. Ursell, "The long-wave paradox in the theory of gravity waves," *Mathematical Proceedings of the Cambridge Philosophical Society*, vol. 49, no. 04, 1953.

[4] D. H. Peregrine, "Long waves on a beach," *Journal of fluid mechanics*, vol. 27, no. 4, pp. 815–827, 1967.

[5] J. M. Kaihatu, *Frequency domain wave models in the nearshore and surf zones*, vol. 67, pp. 43–72. Elsevier, 2003.

[6] P. A. Madsen, R. Murray, and O. R. Sørensen, "A new form of the boussinesq equations with improved linear dispersion characteristics," *Coastal engineering*, vol. 15, no. 4, pp. 371–388, 1991.

[7] H. A. Schäffer and P. A. Madsen, "Further enhancements of boussinesq-type equations," *Coastal Engineering*, vol. 26, no. 1-2, pp. 1–14, 1995.

[8] P. Madsen and H. Schäffer, "Higherorder boussinesqtype equations for surface gravity waves: derivation and analysis," *Philosophical Transactions of the Royal Society of London. Series A: Mathematical, Physical and Engineering Sciences*, vol. 356, no. 1749, pp. 3123–3181, 1998.

[9] O. Nwogu, "Alternative form of boussinesq equations for nearshore wave propagation," *Journal of waterway, port, coastal, and ocean engineering*, vol. 119, no. 6, pp. 618–638, 1993.

[10] Y. Chen and P. L.-F. Liu, "Modified boussinesq equations and associated parabolic models for water wave propagation," *Journal of Fluid Mechanics*, vol. 288, pp. 351–381, 1995.

[11] J. Berkhoff, "Computation of combined refraction-diffraction," *Coastal Engineering Proceedings*, vol. 1, no. 13, 1972.

[12] R. Smith and T. Sprinks, "Scattering of surface waves by a conical island," *Journal of Fluid Mechanics*, vol. 72, no. 2, pp. 373–384, 1975.

[13] A. Radder, "On the parabolic equation method for water-wave propagation," *Journal of fluid mechanics*, vol. 95, no. 1, pp. 159–176, 1979.

[14] C. Lozano and P. L.-F. Liu, "Refractiondiffraction model for linear surface water waves," *Journal of Fluid Mechanics*, vol. 101, no. 4, pp. 705–720, 1980.

[15] P. J. Bryant, "Periodic waves in shallow water," *Journal of fluid mechanics*, vol. 59, no. 4, pp. 625–644, 1973.

[16] P. Bryant, "Stability of periodic waves in shallow water," *Journal of Fluid Mechanics*, vol. 66, no. 1, pp. 81–96, 1974.

[17] J. B. Keller, "Resonantly interacting water waves," *Journal of Fluid Mechanics*, vol. 191, pp. 529–534, 1988.

[18] Y. Agnon, A. Sheremet, J. Gonsalves, and M. Stiassnie, "Nonlinear evolution of a unidirectional shoaling wave field," *Coastal Engineering*, vol. 20, no. 1-2, pp. 29–58, 1993.

[19] Y. Tang and Y. Ouellet, "A new kind of nonlinear mild-slope equation for combined refraction-diffraction of multifrequency waves," *Coastal Engineering*, vol. 31, no. 1-4, pp. 3–36, 1997.

[20] D. K. P. Yue and C. C. Mei, "Forward diffraction of stokes waves by a thin wedge," *Journal of Fluid Mechanics*, vol. 99, no. 01, 1980.

[21] J. M. Kaihatu, "Improvement of parabolic nonlinear dispersive wave model," *Journal of waterway, port, coastal, and ocean engineering*, vol. 127, no. 2, pp. 113–121, 2001.

[22] J. A. Battjes and J. Janssen, "Energy loss and set-up due to breaking of random waves," *Coastal Engineering Proceedings*, vol. 1, no. 16, 1978.

[23] E. B. Thornton and R. Guza, "Transformation of wave height distribution," *Journal of Geophysical Research: Oceans*, vol. 88, no. C10, pp. 5925–5938, 1983.

[24] S. C. Chapra, *Applied numerical methods*. McGraw-Hill Columbus, 2012.

[25] H. Mase and J. T. Kirby, "Hybrid frequency-domain kdv equation for random wave transformation," *Coastal Engineering Proceedings*, vol. 1, no. 23, 1992.

[26] J. M. Kaihatu, "Frequency domain models for nonlinear finite depth water wave propagation," *University of Delaware*, 1994.

[27] J. M. Kaihatu, J. T. Goertz, S. Ardani, and A. Sheremet, "Nonlinear and dissipative characteristics of a combined random-cnoidal wave field," in *ASME 2017 36th International Conference on Ocean, Offshore and Arctic Engineering*, pp. V07AT06A037–V07AT06A037, American Society of Mechanical Engineers, 2017.

[28] J. Zelt, "The run-up of nonbreaking and breaking solitary waves," *Coastal Engineering*, vol. 15, no. 3, pp. 205–246, 1991.